



SAPIENZA
UNIVERSITÀ DI ROMA

**Natural products from higher plants and marine
organisms as sources of new anticancer agents:
synthesis and biological evaluation**

Dipartimento di Chimica e Tecnologie del Farmaco

PhD Thesis

Presented by

Simone Berardozzi

Supervisor:

Prof. Dr. Bruno Botta

2017

To Silvia and my family.

“Not every collision, not every punctilious trajectory by which billiard-ball complexes arrive at their calculable meeting places lead to reaction. Men (and women) are not as different from molecules as they think...”

Roald Hoffmann

Acknowledgments

This thesis results not only from my work in the laboratory, but represents the contribution of many people I have encountered and worked with during the past years, I wish to acknowledge. Since the very beginning of my time at university, I felt at home and enjoyed being part of a research team, in which every contribution is essential for the success of the project.

First and foremost, I would like to express my sincere gratitude to my advisor Prof. Dr. Bruno Botta for the continuous support of my Ph.D study and related research. I am in particular grateful for his patience, motivation, guidance and immense knowledge. Moreover, he supported me emotionally on the journey leading up to this thesis. I could not have imagined better advisor and mentor for my Ph.D study.

Besides my advisor, I am particularly indebted to Prof. Dr. Karl-Heinz Altmann, who provided me the opportunity to join his group as a visiting student. I am very thankful for the excellent example he has provided me as professor and man of science, and I am grateful for his support in the research I did in his lab.

I gratefully acknowledge Dr. Mattia Mori, for performing molecular modeling calculations, Prof. Dr. Lucia Di Marcotullio for the biological tests of CSCs project, Prof. Dr. Gloria Uccello-Barretta for performing the NMR spectroscopy

studies, and Dr. Fernando Diaz for the biological evaluation of antimetabolic compounds.

I would like to express my special appreciation and thanks to my students Pietro Eleuteri and Laura Mangiardi. With their help and support, we successfully synthesized many GlaB derivatives.

The members of Botta's group have immensely contributed to my personal and professional time at Sapienza, while the group has been a source of friendships. In particular, I would like to mention Dr. Francesca Ghirga, Dr. Cinzia Ingallina, Dr. Deborah Quaglio and Patrizio Ghirga for their support and friendship.

In regards to Altmann's group, I would like to thank all the members that made me feel at home since the very first day. A special thank goes to Dr. Bernhard Pfeiffer and Kurt Hauenstein for their scientific support. A special thank goes to my labmates Melanie Zechner, Simon Glauser, Dr. Matthias Gehring and Amer Hadzajlic for the time spent together and their friendship. I would like also to thank Philipp Waser and Dr. Patrick Mäder for all the fun we had playing kicker and at the ski-weekend and my sport mate Dr. Raffael Schrof. Dr. Adriana Edenharter and Patrick Eisenring for their advice and support, and my mate at the beer stand 29 in St. Gallen Openair Lukas Leu. Thanks to all the people I have met at ETH for all the very special moments we shared.

A very special thank goes to my two best friends Pietro Eleuteri and Michele Iannone. We have been friends for a long

time already, and I value our friendship and I feel lucky to have met you two. You have been shared many important moments of my life. Thanks for everything!

I cannot miss to say a big thank to all the people I have met during my university studies: Elisa De Paolis, Eliana Doldo, Federica Di Marcantonio, Virginia D'Ottavio, Sara Antonelli and Chiara Desideri. Thank you for your encouragement to strive towards my goals, and for making our journey special.

A special thank goes to my girlfriend Janne for her constant support, no matter late nights and early mornings, and for keeping me sane over the past few months. Thank you for being my muse, editor and proofreader. But most of all, thank you for being my best friend. I owe you so much.

I wish to thank my parents for supporting me in realizing my aspirations and dreams. All the support you have provided me over the years was the greatest gift anyone has ever given me. Words cannot express how grateful I am to you for all the sacrifices you have made in behalf of me and for your generous support.

The last thought goes to my beloved little sister Silvia. Even though you are not with us anymore, I will always remember the look on your face when you smiled at me. I am sure you will be with me in every single day of my life. I miss you terribly.

Curriculum Vitae

Date of Birth: February 13th 1990

SIMONE BERARDOZZI

Place of Birth: Tarquinia VT, Italy

Hometown: Tolfa RM, Italy

Nationality: Italian

Scientific Experience

PhD Thesis with Prof. Dr. Bruno Botta, Sapienza Università di Roma, Italy **11/2014 - 10/2017**

- Total synthesis, biological evaluation, and SAR studies of Glabrescione B
- Supervision of Master students

Visiting PhD Student in Prof. Dr. Karl-Heinz Altmann, ETH-Zürich, Switzerland **08/2016 - 07/2017**

- (+)-Dactylolide, 19-*epi*-(+)-dactylolide and (+)-zampanolide: synthesis and biological evaluation
- Synthesis and biological evaluation of *seco*-C/D ring analogues of *Ergot* alkaloids

Education

Pharmacist Habilitation

12/2014

Master in Medicinal Chemistry at Sapienza Università di Roma, Italy 11/2009-07/2014

- Focus on organic chemistry
- Master thesis in the group of Prof. Dr. Bruno Botta: "Supramolecular control of S_EAr reactions on Resorc[4]arenes variously substituted".

Master in Clarinet at Conservatorio di Musica "S. Cecilia" in Roma, Italy 11/2009-09/2012

- Supervisor: Prof. Piero Iacobelli

Matura at Liceo Scientifico "G. Galilei" Civitavecchia, Italy
09/2004 - 06/2009

Teaching and Mentoring Experience

- Supervision of Master students (2 years).

- Teaching assistant for the Organic Chemistry course for Pharmacy at Sapienza Università di Roma (09/2017 - 12/2017).

List of Publications

B. Cevatemre, M. Erkisa, N. Aztopal, D. Karakas, P. Alper, C. Tsimplouli, E. Sereti, K. Dimas, E. I. Ikitimur Armutak, E. G. Gurevin, A. Uvez, M. Mori, S. Berardozzi, C. Ingallina, I. D'Acquarica, B. Botta, B. Ozpolat, E. Ulukaya*. A promising natural product, pristimerin, results in cytotoxicity against breast cancer stem cells *in vitro* and xenografts *in vivo* through apoptosis and an incomplete autophagy in breast cancer. *Pharmacol. Res.* **2017**, ASAP.

R. Pingwara, K. Witt-Jurkowska, K. Ulewicz, J. Mucha, K. Tonecka, Z. Pilch, B. Taciak, K. Zabielska-Koczywas, M. Mori, S. Berardozzi, B. Botta, T.P. Rygiel, M. Krol*. Interferon lambda 2 promotes mammary tumor metastasis via angiogenesis extension and stimulation of cancer cell migration. *J. Physiol. Pharmacol.* **2017**, August, 68 (4).

C. Ingallina, P.M. Costa, F. Ghirga, R. Klippstein, J.T. Wang, S. Berardozzi, N. Hodgins, P. Infante, S.M. Pollard, B. Botta*, K.T. Al-Jamal*. Polymeric glabrescione B nanocapsules for

passive targeting of Hedgehog-dependent tumor therapy *in vitro*. *Nanomedicine* **2017**, 12 (7), 711-728.

E. Evain-Bana, L. Schiavo, C. Bour, D-A Lanfranchi, S. Berardozzi, F. Ghirga, D. Bagrel, B. Botta, G. Hanquet, M. Mori*. Synthesis, biological evaluation and molecular modeling studies on novel quinonoid inhibitors of CDC25 phosphatases. *J. Enz. Inhib. & Med. Chem.* **2016**, 32 (1), 113-118.

B. Cevatemre, B. Botta, M. Mori , S. Berardozzi, C. Ingallina, E Ulukaya*. The plant-derived triterpenoid tingenin B is a potent anticancer agent due to its cytotoxic activity on cancer stem cells of breast cancer *in vitro*. *Chem. Biol. Interact.* **2016**, S0009-2797(16), 30423-30429.

V. Iovine, M. Mori*, A. Calcaterra, S. Berardozzi, B. Botta. One Hundred Faces of Cyclopamine. *Curr. Pharm. Des.* **2016**, 22 (12), 1658-1681.

F. Ghirga, D. Quaglio, P. Ghirga, S. Berardozzi, G. Zappia, B. Botta, M. Mori*, I. D'Acquarica*. The occurrence of enantioselectivity in nature: the case of (S)-Norcoclaurine. *Chirality* **2016**, 28 (3), 169-180.

C. Ingallina, I. D'Acquarica, G. Delle Monache, F. Ghirga, D. Quaglio, P. Ghirga, S. Berardozzi, V. Markovic, B. Botta*. The Pictet-Spengler reaction still on stage. *Curr. Pharm. Des.* **2016**, 22 (12), 1808-1850.

List of Oral Presentations

S. Berardozzi, K.-H. Altmann "Total synthesis and biological investigation of (+)-dactylolide and 19-*epi*-(+)-dactylolide". **X European Conference on Marine Natural Products**. *Kolymbari, Crete. September 3-7, 2017.*

S. Berardozzi, K.-H. Altmann "Total synthesis of (+)-dactylolide and 19-*epi*-(+)-dactylolide". **XLII International Summer School on Organic Synthesis**. "A. Corbella", Gargnano, Italy, *June 18-22, 2017.*

S. Berardozzi, F. Ghirga, C. Ingallina, D. Quaglio, P. Infante, L. Di Marcotullio, B. Botta, M. Mori "Gli1/DNA interaction is a druggable target for Hedgehog-dependent tumors". **COST Action CM1407 - Challenging organic syntheses inspired by**

nature: from natural products chemistry to drug discovery,
Krakow, Poland. *March 2-3, 2017.*

S. Berardozzi, P. Infante, R. Alfonsi, L. Di Marcotullio, B. Botta,
M. Mori, I. D'Acquarica "Anthranoids from *Vismia baccifera*
as Potential Inhibitors of the Hedgehog Pathway". **COST
Action CM1106 - "Chemical Approaches to Targeting Drug
Resistance in Cancer Stem Cells"**. Barcelona, Spain, *January
19-20, 2015.*

List of Poster Presentations

S. Corradi, F. Ghirga, M. Mori, C. Ingallina, S. Berardozzi, E.
De Paolis, L. di Marcotullio, R. Alfonsi, B. Botta, D. Quaglio
"Identification of novel natural products chemotypes of
Hedgehog-dependent tumors inhibitors". **COST Action
CM1407 - Training School In Lisbon**, Lisbon, Portugal,
September 18-22, 2017.

S. Berardozzi, C. Tortolini, F. Ghirga, C. Ingallina, L.
Mangiardi, D. Quaglio, B. Botta, F. Mazzei "Synthesis of a new
artificial linker resorc[4]arene-based system for
immunosensors development" **XII International Conference**

on Surfaces, Coatings and Nanostructured Materials

NANOSMAT. *Paris, France. September 11-14, 2017.*

S. Corradi, E. De Paolis, C. Ingallina, S. Berardozzi, F. Ghirga, D. Quaglio, M. Mori, L. Di Marcotullio, P. Infante, R. Alfonsi, B. Botta "Gli1/DNA interaction is a druggable target for Hedgehog-dependent tumors". **XLII International Summer School on Organic Synthesis.** "A. Corbella", Gargnano, Italy, *June 18-22, 2017.*

F. Ghirga, M. Mori, C. Ingallina, S. Berardozzi, E. De Paolis, L. di Marcotullio, R. Alfonsi, B. Botta, D. Quaglio "Inhibition of Hedgehog-dependent tumors and cancer stem cells by a newly identified naturally occurring chemotype". **COST Action CM1407 - Challenging organic syntheses inspired by nature: from natural products chemistry to drug discovery,** Krakow, Poland. *March 2-3, 2017.*

S. Berardozzi, F. Ghirga, D. Quaglio, C. Ingallina, M. Mori, I. D'Acquarica, I. Screpanti, R. Palermo, B. Botta: "Synthesis of chalcones as inhibitors of the Notch signaling pathway in the treatment of T-cell acute lymphoblastic leukemia". **VI European Workshop in Drug Synthesis,** Siena, Italy. *May 15-19, 2016.*

E. De Paolis, C. Ingallina, S. Berardozzi, F. Ghirga, D. Quaglio, M. Mori, L. Di Marcotullio, P. Infante, R. Alfonsi, B. Botta: "Gli1/DNA interaction is a druggable target for Hedgehog-dependent tumors". **VI European Workshop in Drug Synthesis**, Siena, Italy. *May 15-19, 2016.*

C. Ingallina, S. Berardozzi, F. Ghirga, M. Mori, P. Infante, R. Alfonsi, L. Di Marcotullio, B. Botta "Natural polyphenols and derivatives as inhibitors of the hedgehog signaling pathway". First meeting of **COST Action CM1407 - Challenging Organic Syntheses Inspired By Nature: From Natural Products Chemistry To Drug Discovery**, Rome, Italy. *October 5-6, 2015.*

A. Calcaterra, S. Berardozzi, V. Iovine, I. D'Acquarica, B. Botta, F. Aiello, F. Balzano, G. Uccello-Barretta "Synthesis and NMR investigation of N-peptidoresorc[4]arenes as α -chymotrypsin inhibitors". **ChirItaly**. Sapienza University, Rome, Italy. *September 8-10, 2015.*

D. Quaglio, B. Botta, S. Berardozzi, S. Menta, M. Pierini, I. D'Acquarica, F. Ghirga "Synthesis of a basket-resorc[4]arene *via* metathesis reaction and encapsulation studies of fullerenes C₆₀ and C₇₀". **ISOM XXI, International Symposium on Olefin Metathesis and Related Chemistry**, Graz, Austria. *July 12-16, 2015.*

Table of Contents

Abstract Part A.....	vii
Abstract Part B	ix
List of Abbreviations, Acronyms and Symbols.....	xiii
Natural Products as Anticancer Agents	1
1. Gli1/DNA Interaction: a Druggable Target for Hedgehog- Dependent Tumors.....	5
1.1. Cancer Stem Cells Theory	5
1.1.1. The Hypothesis.....	5
1.1.2. Therapeutic Strategies	7
1.2. The Hedgehog Signalling Pathway.....	10
1.2.1. The Pathway	10
1.2.2. Alteration of the Hedgehog Pathway and Cancer.....	11
1.3. Hedgehog Pathway and CSCs.....	15
1.3.1. Targeting the Hedgehog Pathway in Cancer	15
1.4. Identification of the Active Site of Gli1.....	21
1.5. <i>In Silico</i> Screening	23
1.6. Aims and Scope	25
2. Total Synthesis, Biological Evaluation, and SAR Studies of GlaB.....	27

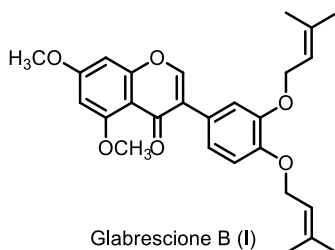
2.1. Chromones: A Privileged Structure in Medicinal Chemistry.....	27
2.2. Synthetic Strategies for Isoflavones	29
2.3. First Total Synthesis of GlaB	31
2.3.1. Retrosynthesis.....	31
2.3.2. Synthesis.....	32
2.4. NMR Analysis of the Interaction GlaB/Gli1.....	34
2.5. Biological Evaluation of GlaB	39
2.5.1. Influence of GlaB on Gli1/DNA Binding and Transcriptional Activity	39
2.5.2. Effect of GlaB on Gli-dependent MB Cells and Tumor SCs: <i>Ex vivo</i> Experiment.....	40
2.5.3. Effect of GlaB on Gli-dependent MB Cells <i>In Vivo</i>	42
2.5.4. GlaB Inhibits the Growth of Gli-dependent Basal Cell Carcinoma <i>In Vitro</i> and <i>In Vivo</i>	43
2.6. Second Total Synthesis of GlaB	45
2.6.1. First Generation of GlaB Derivatives.....	46
2.6.2. Second Generation of Derivatives.....	48
2.7. Conclusions and Outlook	50
3. Microtubules: a Successful Target in Cancer Therapy	53
3.1. Microtubules: a Successful Target against Cancers.....	53
3.2. Microtubule-Targeting Agents	57
3.2.1. Microtubule-Destabilizing Agents.....	57
3.2.2. Microtubule Stabilizing Agents.....	61

3.3. Limitations of the MTAs.....	64
3.4. Marine Macrolides (-)-Zampanolide and (+)-Dactylolide: new MSAs 65	
3.4.1. Isolation and Structure Elucidation	65
3.4.2. Biological Activity	69
3.5. Aims and Scope	74
4. (+)-Dactylolide, 19-<i>epi</i>-(+)-Dactylolide and (+)-Zampanolide: Synthesis and Biological Evaluation.....	77
4.1. Retrosynthesis	77
4.2. Synthesis of (+)-Dactylolide and 19- <i>epi</i> -(+)-Dactylolide	79
4.2.1. Synthesis of Acid 67	79
4.2.2. Synthesis of THP-vinyl Iodide 72.....	80
4.2.3. Completion of the Synthesis of (+)-Dactylolide (64).....	82
4.2.4. Completion of the Synthesis of 19- <i>epi</i> -(+)-Dactylolide (64).84	
4.3. Synthesis of (+)-Zampanolide	85
4.4. Biological Evaluation of Zampanolide Analogs.....	88
4.4.1. <i>In Vitro</i> Antiproliferative Activity	88
4.5. Conclusions and Outlook	89
5. Experimental Section.....	91
5.1. General Methods for Sapienza project.....	91
5.2. First Total Synthesis of GlaB (13).....	94
5.3. Second Total Synthesis of GlaB and GlaB Ring-B Derivatives	104

5.3.1. General procedure for the preparation of deoxybenzoines (30, 34-36).....	104
5.3.2. General procedure for the Vilsmeier-Haack reaction for the preparation of isoflavones (21, 37-39).....	109
5.3.3. General procedure for the alkylation/benzylation reaction (13, 40-49).....	114
5.4. General Methods for ETH project	124
5.5. Synthesis of (+)-dactylolide (62).....	127
5.6. Synthesis of 19- <i>epi</i> -(+)-dactylolide (64)	177
5.7. Stereoselective Aza-Aldol Addition.....	195
6. Bibliography	201

Abstract Part A

The dysregulation of the Hedgehog (Hh) signaling pathway plays a pivotal role in the generation and cell-maintenance of many human cancers. Gli transcription factors, the final effectors of the pathway, represent the most promising target for the development of new drugs targeting the Hh pathway in tumors. In a previous work, a natural isoflavone, glabrescione B (GlaB) (I), was identified as the first small molecule binding Gli1. It is able to inhibit the transcriptional activity of Gli1, by interfering with its interaction with DNA.



In order to perform further studies on the mechanism of action of GlaB (I) we developed a total synthesis, while NMR studies demonstrated the interaction of GlaB with Gli1

Biological studies have demonstrated its ability to interfere with the activity of Gli1 by inhibiting the growth of Gli-dependent-Hh-dependent tumor cells such as medulloblastoma (MB) and basal cell carcinoma (BCC) both *in vitro* and in allograft mouse models.

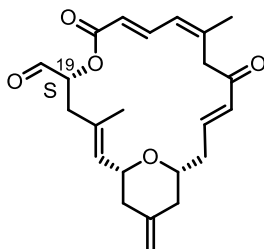
In addition, our new synthetic route, which encompasses just three steps with an overall yield of 15%, provided an efficient synthetic means to enable the investigation of the role of GlaB ring-B in the interaction Gli1-GlaB. In fact, our synthetic strategy allowed the preparation of several GlaB derivatives in order to elucidate the structure-activity relationships (SARs) and to clarify the molecular mechanism underlying its Hedgehog signalling modulation.

Abstract Part B

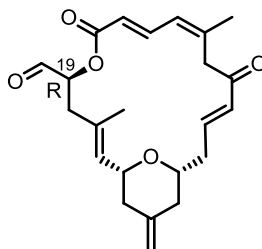
The second part of this PhD thesis describes the work I have carried out during my research stay abroad at Swiss Federal Institute of Technology (ETH) in Zürich (Switzerland) in Prof. Dr. Karl-Heinz Altmann's laboratory.

Marine natural products show higher incidence of bioactivity compared to terrestrial natural products. This is due to a high degree of chemical novelty and their high dilution in ocean water.

(+)-Dactylolide (**I**) was isolated by Riccio and co-workers from a sponge of the genus *Dactylospongia*, collected off the coast of Vanuatu islands, in the South Pacific Ocean. The absolute and the relative configuration at C19 of the compound remained unassigned.



(+)-Dactylolide (**I**)

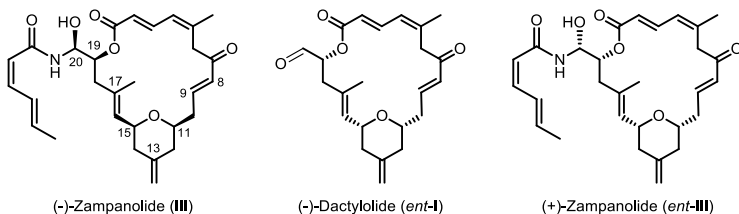


19-*epi*-(+)-dactylolide (**II**)

The assignment of the relative and absolute configuration of (+)-dactylolide (**I**) is based on its first total synthesis by Smith and co-workers. As had been described for the natural product, synthetic dactylolide has been found to be dextrorotatory, but the magnitude of

the specific rotation reported for the natural product and synthetic **I** were significantly different from each other. In addition, the discrepancies between the ^{13}C -NMR spectra of synthetic and natural (+)-dactylolide (if ever so slight), also leave open the possibility that the configuration of C19 in natural (+)-dactylolide is *R* and not *S* (i. e. natural dactylolide could have the structure **II** instead of **I**). In order to demonstrate that, a total synthesis of both compounds was established.

(+)-Dactylolide (**I**) is related to (-)-zampanolide (**III**), another marine macrolide. The latter shows low nanomolar cytotoxicity against both drug-sensitive and multi-drug resistant cancer cell lines, and induces microtubule bundle formation.



While (-)-zampanolide (**III**) is a nM inhibitor of cancer cell growth *in vitro*, not many data about the activity of (+)-dactylolide (**I**) have been published. On the other hand, the biological activity of synthetic (-)-dactylolide (*ent*-**I**) is well known. This compound exhibits sub- μM IC_{50} values against a multitude of cancer cell lines, although (-)-zampanolide (**III**) is still 100- to 300-fold more potent. At the same time, not even synthetic (+)-zampanolide (*ent*-**III**) has ever been tested and the importance of the configuration of the macrocycle for the potency of dextrorotatory compounds remains unclear. Our goal was

to synthesize (+)-dactylolide (**I**) and (+)-zampanolide (*ent*-**III**), in order to investigate how the macrocycle configuration would affect the biological activity of the compounds.

List of Abbreviations, Acronyms and Symbols

A

$[a]_D^T$	specific rotation at temperature T at the sodium D line
Å	Ångstrom
Ac	acetyl
Ac ₂ O	acetic anhydride
AcOH	acetic acid
ALL	acute lymphoblastic leukemia
AML	acute myeloid leukemia
ATO	arsenic trioxide

B

BALB	albino laboratory-bred strain of the house mouse
BCC	basal cell carcinoma
BINAL-H	2,2'-dihydroxy-1,1'-binaphthyl lithium aluminum hydride
BINOL	1,1'-binaphthyl-2,2'-diol
br	broadened (signal)
Bu	butyl
BuLi	butyl lithium
Bu ₃ SnH	tributyltin hydride

C

18-crown-6	1,4,7,10,13,16-hexaoxacyclooctadecane
ca.	about, approximately

°C	degree centigrade
cDNA	complementary DNA
CK1- α	casein kinase 1 α
Cpm	carboxypeptidase M
CPS	Ce ₂ (SO ₄) ₃ /phosphomolybdic acid/H ₂ SO ₄
CSC	cancer stem cell
CsOAc	cesium acetate
D	
δ	NMR chemical shift in ppm
ΔG	delta energy
d	doublet or days
Da	Dalton
DCC	N,N'-
dicyclohexylcarbodiimide	
DCM	dichloromethane
DDQ	2,3-dichloro-5,6-dicyano-1,4-benzoquinone
DEAD	diethyl azodicarboxylate
DET	diethyl tartrate
Dhh	desert hedgehog
DIBAL-H	diisobutylaluminum hydride
DMAP	4-dimethylamino pyridine
DME	dimethoxyethane
DMEM	Dulbecco's modified Eagle's
medium	
DMF	N,N-dimethylformamide
DMF-DMA	N,N-dimethylformamide dimethyl acetal
DMP	Dess-Martin periodinane
DMSO	dimethyl sulfoxide
DNA	deoxyribonucleic acid

<i>dr</i>	diastereomeric ratio
E	
EGL	external germinal layer
EI	electron ionization
EMSA	electrophoretic mobility shift assay
<i>ent</i>	enantiomeric
ESI	electrospray ionization
equiv.	equivalent
<i>epi</i>	epimeric
Et	ethyl
Et ₂ O	diethyl ether
EtOAc	ethyl acetate
EtOH	ethanol
F	
FBS	fetal bovine serum
FC	flash chromatography
FDA	Food and Drug Administration
FT-ICR	Fourier transform ion cyclotron resonance
G	
g	gram
GCP	granule cell progenitors
GDP	guanosine diphosphate
GI ₅₀	half maximal growth inhibitory concentration
GlaB	glabrescione B
Gli	glioma associated oncogene
GSK3-β	glycogen synthase kinase 3 β

GST	glutathione S-transferases
GTP	guanosine triphosphate
<i>H</i>	
h	hour
HCC	hepatocellular carcinoma
HEK	human embryonic kidney
Hex	hexane
Hh	hedgehog
HPI	hedgehog pathway inhibitor
HPLC	high-performance liquid chromatography
HPRT	hypoxanthine-guanine phosphoribosyltransferase
HR-FABMS	high resolution fast-atom bombardment mass spectrometry
HRMS	high resolution mass spectrometry
HWE	Horner-Wadsworth-Emmons
Hz	Hertz (s^{-1})
<i>I</i>	
<i>i</i>	<i>iso</i>
IC ₅₀	half maximal inhibitory concentration
IGF	insulin-like growth factor
Ihh	indian hedgehog
IL-6	interleukin-6
ImH	imidazole
<i>i</i> -PrOH	<i>iso</i> -propanol
IR	infrared

<i>J</i>	
<i>J</i>	coupling constant
<i>K</i>	
-	
<i>L</i>	
LAH	lithium aluminum hydride
LE	ligand efficiency
<i>M</i>	
μ	micro
m	multiplet
MB	medulloblastoma
MD	molecular dynamics
MDA	microtubule destabilizing agent
MDR	multidrug-resistant
Me	methyl
MEF	mouse embryonic fibroblasts
MeOH	methanol
MePh ₃ PBr	methyltriphenylphosphonium bromide
mg	milligram
MHz	Megahertz
min	minute
mL	milliliter
mM	millimole per liter
MM-GBSA	molecular mechanics energies combined with generalized Born and surface area continuum solvation
mmol	millimole

μL	microliter
Mp	melting point
mRNA	messenger RNA
MS	mass spectrometry
M.S.	molecular sieves
MSA	microtubule stabilizing agent
MTA	microtubule-targeting agent
MTT	3-(4,5-dimethylthiazol-2-yl)- 2,5-diphenyltetrazolium bromide
N	
<i>n</i>	normal
NaOAc	sodium acetate
NCI	National Cancer Institute
NEt ₃	triethyl amine
ng	nanogram
NIS	<i>N</i> -Iodosuccinimide
nM	nanomol per liter
NMR	nuclear magnetic resonance
NOD/SCID	non-obese diabetic/ severe combined immunodeficiency mouse
O	
-	
P	
PCR	polymerase chain reaction
PDA	photodiode array
Pd EnCat™ 40	encapsulated palladium catalyst 0.4 mmol/g Pd loading

PE	petroleum ether
P-gp	P-glycoprotein 1
Ph	phenyl
PhD	doctor of philosophy
P _i	inorganic phosphate
PKA	protein kinase A
PMB	4-methoxybenzyl
PMBOH	4-methoxybenzyl alcohol
ppm	parts per million
PPTS	pyridinium <i>para</i> -toluenesulfonate
Ptch1	protein patched homolog 1
py	pyridine
Q	
q	quartet
q-RT-PCR	real time quantitative PCR
R	
R	stathmin-like protein <i>or</i>
residue	
R ₁ ^{SE}	selective relaxation rate
R ₁ ^{NS}	non-selective relaxation rate
Red-Al [®]	sodium bis(2-methoxyethoxy)aluminumhydride
R _f	retention factor
RNA	ribonucleic acid
RP	reversed-phase
R _t	retention time
rt	room temperature

S

s	second or singlet
SAR	structure-activity relationship
SC	stem cell
SD	standard deviation
siRNA	small interfering RNA
Shh	sonic hedgehog
Smo	smoothened
SuFu	suppressor of fused homolog

T

t	triplet
<i>t</i>	<i>tert</i>
T	tubulin
TBAI	tetrabutylammonium iodide
TBDPS	<i>tert</i> -butyldiphenylsilyl
TBDPSCI	<i>tert</i> -butyldiphenylsilyl
chloride	
TBS	<i>tert</i> -butyldimethylsilyl
TBSCI	<i>tert</i> -butyldimethylsilyl
	chloride
TCBC	2,4,6-trichlorobenzoyl
	chloride
THF	tetrahydrofuran
THP	tetrahydropyran
TIPS	triisopropylsilyl
TLC	thin layer chromatography
TMS	trimethylsilyl
TMSI	trimethylsilyl iodide
TRIP	3,3'-bis(2,4,6-
	triisopropylphenyl)-1,1'-
	binaphthyl-2,2'-diyl
	hydrogenphosphonate

TTL tubulin tyrosine ligase
TUNEL terminal deoxynucleotidyl
transferase dUTP nick end
labeling

U

USA United States of America
UV ultraviolet

V

VEGF vascular endothelial growth
factor

W

WT wild type

X

-

Y

-

-

Z

ZF zinc finger

Natural Products as Anticancer Agents

Modern pharmaceutical research relies strongly on the search for and identification of novel lead compounds.

In the 1950s, the U.S. National Cancer Institute (NCI) started a screening of about 35,000 plant samples to evaluate their growth inhibitory effects against the mouse leukemia cell lines L1210 and P388. From this screening, paclitaxel (Taxol™), obtained from the bark of the Pacific yew *Taxus brevifolia*, emerged as the most important drug. By 1985 on, the NCI extended that screening against 60 human cancer cell lines, comprising cell lines derived from solid tumors, such as lung, colon, skin, kidney, ovary, brain, breast and prostate cancers, and other types of leukemia. Extracts from plants, animals, microorganisms, and compounds derived from microorganisms of marine origin were involved.^[1] Since these early initiatives, the NCI has continued to support the discovery of new naturally occurring anticancer agents. Hence, natural products have proven to be successful in the course of anticancer drug discovery.

But why are natural products so important? In the introductory chapter of “Anticancer Agents from Natural Products” the authors give a number of reasons.^[2] First, the non-mobility of plants and marine invertebrates required these organisms to produce bioactive secondary metabolites, in order to develop a complex chemical defense against predators and parasites.^[3] Secondly, for thousands of years natural products have provided the sole source for pharmaceuticals, and allowed for the development of many important drugs.^[4-9] To give a practical example for the importance of natural products in cancer treatment. By 2010 178 new drugs were approved for the treatment of cancers and 52% of them originated from natural products. In fact, 14% are non-modified natural products, 27% modified natural products, and 11% synthetic compounds derived from natural product optimization.^[10] The latter percentage is crucial as natural products can be used as templates for drug design. Even though a natural product is not an effective drug itself, it still serves as a good starting point for further developments.

The major problem encountered during natural product development towards new drugs is to find a scalable and inexpensive route to produce the desired material. Extraction processes are limited as they typically obtain very low quantities of natural product and this is particularly true for marine secondary metabolites. The problem can be overcome by large-scale fermentation,^[11] but some organisms, like sponges, are difficult to cultivate.^[12] On the other hand, the chemical synthesis of natural products and their analogs are a very effective tool to solve these limitations. In fact, several new synthetic methodologies

have been developed during the last decade, providing new routes for the synthesis of complex scaffolds. Furthermore, the total synthesis allows the preparation of natural product derivatives for the structure-activity-relationship (SAR) studies, which are very difficult to perform through semi-synthesis or genetic manipulation of the organisms.^[13] In the development of a new drug, SAR studies are fundamental because they can lead to the discovery of more potent and less complex analogs.

In summary, the use of natural sources in drug discovery is justified by their contributions to the development of approved drugs to date. While the unique position of marine organisms and plants in the ecosystem provides us with a biochemical rationale, the chemical motivation is based on the natural product as drug design templates.

1. Gli1/DNA Interaction: a Druggable Target for Hedgehog-Dependent Tumors

1.1. Cancer Stem Cells Theory

1.1.1. The Hypothesis

The concept of cancer arising from a population of stem-like cells was proposed about 150 years ago. Yet only in the last 40 years cancer research has demonstrated that tumor cells are very different. The official definition is:^[14]

a cell within a tumor that possess the capacity to self-renew and to cause the heterogeneous lineages of cancer cells that comprise the tumor.^[14]

Cancer stem cells (CSCs) can thus only be defined experimentally by their ability to regenerate a continuously growing tumor. Heterogeneous populations of cancer cells at various differentiation stages could be the result of both acquired mutations and aberrant but hierarchical differentiation programmes. As cancer is

Interaction: a Druggable Target for Hedgehog-Dependent Tumors

both a proliferation and a differentiation disease, the 'clonal evolution' and 'cancer stem cell' models might not be mutually exclusive, as initially thought. Owing to genetic instability, the tumor-initiating cells isolated from a clinically detectable tumor probably differ substantially from the genetic profile of the initial transformed cells that originated from the tumor.^[15]

Cancer cells also frequently display resistance to chemotherapy and they are related to cancer initiation, recurrence and metastasis due to their asymmetric divisions, ability to drug efflux, immortality, and mesenchymal phenotype. Therefore, the possibility of identifying and isolating these cells has provided a promising opportunity for novel therapeutic strategies. It should be noted that proliferation is not synonymous with self-renewal. A self-renewing cell division results in one or both daughter cells which have essentially the same ability to replicate and to generate differentiated cell lineages as the parental cell. Stem cells have the ability to undergo a symmetrical self-renewing cell division, causing identical daughter stem cells, which retain self-renewal capability. Alternatively, stem cells also display asymmetrical self-renewing cell division, resulting in one stem cell and one more differentiated progenitor cells. In addition, it seems that stem cells may

divide symmetrically to form two progenitor cells, which could lead to stem cell depletion.^[14]

1.1.2. Therapeutic Strategies

Nowadays, various therapeutic strategies are able to target tumor-initiating cells. Killing these cells can be achieved by inhibiting their survival pathways or sensitizing them to chemotherapeutic agents. Current failure with cancer treatment is usually not due to the lack of primary response or initial induction of remission, but due to relapse or tumor recurrence after therapy. In this case tumor-initiating cells seem to play a critical role. If therapies can be targeted against CSCs, this will render the tumors unable to maintain themselves or grow. Potential approaches to kill tumor-initiating cells include blocking essential selfrenewal signalling, inhibiting the survival mechanisms of these cells, or targeting tumor-initiating cell surface markers through antibody-based cytotoxic approaches.^[16] Alternatively, differentiating the CSCs can be a successful therapeutic strategy as the bulk of the tumor has limited proliferative potential.^[17]

Targeting CSCs alone is probably not sufficient to get effective cures or long-term remission for most cancers. A combined therapy, using conventional chemotherapeutic drugs with an agent able to target CSCs, may provide a good approach to eradicate both cancer cells and cancer stem cells. Moreover, agents targeting single hits are more susceptible to become resistant if the signalling network system

Interaction: a Druggable Target for Hedgehog-Dependent Tumors

is more complex. Multi-targeted anti CSCs therapy have a more reasonable potential to target CSCs (Figure 1).^[18]

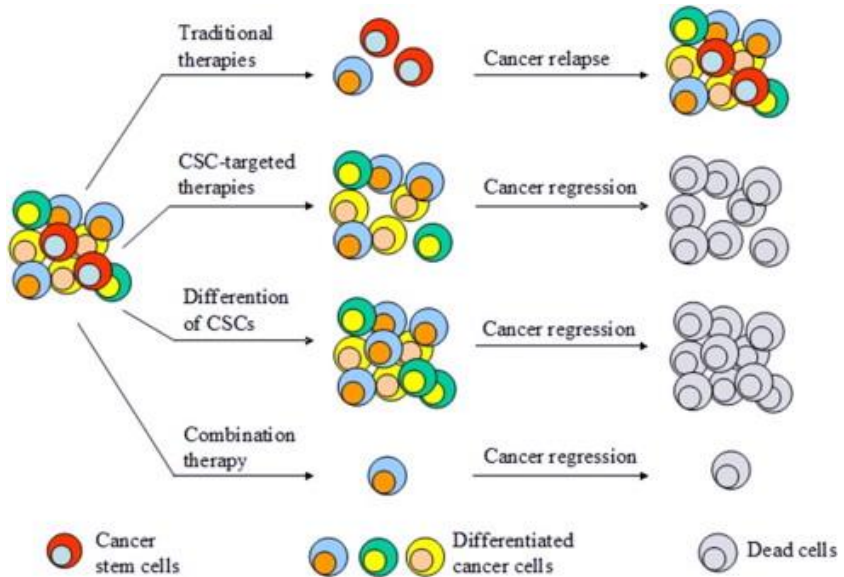


Figure 1: Conventional therapies vs CSCs targeted therapies (Reproduced with permission).^[19]

Several signalling pathways that regulate normal stem cells can cause neoplastic proliferation when dysregulated by mutation. In tumor initiating cells those pathways may be constitutively activated or improperly regulated, leading to uncontrolled growth. Developmental signalling pathway responsible for normal stem cell self-renewal, including Wnt, Hedgehog (Hh) and Notch, have been shown to be hyperactivated in various cancers (Figure 2). In our investigation, we focused our attention on the Hh signalling pathway.

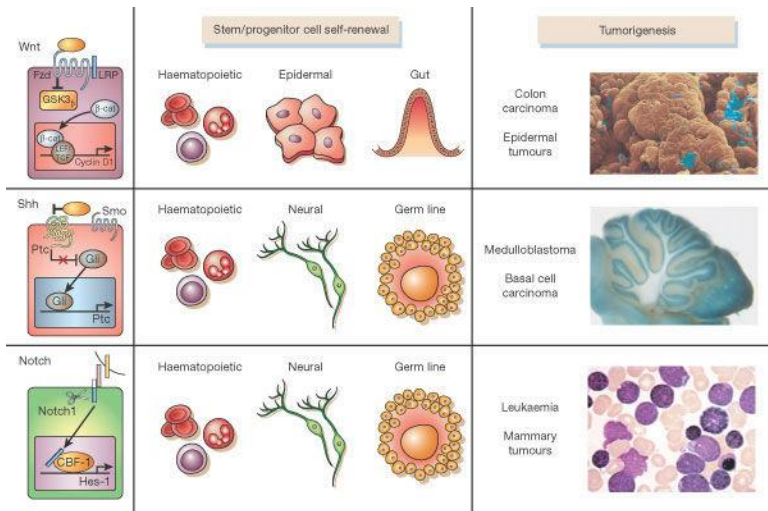


Figure 2: Wnt, Shh and Notch pathways: their contribution in the self-renewal of stem cells and/or progenitors, and in tumorigenesis (Reproduced with permission).^[20]

1.2. The Hedgehog Signalling Pathway

The Hh signalling pathway controls tissue polarity, patterning and stem cell maintenance. In 1980 Christiane Nusslein-Volhard and Eric F. Weischaus identified the Hh gene by genetic screens in *Drosophila melanogaster*. It earned its name from the appearance of embryos with null alleles of Hh, which display a larval of disorganized, hair-like bristles reminiscent of hedgehog spines. Duplication of the vertebrate genome resulted in the identification of the Hh genes, which can be classified into three groups: Desert (Dhh), Indian (Ihh) and Sonic (Shh).

1.2.1. The Pathway

The precise mechanism of Hh signalling is not fully understood. Hh pathway activation begins when the ligand Hh is released from the cells through a transmembrane transporter Dispatched and binds the transmembrane receptor Patched1 (Ptch1). In basal conditions, Ptch1 is linked to the receptor Smoothed (Smo) and prevents location to the primary cilium (Figure 3a). In the presence of Hh, Ptch1 loses its inhibitory activity against Smo, allowing Smo activation. Localization of Smo in the primary cilium initiates a signalling cascade, which leads to the activation of the glioma associated oncogene (Gli) family of zinc-finger transcription factors (Gli1, Gli2 and Gli3). Activated Glis, the final effectors of the pathway, translocate into the nucleus to induce the expression of various specific genes, such as those encoding the D-type cyclins, *c-MYC* (also called *MYC*), *BCL2* and *SNAIL* (also called *SNAIL1*), which regulate cellular differentiation, proliferation and survival.^[21,22] Furthermore, Hh target genes include *Gli1* itself, *PTCH1*

and the gene encoding for the Hh ligand.^[23] The signalling of Gli is also regulated by several protein mediators (PKA, GSK3- β , CK1- α), including suppressor of fused (SuFu). SuFu is a negative regulator of the Hh pathway because it is a sequester of Gli factors in the cytoplasm, thus repressing transcriptional activation (Figure 3b).^[24,25]

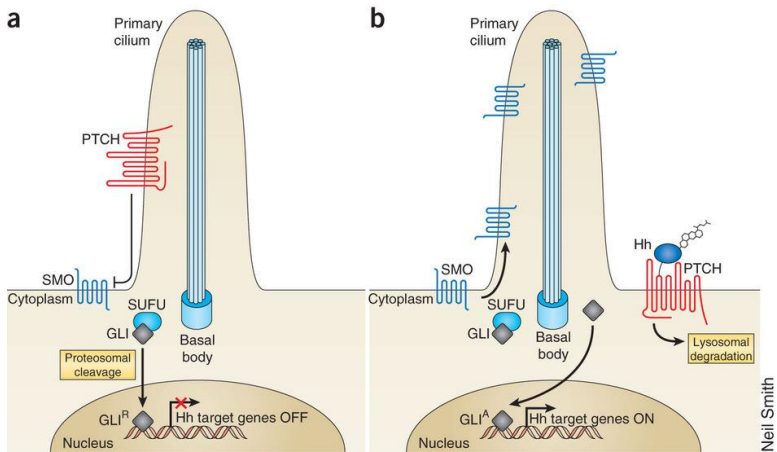


Figure 3: Hh pathway activation. (a) Inactive Hh pathway. (b) Activated Hh pathway (Reproduced with permission).^[26]

1.2.2. Alteration of the Hedgehog Pathway and Cancer

In recent years, a multitude of studies have shown a correlation between the aberrant activation of the Hh pathway and cancer. In adults, Hh pathway mutation or dysregulation plays a crucial role in both proliferation and differentiation, leading to tumorigenesis or tumor growth acceleration. Basal cell carcinoma (BCC) and

Interaction: a Druggable Target for Hedgehog-Dependent Tumors

medulloblastoma (MB) are two well-recognized cancers with mutations in components of the Hh pathway. Inappropriate activation of the Hh signaling pathway implies the development of several other types of cancer such as lung, prostate, breast, and pancreas cancer. Three basic models have been proposed for Hh pathway activity in cancer (Figure 4).^[21,27]

1.2.2.1. Type I: ligand-independent

First the type I cancers were discovered. These feature harbouring Hh pathway-activating mutations which are independent of the Hh ligand, such as BCCs and MBs (Figure 4a). Most of these tumors either display inactivating mutations in Ptch1 (85%) or activating mutations in Smo (10%).^[28] Furthermore, about one third of all medulloblastomas and occasional rhabdomyosarcomas were shown to have inappropriate Hh pathway activation, often due to Ptch1 mutations or sometimes due to SuFu mutations.^[29,30] Since these tumors are ligand independent, Hh pathway inhibitors must act at or below the Smo level to be effective.

1.2.2.2. Type II: ligand-dependent autocrine mechanism

Autocrine activation of the Hh pathway in tumor cells through increased Hh ligand expression has been reported in a variety of tumors, such as lung, breast, stomach and prostate cancers (Figure 4b).^[31] The relevance of this mechanism is not clearly understood. But most of these tumors are dissimilar to BCC or MBs as they do not harbor any somatic mutations in the Hh signaling pathway. Instead, they demonstrate an autocrine, ligand-dependent, abnormal Hh

pathway activation. Most of these tumors have an elevated expression of the Hh ligand (Shh or Ihh) and/or ectopic Ptch1 and Gli expression within the epithelial compartment. This autocrine tumor growth can be effectively suppressed by various pathway inhibitors such as Hh neutralizing antibodies or Smo antagonists.

1.2.2.3. Type III: ligand-dependent paracrine mechanism

In contrast to the autocrine model, Bushman and colleagues were the first to propose that at least one model of prostate cancer signals in a paracrine manner to the stroma.^[32] In paracrine signaling, Hh produced by the tumor cells is received by the stroma, which signals back to the tumor to promote its growth or survival (Figure 4c). The precise mechanisms by which the Hh-stimulated stroma positively regulates tumor cell growth are not completely understood. However, it has been proposed that Hh regulates signaling mediators in the stroma, including insulin-like growth factor (IGF), Wnt, interleukin-6 (IL-6) and vascular endothelial growth factor (VEGF), which in turn promote tumor growth. Inhibition of this paracrine signaling in epithelial tumors may be of therapeutic value as specific inhibition of Hh signaling in the stroma did result in growth inhibition of tumor xenografts. Although the most effective way of treating these tumors relies possibly on a combination of a Hh pathway inhibitor targeting the stroma and other drugs targeting the tumor cells.

Interaction: a Druggable Target for Hedgehog-Dependent Tumors

1.2.2.4. Type IIIb: reverse paracrine mechanism

Very recently, a “reverse paracrine” signalling model has also been introduced in which Hh is secreted from the stroma and is received by the tumor cells (Figure 4d). In this model, stromal Hh is thought to provide the appropriate microenvironment for potentiating tumor growth and would thus be a suitable therapeutic target as well.^[31]

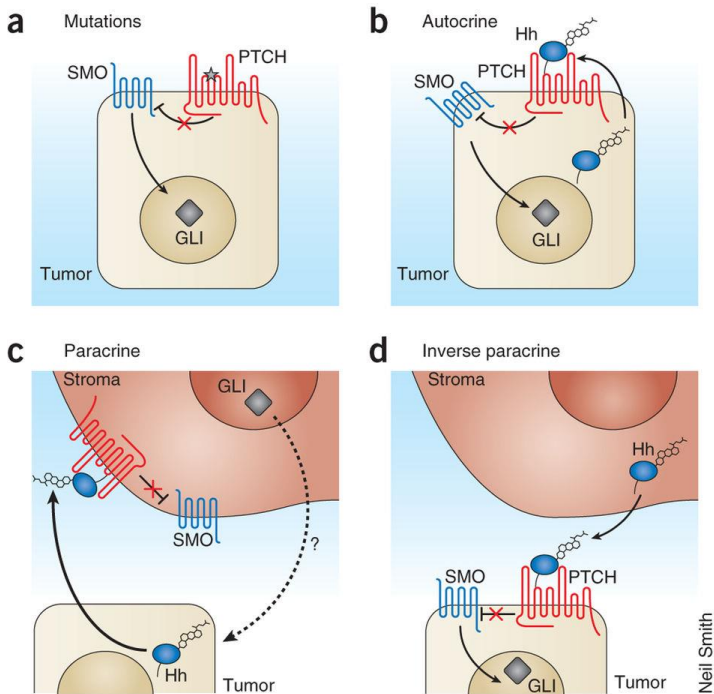


Figure 4: Different models of Hedgehog pathway activation in cancers. (a) Type I ligand-independent cancers. (b) Type II ligand-dependent autocrine cancers. (c) Type III ligand-dependent paracrine cancers. (d) Type IIIb reverse paracrine tumors (Reproduced with permission).^[26]

1.3. Hedgehog Pathway and CSCs

Remarkably, Hh signaling is active in CSCs of various tumor types. It is responsible to sustain the proliferation of these cells, which are responsible for tumor relapse and resistance to conventional anticancer therapies. Indeed, the Hh pathway controls the functional properties of CSCs, such as self-renewal, survival, metastatic spread, and neoangiogenesis by the regulation of stemness-determining genes such as *Nanog*, often overexpressed in cancer. Given the increasing evidences supporting the crucial role of the Hh pathway in cancer initiation, proliferation, metastasis, chemoresistance, and in the survival of CSCs, its components represent attractive druggable targets for anticancer therapy.^[33,34]

1.3.1. Targeting the Hedgehog Pathway in Cancer

Four major modes of Hh inhibition have been exploited therapeutically: 1) Smo inhibition; 2) receptor-ligand disruption; 3) inhibition of ligand processing; and 4) Gli inhibition (Figure 5).

Interaction: a Druggable Target for Hedgehog-Dependent Tumors

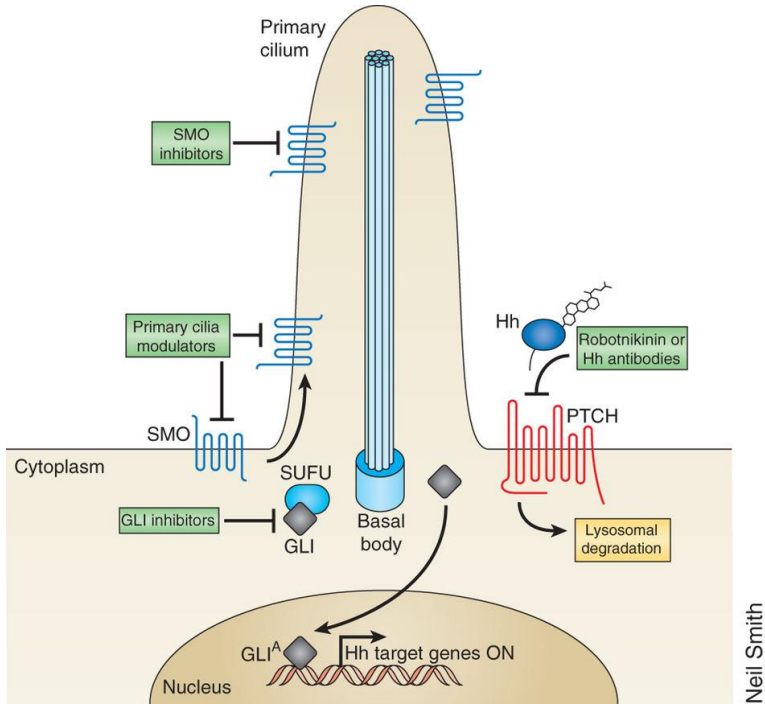


Figure 5: Potential sites for blocking the Hh pathway with therapeutic agents (Reproduced with permission).^[26]

In recent years, drug discovery efforts directed against the Hh pathway have focused predominantly on the development of Smo antagonists. As a consequence a remarkable number of small molecules of natural, semisynthetic or synthetic origin have been developed and reviewed extensively.^[35] Despite the initial enthusiasm, clinical development of Smo antagonists has ultimately proved disappointing, due to scarce pharmacokinetics, low selectivity on CSCs, severe side

effects, and the emergence of drug resistance.^[35] Advanced tumors can evolve resistance through pathway-dependent genetic mechanisms or through compensatory adaptation. Pathway-dependent genetic alterations discovered in resistant tumors from patients and animal models directly affect Hh pathway members. Vismodegib resistance is due to genetic alterations at the level of, or downstream from, Smo. Resistance can originate from Smo point mutations that ablate Smo–drug interaction while maintaining Hh pathway activation (Figure 6a).^[36] These mutations occur in the ligand-binding pocket of Smo. Other genetic alterations that lead to resistance come from gene duplications of *Gli2* or Hh target gene *cyclin D1* (Figure 6b) which bypass the requirement of Smo to inappropriately maintain or increase Gli target gene induction. These mutations promote high Hh pathway activation in the presence of Smo antagonists and mediate resistant tumor growth.

Compensatory alterations outside the Hh pathway have been found to mediate tumor resistance. In this case, Hh activation occurs in the absence of direct genetic mutation or copy number of variation of Hh members, and is epigenetic in nature. Developing Hh inhibitors that modulate targets acting downstream of Smo or independently from Smo, such as Gli, has recently emerged as a more promising therapeutic strategy for the treatment of Hh-dependent tumors. This approach could potentially overcome anti-Smo resistance and adverse effects, which are responsible for more than 50% dropout's rates in Smo antagonists clinical trials.

Interaction: a Druggable Target for Hedgehog-Dependent Tumors

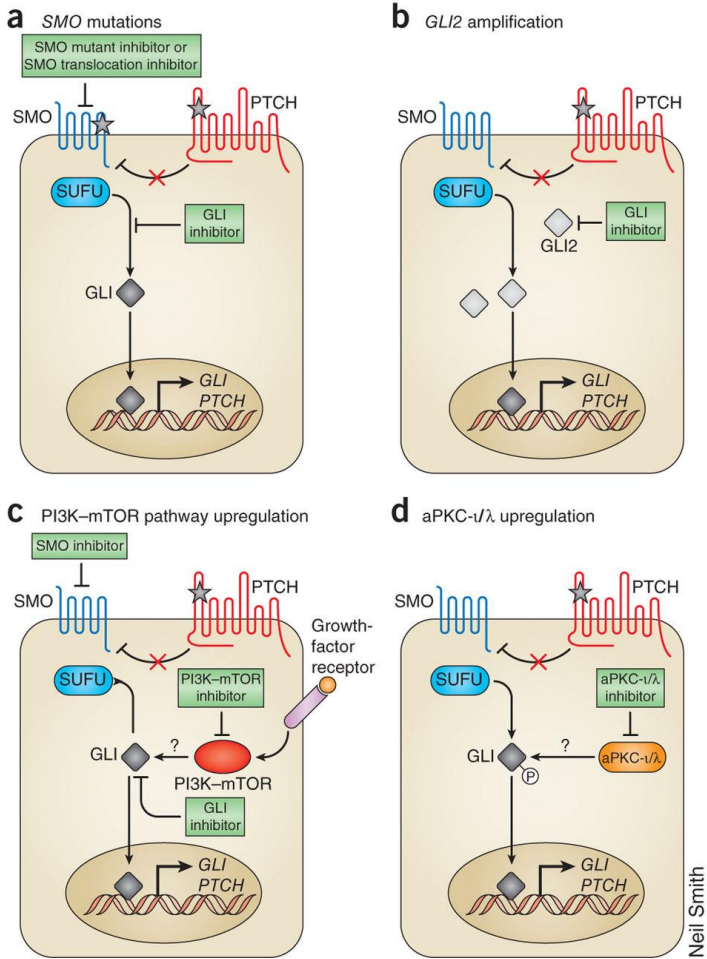


Figure 6: Genetic escape pathways evolving during Smo antagonist treatment and approaches to overcome resistance. (a) Smo point mutations. (b) Gli target gene amplification of *Gli2*. Compensatory escape pathways including (c) PI3K pathway upregulation or (d) inappropriate activation of aPKC-1/λ (Reproduced with permission).^[26]

1.3.1.1. Gli inhibitors

Gli transcription factors are the final effectors of the Hh pathway. Gli proteins have different functions *in vivo*: Gli1 acts as a transcriptional activator, whereas Gli2 and Gli3 can act both as activators and as repressors. It is important to consider that, whatever alteration leads to aberrant Hh pathway activation, all trigger the downstream effector Gli1. For this reason, in the last few years, Gli factors are emerging as the most attractive targets for the development of new anticancer drugs. However, not many Gli antagonists have been identified.

GANT58 (1) and GANT61 (2) are the first Gli antagonists that have been identified by Lauth *et al* in 2007 (Figure 7).^[37] GANT61 (2) has become the reference compound in many biological studies since it proved to inhibit the Hedgehog pathway in five different human colon carcinoma cell lines and in prostate cancer human xenografts. Recently, Chen and coworkers discovered a class of compounds named HPIs (Hedgehog Pathway Inhibitors) (3-6) by as Gli antagonist (Figure 7).^[38] The most promising compound, HPI-1 (3), was encapsulated in a polymeric nanoparticle. The formulation has undergone early preclinical testing showing a potent activity in HCC xenografts and inhibition of the proliferation and invasion of human HCC cell lines. Arsenic trioxide (ATO) (7), a drug approved by the FDA for the treatment of acute promyelocytic leukemia, was found to interfere directly with the Gli transcriptional factors, with efficacy both *in vitro* and *in vivo* (Figure 7).^[39] Many other studies pointed out the efficacy of ATO in targeting Gli proteins in different cancer types. In 2013 a clinical

Interaction: a Druggable Target for Hedgehog-Dependent Tumors

trial study started to check the efficacy of ATO in treating patients with BCC.

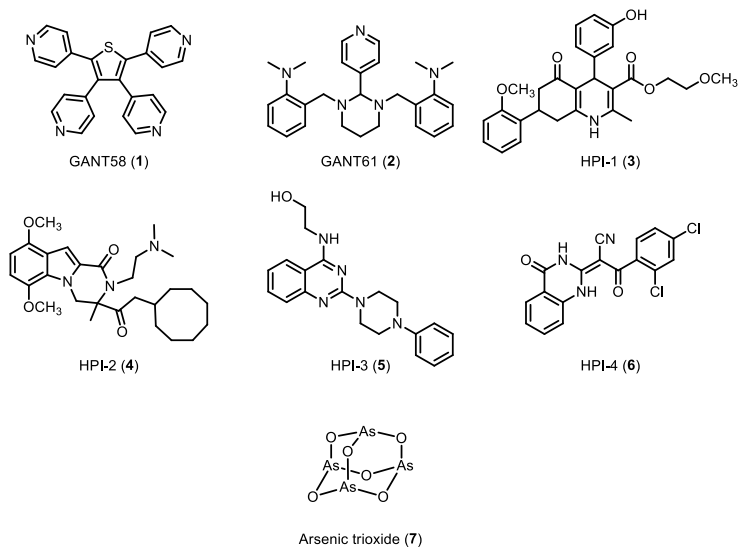


Figure 7: Gli direct antagonists.

In conclusion, Gli transcriptional factors represent the most promising target for the development of new drugs targeting the Hh pathway in tumors.

1.4. Identification of the Active Site of Gli1

A previous study identified the active site of Gli1.^[40] The starting point of the investigation was the X-ray structure of cobalt ion-coordinated Gli1ZF in complex with DNA.^[41] A representative Gli1ZF structure was extracted after molecular dynamics (MD) simulations (Figure 8A). Based on MD analysis and X-ray structure, a computational alanine scanning experiment was performed to evaluate which basic residues in ZF4 and ZF5 domains are relevant for the thermodynamic stability of the Gli1ZF/DNA adduct.^[40] The delta energy (ΔG) of binding to DNA of Gli1 mutants (Figure 8B) and wild-type Gli1ZF (Gli1ZF-WT) ($\Delta\Delta G$) were calculated. Basic residues in ZF4 (K340, K350, R354) and ZF5 (K360, K371, R380 and K381) domains exhibit the strongest $\Delta\Delta G$ contribution (Figure 8B), indicative of their role in the Gli1/DNA interaction.^[40]

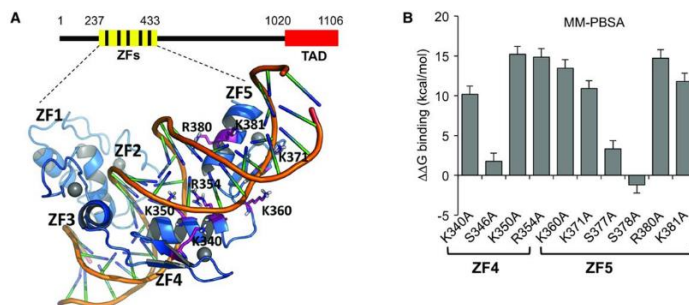


Figure 8: Structure-based analysis of Gli1/DNA complex. (A) Gli1ZF/DNA structure extrapolated from MD analysis. Gli1ZF (blue cartoon), residues involved in binding to DNA (magenta sticks), Zn ions (grey spheres) are shown. (B) Effect of Gli1ZF mutants on the binding affinity to DNA as predicted by *in silico* alanine scanning (Reproduced with permission).^[40]

Interaction: a Druggable Target for Hedgehog-Dependent Tumors

To correlate computational with experimental studies, a mutation experiment was performed on HEK293T cells. These cells have the peculiarity to transiently express ectopic Gli1 or different Gli1 mutants and a Gli-dependent luciferase reporter. The mutagenesis studies confirmed the role played by those residues in ZF4 and ZF5 domains in the transcriptional activity of Gli1 (Figure 9).^[40] The representative Gli1ZF structure extracted from MD trajectories served as a starting point for *in silico* ligand design.^[40]

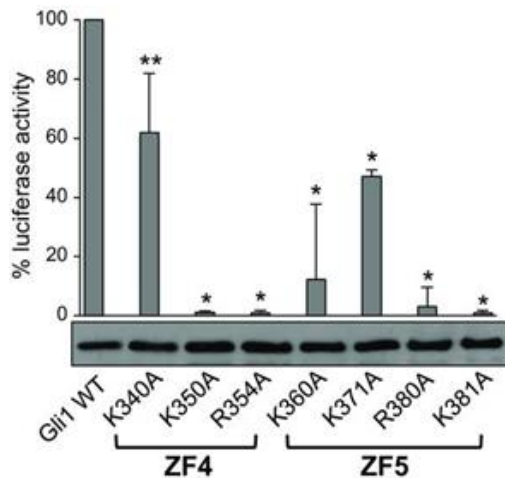


Figure 9: Luciferase assay on HEK293T cells. Effect of Gli1ZF mutants on Gli1-dependent transcriptional activity (Reproduced with permission).^[40]

1.5. *In Silico* Screening

In Prof. Bruno Botta's laboratory an *in house* library composed of more than 800 unique natural compounds belonging to different clusters is available. Literature data^[42] and results of the mutagenesis studies were used as starting point for a docking of the library.^[42] The docking analysis was set so that at least one of the basic residues, highlighted by the previous studies, would be able to interact with small molecules.^[40] The *in silico* study identified six molecules (three vismiones, GlaB, the chalcone V94 and the opioid alkaloid narceine) (Figure 10) as potential Gli1 inhibitors.^[40]

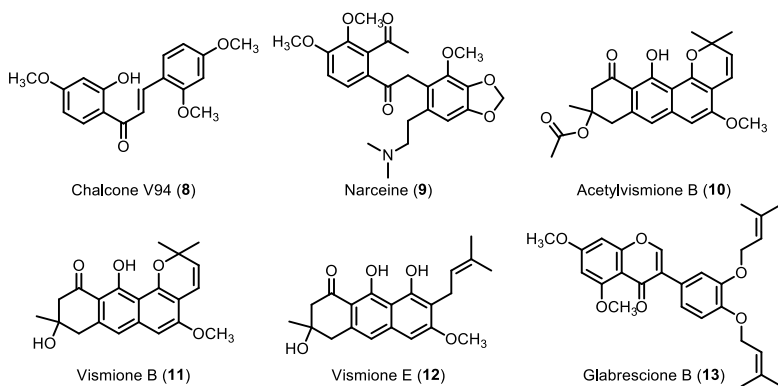


Figure 10: Structure of the six virtual hits.

The biological activity of the selected hits as specific modulators of Gli1 was evaluated by a Gli-dependent luciferase reporter assay, using HEK293T cells (Figure 11).^[40]

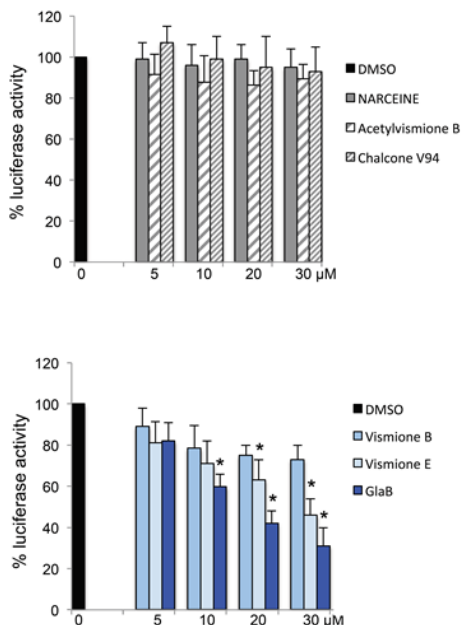
Interaction: a Druggable Target for Hedgehog-Dependent Tumors

Figure 11: Gli1-induced transcription in HEK293T cells, treated with increasing concentrations of different compounds or DMSO as control (Reproduced with permission).^[40]

The results of the biological tests showed that chalcone V94 (8), narceine (9) and acetylvismione B (10) were not active, yet vismione B (11) was partially active.^[40] In contrast, vismione E (12) and glabrescione B (GlaB) (13) strongly inhibited the luciferase activity (2) (Figure 11).^[40] Since vismiones display chemical instability under various conditions, further studies focused on GlaB (13).^[40]

1.6. Aims and Scope

Aberrant Hh pathway activation is responsible for the tumorigenesis of several human cancers, including medulloblastoma (MB), rhabdomyosarcoma, melanoma, basal cell carcinoma (BCC), and breast, lung, liver, stomach, prostate, and pancreas tumors,^[43–46] through the aberrant regulation of the functional properties of CSCs, such as self-renewal, survival, metastatic spread, and neoangiogenesis. Since much evidence supports the crucial role of the Hh pathway in cancer initiation, proliferation, metastasis, chemoresistance, and in the survival of CSCs,^[45,47] its components represent attractive druggable targets for anticancer therapy.

In this contest, targeting Gli transcription factors are extremely important to overcome the resistance to clinically available Smo antagonists. We previously identified GlaB (**13**) as the first Gli1 direct inhibitor. At the outset of this PhD thesis, no total synthesis of GlaB had been reported in literature, while the extremely limited supply of natural material had already been used for preliminary biological studies. In this context, it was a major goal of this PhD thesis to develop an efficient total synthesis of GlaB, in order to provide material for the assessment of its effects on human cancer cell growth. The chemistry developed in the course of this total synthesis was designed to also provide a basis for the synthesis of analogs to study theSAR and the underlying mechanism of action.

2. Total Synthesis, Biological Evaluation, and SAR Studies of GlaB¹

2.1. Chromones: A Privileged Structure in Medicinal Chemistry

Chromones are benzoannulated γ -pyrone (4H-chromen-4-one, 4H-1-benzopyran-4-one) heterocycles (Figure 12). Since ancient times they have been used in traditional medicine^[48] and are well-known for their broad range of pharmacological properties, such as anti-allergic, anti-inflammatory, antidiabetic, antimicrobial, and antitumor.^[49–51] Extensive research on chromones and their derivatives have proven the pharmacological importance of their heterocyclic moiety. Also in medicinal chemistry, chromones play an important role: their synthetic accessibility and structural diversity make them privileged structures for drug discovery.^[52]

¹ This work of my PhD research was carried out in the laboratories of Prof. Bruno Botta, Sapienza University of Rome (Italy).

The chromone ring system is the core fragment of several flavonoids, such as flavones and isoflavones (Figure 12).^[49] In particular, isoflavones are a class of natural compounds mainly occurring in plants of the *Leguminosae* family. The isoflavone nucleus consists of two phenyl rings linked by a propane bridge to form an oxygenated heterocyclic ring, resulting in the typical 15 carbon atoms (C6-C3-C6) skeleton with three rings, labelled A, B and C (Figure 12). Due to their interesting biological activity and benefits to human health, isoflavones have recently received attention.^[53,54] Furthermore, as underlined by genistein and its derivatives in differentiated pancreatic cancer cells and CSCs, isoflavones have displayed a noticeable pharmacophoric preference for Hh targets.^[35]

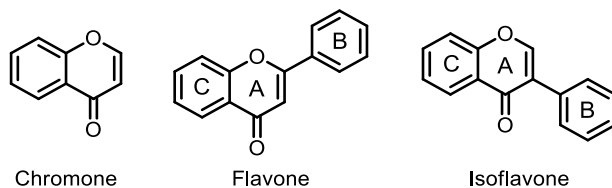
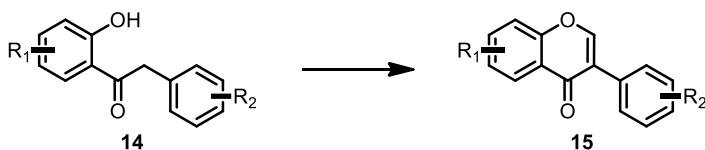


Figure 12: Chromones, flavones and isoflavones skeleton.

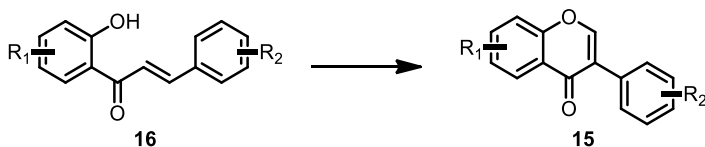
Most of the isoflavones have been isolated from natural sources, but extraction methods provide only very limited amounts of pure samples. However, their simple structure features can be addressed conveniently by synthetic methods.

2.2. Synthetic Strategies for Isoflavones

Several synthetic procedures have been developed for the preparation of isoflavones.^[55] Nevertheless, many of these new synthetic approaches have not been demonstrated in the synthesis of polyhydroxylated isoflavones and isoflavones bearing other naturally-occurring substitution patterns. The most popular procedures are mainly based on two strategies, namely (i) the deoxybenzoin route (Scheme 1)^[56] and (ii) the chalcone route (Scheme 2).^[57]

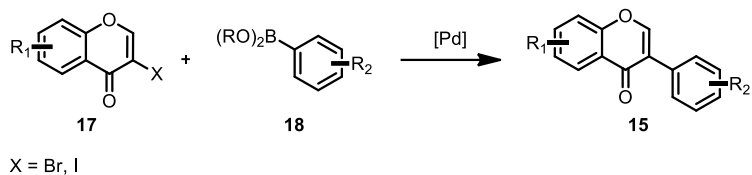


Scheme 1: Deoxybenzoin route.

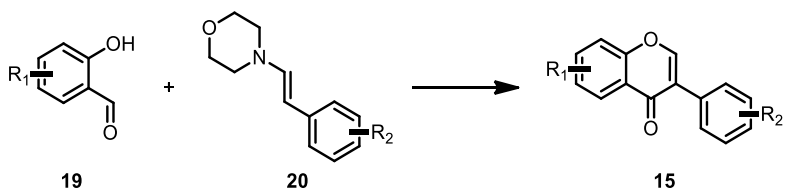


Scheme 2: Chalcone route.

Two other methods towards the synthesis of isoflavones include first the palladium catalyzed cross coupling reaction of a 3-alo chromone (17) with an arylboronic acid/ester (18) (Scheme 3)^[58,59], and second the condensation of enamine (20) with salicylaldehyde (19).^[60]



Scheme 3: Suzuki cross coupling route.



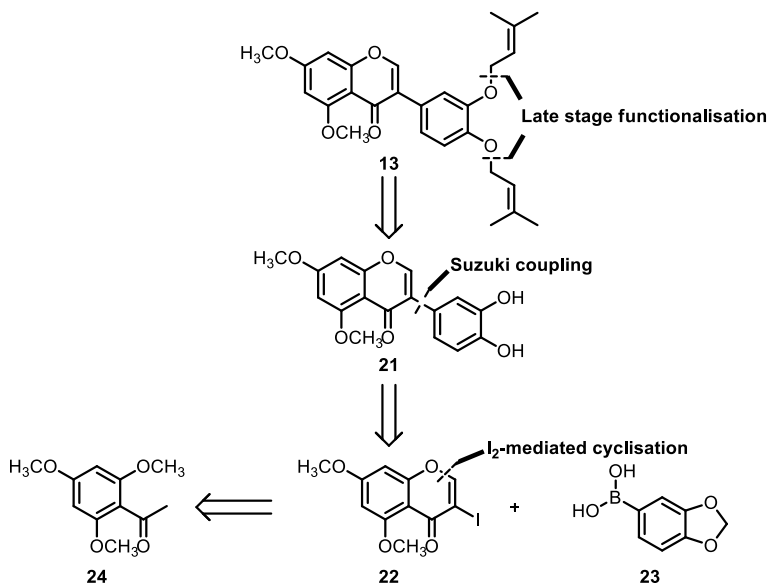
Scheme 4: Enamine-salicylaldehyde condensation.

Most of the available methods have major drawbacks, including the use of special and expensive reagents in large excess, long reaction times, vigorous conditions and very low yields. Hence, these approaches are overall unfeasible for the synthesis of GlaB, in particular for *in vitro* and *in vivo* studies requiring larger quantities. This prompted us to develop a mild and cost effective method, which also allows for scale up to gram quantities.

2.3. First Total Synthesis of GlaB

2.3.1. Retrosynthesis

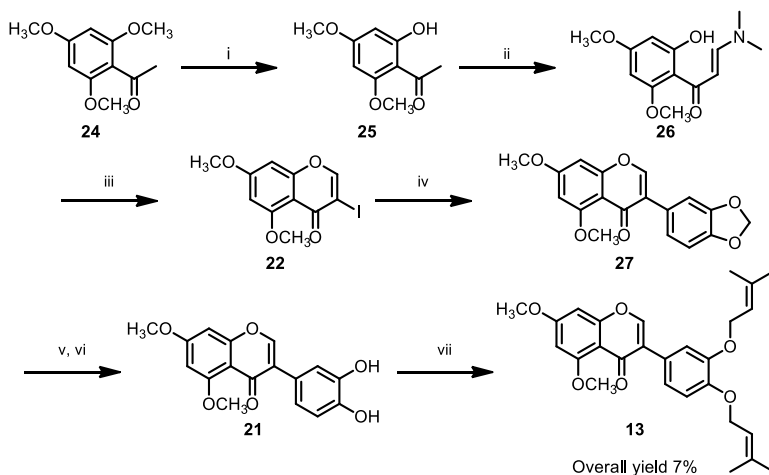
The strategy to be followed for the synthesis of GlaB (**13**) entails a late stage functionalization (Scheme 5). The isoflavone **21**, as the crucial precursor for the prenylation reaction, will be obtained by Suzuki coupling with protected boronic acid (**23**) and 3-iodochromone (**22**), respectively, followed by protecting group manipulation. **22** can be prepared from commercially available 2',4',6'-trimethoxyacetophenone (**24**) in a 3-step sequence (Scheme 5).



Scheme 5: Retrosynthesis of GlaB (**13**).

2.3.2. Synthesis

Our synthetic endeavours started from commercially available 2',4',6'-trimethoxyacetophenone (**24**) (Scheme 6).^[61] Treatment of **24** with BBr₃ led the selective ortho-*O*-demethylation to give 2'-hydroxy-4',6'-dimethoxyacetophenone (**25**). **25** was first treated with *N,N*-dimethylformamide dimethyl acetal (DMF-DMA), which gave the enamino ketone **26**. Stirring the latter with I₂ excess has resulted in tandem cyclization and iodination, to afford 3-iodo-chromone (**22**). Pd catalyzed Suzuki cross-coupling of **22** with 3,4-(methylenedioxy)-phenylboronic acid (**23**) using polyurea-encapsulated palladium (Pd EnCatTM 40)^[62] gave the isoflavone **27**. Methylendioxy group was then removed in acidic conditions after the formation of the acetoxy acetal by treatment with Pb(OAc)₄ allowing the formation of the desired catechol **21**. The prenylation reaction of the phenolic hydroxyl groups of **21** completed the synthesis of glabrescione B (**13**), with an overall yield of 7% (Scheme 6).^[61] In total, the linear sequence from **24** to **13** comprises 7 discrete steps.



Scheme 6: Forward synthesis of GlaB (**13**). i) BBr_3 , 98%; ii) DMF-DMA, quantitative crude; iii) **1**, 33%; iv) **23**, PdEnCatTM, Na_2CO_3 , 57%; v) $\text{Pb}(\text{OAc})_4$; vi) AcOH, 42% over two steps; vii) 3,3-dimethylallyl bromide, K_2CO_3 , 90%.

2.4. NMR Analysis of the Interaction GlaB/Gli1²

Virtual screening predicted GlaB (**13**) binding to Gli1 within ZF4 and ZF5 as well as interactions within K340 and K350 (Figure 13).

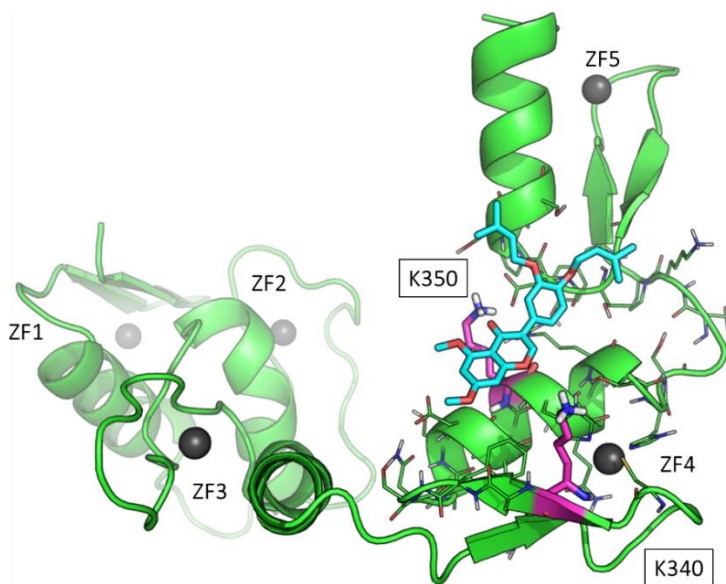


Figure 13: The predicted binding mode of GlaB (**13**) (blue sticks) to Gli1ZF (green cartoons). Residues K340 and K350 of the GlaB binding site are colored magenta.

NMR relaxation parameters, and in particular selective spin-lattice relaxation rates (R_1^{SE}), are highly sensitive indicators for binding

² These experiments were carried out in collaboration with Prof. Gloria Uccello-Barretta, University of Pisa, Italy. For detailed data about GlaB NMR conditions check the following article.^[40]

processes between macromolecules and small molecules.^[63,64] The method relies on the change in molecular motion of the small molecule, i.e. its correlation time τ_c , upon interacting with a macromolecule. In its free state the small molecule performs fast molecular motions ($\omega_0^2 \tau_c^2 \ll 1$, Figure 14) and enter the slow motional regime ($\omega_0^2 \tau_c^2 \gg 1$, Figure 14) only when bound to a macromolecule. R_1^{SE} increases strongly upon passing $\omega_0^2 \tau_c^2 = 1$ as the slow motional regime is reached (Figure 14). R_1^{SE} based NMR relaxation studies rely on the favorable dependence of R_1^{SE} on τ_c , while non-selective relaxation rates (R_1^{NS}) scale differently in this motional regime (Figure 14).

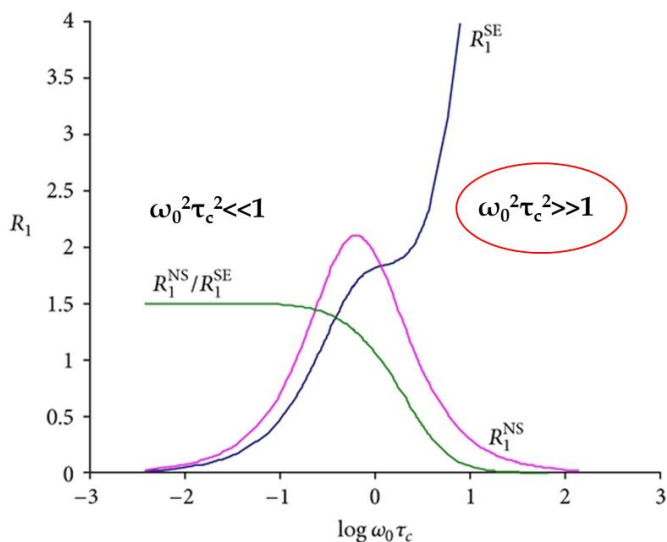


Figure 14: Dependence of the specific and non-specific spin-lattice relaxation rates R_1^{SE} and R_1^{NS} , respectively, on $\omega_0 \tau_c$.

To demonstrate the predicted binding of GlaB (**13**) to Gli1 by means of NMR, a relaxation study was performed. For this mono-selective relaxation rates were determined for a chosen subgroup of GlaB (**13**) protons (Figure 15) by selectively inverting the corresponding proton signals.

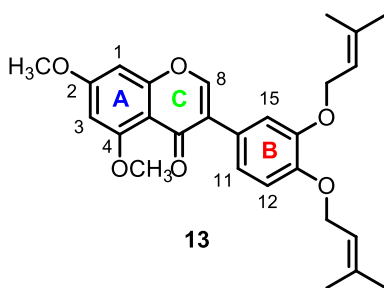


Figure 15: Chosen subgroup of GlaB (**13**) protons for NMR based study of GlaB/Gli1 interaction, namely H-1 and H-3 and proton groups at 2-OCH₃ and 4-OCH₃ of methoxy groups of ring A, H-11, H-12 and H-15 of ring B, and H-8 of ring C.

Mono-selective relaxation rates were obtained both for free GlaB (**13**) (R_f) and GlaB/Gli1 mixtures (R^{ms}). The former allows normalization of R^{ms} , yielding $\Delta R/ R_f$ with $\Delta R = R^{ms} - R_f$ (Table 1). In addition to the GlaB/Gli mixtures, a GlaB/GST sample was included into the relaxation study and ensured that no specific contribution arises from a GlaB/GST interaction (Table 1).

Table 1: $^1\text{H-NMR}$ mono-selective relaxation rate (R_i , s^{-1}) of 0.412 mM free GlaB (**13**) in $\text{DMSO-}d_6$ measured at 25°C and 600 MHz for specified protons. Associated normalized relaxation rates ($\Delta R/R_i$ with $\Delta R=R^{\text{ms}}-R_i$) are listed for four different GlaB/protein mixtures (Reproduced with permission).^[40]

Proton ^a	Ring	GlaB (13) ^a	GlaB/GST-Gli1ZF	GlaB/GST-Gli1ZFK340A	GlaB/GST-Gli1ZFK340A/K350A	GlaB/GST
		R_i (s^{-1})	$\Delta R/R_i$	$\Delta R/R_i$	$\Delta R/R_i$	$\Delta R/R_i$
H-1	A	0.41	0	0	0.03	0.02
2-OCH ₃	A	1.20	0	0	0.05	0.06
H-3	A	0.63	0	0	0.05	0.06
4-OCH ₃	A	1.39	0	0	n. d. ^b	0
H-8	C	0.36	0.13	0.05	0.07	0
H-11	B	0.63	1.20	0.15	0.38	0.22
H-12	B	0.89	0.95	0.23	n. d. ^c	0.03
H-15	B	0.76	0.22	0.22	0.14	0.14

^a According to the proton number scheme of GlaB (Figure 15).

^b R^{ms} could not be determined due to overlapping water signal.

^c R^{ms} could not be determined due to the large linewidth.

In order to demonstrate the predicted interaction of GlaB (**13**) to Gli1 within K340 and K350 (Figure 13), a mutagenesis NMR study was carried out. To this end, R^{ms} values of GlaB in combination with the single mutant GST-Gli1ZF-K340A and the double mutant GST-Gli1ZF-K340A/K350A were determined. An overall smaller increase of the R^{ms} values upon addition of GST-Gli1ZF-K340A was observed, though preserving the stronger affinity towards ring B over ring A and C (Table 1; Figure 16). In case of the double mutant, change in R^{ms} values for the

protein mixture is comparable to the GST sample (Table 1; Figure 16). These results suggest a comparable binding conformation of GlaB (**13**) upon interacting with GST-Gli1ZF-WT and the single mutant. Instead, double mutation to GST-Gli1ZF-K340A/K350A prohibits the specific binding via the GlaB ring B.

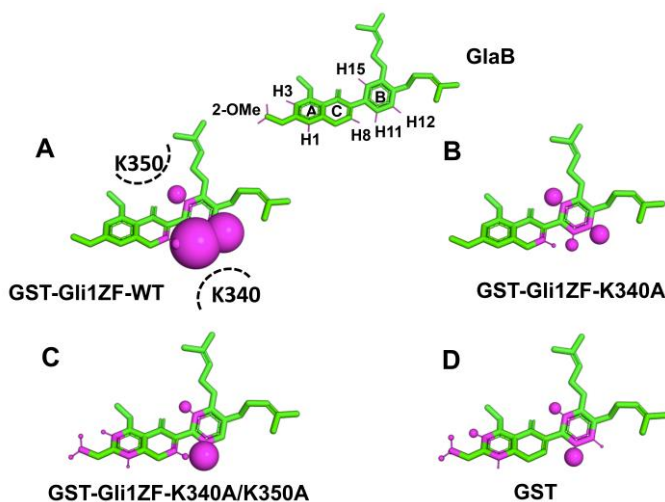


Figure 16: GlaB (**13**) is shown as green sticks, protons highlighted by the NMR study as magenta spheres and the radius is proportional to the normalized R^{ms} value (Reproduced with permission).^[40]

In summary, results of NMR studies show that GlaB (**13**) interacts directly with Gli1 and further emphasize the role of K340 and K350. The ring B turns out to be the key determinants for GlaB (**13**) activity.

2.5. Biological Evaluation of GlaB³

2.5.1. Influence of GlaB on Gli1/DNA Binding and Transcriptional Activity

Biological tests validated the potency of GlaB (**13**) against Gli1. First, it was shown that GlaB reduces the luciferase activity arising from Gli-responsive element reporter in *Smo*^{-/-} mouse embryonic fibroblasts (MEFs) (Figure 17).^[40] Second, **13** affects the transcriptional activity specifically of a number of endogenous Gli target genes, while non-related genes were not influenced (Figure 18).^[40]

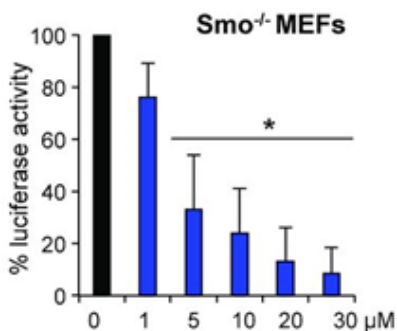


Figure 17: Inhibition of Gli1-induced transcription in transfected *Smo*^{-/-} MEF cells (Reproduced with permission).^[40]

³ These experiments were carried out in collaboration with Prof. Lucia Di Marcotullio, Sapienza University of Rome, Italy. For detailed data about GlaB activity check the following article.^[40]

Specifically, related experiments proofed that **13** suppresses Hh-gene expression in *Ptch1*^{-/-} MEFs (Figure 18).^[40] In the latter cells, the *Ptch1* receptor on *Smo* (Figure 18) is deleted along with its prohibiting effect, increasingly activating *Gli* transcription factors (Figure 18).^[65] In addition, the downstream activity of GlaB was demonstrated on *SuFu*^{-/-} MEFs cells, which also feature high *Gli1* reporter activity due to loss of *SuFu* inhibition (Figure 18).^[66] As for *Ptch1*^{-/-} MEFs cells, **13** also decreases the Hh target gene expression in *SuFu*^{-/-} MEFs cells (Figure 18).^[40]

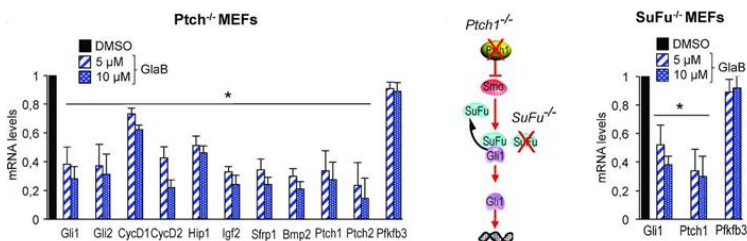


Figure 18: Hh target genes expression levels in *Ptch1*^{-/-} MEFs treated for 48h with GlaB (**13**) or DMSO only (left). Representative model of Hh signaling hyperactivation: in *Ptch1*^{-/-} MEFs and in *SuFu*^{-/-} MEFs cells (center). *SuFu*^{-/-} MEFs were treated for 48h with GlaB (**13**) or DMSO as control (right) (Reproduced with permission).^[40]

2.5.2. Effect of GlaB on Gli-dependent MB Cells and Tumor SCs: *Ex vivo* Experiment

The potency of GlaB to prevent tumor growth was tested on primary MB cells, isolated from *Ptch1*^{+/-} mice tumors. These MB cells were treated with either GlaB (**13**), GANT61 (**2**) or DMSO and resulted in comparable inhibition of MB cell growth in case of GANT61 (**2**) and

GlaB (**13**) (Figure 19).^[40] Besides, GlaB (**13**) treated MB cells showed a strong reduction in *Gli1* mRNA levels in those cells (Figure 19).^[40]

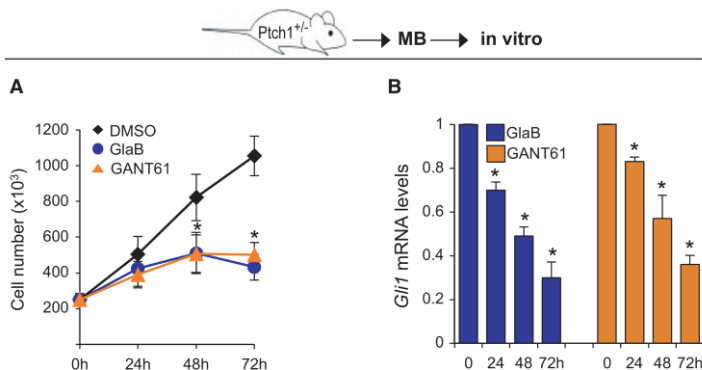


Figure 19: Inhibition of Gli-dependent MB tumor cell growth. (A) *Ex vivo* cultures from *Ptch1*^{+/-} mice MBs were treated with GlaB (**13**) (5 μ M), GANT61 (**2**) (10 μ M) or DMSO only. (B) *Gli1* mRNA expression levels (Reproduced with permission).^[40]

Hh-dependent tumors, generally and including MB, feature a variety of stem cells (SCs) which cause the self-renewal of cancer cells, tumorigenesis and resistance towards conventional chemotherapies as well as tumor relapse.^[67] In this context, the Hh pathway plays a central role both in humans and mice as it regulates the generation and maintenance of these SCs.^[68] Due to these features, MB-SCs were chosen as a target for evaluating the efficiency and selectivity of GlaB (**13**) against the described pathway. This test showed that **13** firstly inhibits the neurosphere formation by *Ptch1*^{+/-} MB-SC (Figure 20),^[40] which is otherwise part of their clonogenic self-renewal activity. Secondly, **13** was able to decrease the mRNA levels of the Hh pathway,

stemness markers, growth and oncogenic related signals (Figure 20).^[40] All in all, this experiment is the final proof that GlaB (**13**) acts as an efficient Hh pathway inhibitor.^[40]

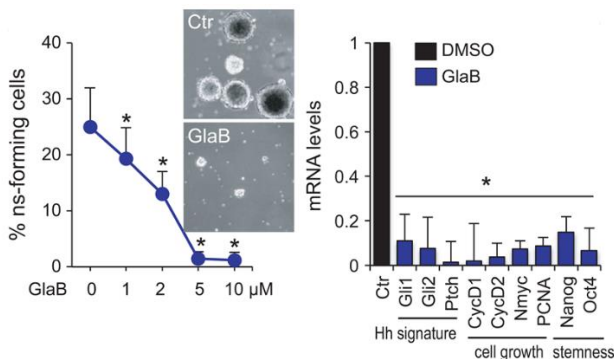


Figure 20: Inhibition of MB-SCs cell growth. MB-SCs were isolated from *Ptch1^{+/-}* mice and allowed to form neurospheres. The neurospheres were treated with increasing concentrations of GlaB (**13**) or DMSO as control (left). mRNA levels of Hh, proliferation and stemness in MB-SCs after treatment with GlaB (**13**) (5 μM) or DMSO only for 48 h (right) (Reproduced with permission).^[40]

2.5.3. Effect of GlaB on Gli-dependent MB Cells *In Vivo*

An allograft model of MB cells was set in order to study the GlaB (**13**) effect *in vivo*.^[40] Nude mice were grafted with spontaneous primary MB from *Ptch1^{+/-}* mice and treated every two days with sub cutaneous (s. c.) injections of **13** at a concentration of 75 μmol/kg or solvent as control (n = 6 for each group).^[40] After 18-days, GlaB (**13**) was able to suppress tumor growth (Figure 21).^[40]

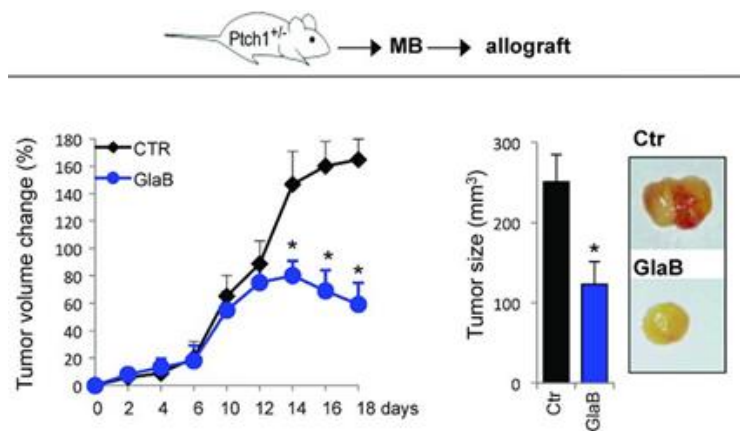


Figure 21: $Ptch1^{+/-}$ MB allograft experiments. Change of tumor volume during GlaB (13) or vehicle treatment period (18 days) (Reproduced with permission).^[40]

2.5.4. GlaB Inhibits the Growth of Gli-dependent Basal Cell Carcinoma *In Vitro* and *In Vivo*

Another Gli-dependent Hh tumor is basal cell carcinoma (BCC). *In vitro* tests of GlaB on ASZ001 BCC cells showed that GlaB (13) is able to inhibit tumor cell growth and to reduce Gli1 mRNA levels.

Furthermore, 13 (100 $\mu\text{mol/kg}$) induced tumor growth inhibition in BCC allografts (*in vivo* experiments) after 18 days of s. c. injection compared to the control (Figure 22).^[40]

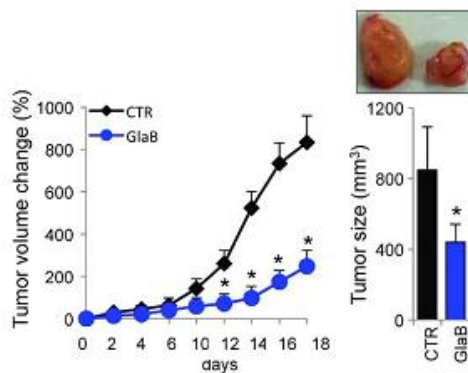
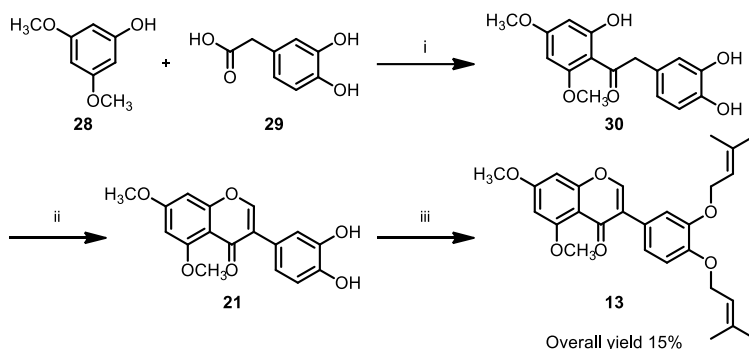


Figure 22: Inhibition of Gli-dependent BCC tumor cell growth. Change of tumor volume during GlaB (13) or vehicle treatment period (18 days) (Reproduced with permission).^[40]

2.6. Second Total Synthesis of GlaB

With the aim of investigating the role of the isoprenyl chains on GlaB-ring B and improving the quantities of **13** obtained, reducing in the meantime the reaction steps, we investigated a different approach: the deoxybenzoin route.

3,5-dimethoxyphenol (**28**) (Scheme 7) was treated with 3,4-dihydroxyphenylacetic acid (**29**) in presence of $\text{BF}_3 \cdot \text{OEt}_2$ as Lewis acid, providing the corresponding deoxybenzoin (**30**). (Chloromethylene)dimethyliminium chloride, generated *in situ* from DMF and PCl_5 , accomplished the addition of one carbon atom and cyclization of the deoxybenzoin, affording the formation of the isoflavone (**21**). The late stage functionalization of the isoflavone ring B was performed using 3,3-dimethylallyl bromide and K_2CO_3 in refluxing acetone to yield GlaB (**13**), with overall yield of around 15% (Scheme 7).



Scheme 7: Second total synthesis of GlaB (**13**). i) $\text{BF}_3 \cdot \text{OEt}_2$, 55%; ii) $\text{BF}_3 \cdot \text{OEt}_2$, (chloromethylene)dimethyliminium chloride, 30%; iii) 3,3-dimethylallyl bromide, K_2CO_3 , 90%.

This synthetic strategy allowed us to obtain higher amounts of GlaB (**13**) (up to 5 grams) in much shorter time.

2.6.1. First Generation of GlaB Derivatives

As discussed above, this synthetic strategy not only improved the efficiency of the synthesis of **13**, but also provided us with a tool to investigate the interactions involving the GlaB-ring B.

NMR analysis of *O*-prenyl groups was not very informative, because of the broad proton signals. As suggested by molecular docking studies, prenyls might be crucial for the correct positioning of the GlaB-ring B. In fact, as we can see in Figure 23, GlaB, vismione B and vismione E preferably bind within the same site at the interface between ZF4 and ZF5. The *O*-prenyl groups seems to be essential for the correct positioning of GlaB-ring B. In particular, the prenyl group at C13 of GlaB is clearly overlapped over the corresponding feature of Vismione E, suggesting that this prenyl chain is not only important for the correct positioning, but is moreover relevant for Gli1 inhibition.

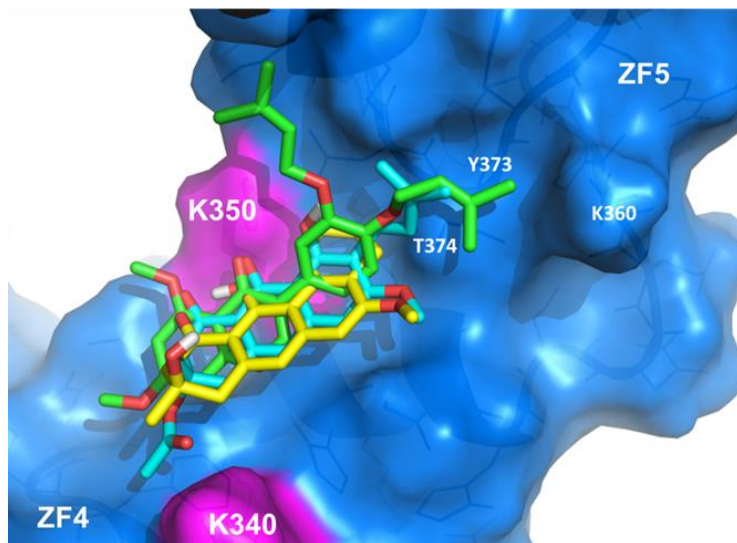
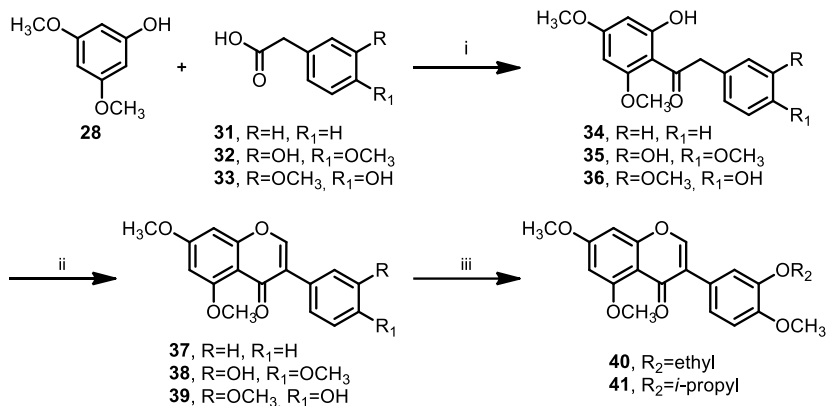


Figure 23: Overimposition between GlaB (green sticks), vismione B (yellow sticks) and vismione E (cyan sticks) on Gli1ZF (blue) (Reproduced with permission).^[40]

GlaB derivatives without prenyl chains were synthesized following the same procedure developed for GlaB (**13**), using a non-symmetrical substituted phenylacetic acid. In a general experiment, 3,5-dimethoxyphenol (**28**) (Scheme 8) was treated with the corresponding 3,4-disubstituted phenylacetic acid (**31-33**) in presence of $\text{BF}_3 \cdot \text{OEt}_2$, providing the corresponding deoxybenzoin (**34-36**). Vielsmyer reaction then allowed for the formation of the isoflavones (**37-39**). **38** was then functionalized using either ethyl- or isopropyl bromide affording **40** or **41** (Scheme 8).

The compounds were tested through the Gli-dependent luciferase reporter assay, but none of them was active, reinforcing that ring-B prenyl chains may be important for GlaB biological activity.



Scheme 8: Synthesis of GlaB-ring B derivatives lacking prenyl-chains. i) BF₃·OEt₂, 55%; ii) BF₃·OEt₂, (chloromethylene)dimethyliminium chloride, 30%; iii) 38, ethyl bromide or isopropyl bromide, K₂CO₃, 90-92%.

2.6.2. Second Generation of Derivatives

The biological data showed the importance of substitution on ring-B of the isoflavone system. In order to investigate which position on ring-B is important for the interaction with Gli1, we planned to synthesize non-symmetrical isoflavones bearing substituents with similar electronic properties of prenyl groups.

This synthetic strategy allowed for the preparation of a new generation of derivatives 3- (**42-45**) or 4-substituted (**46-49**), starting from isoflavones **38** or **39** respectively (Figure 24).

The biological evaluation of the latter compounds is still ongoing.

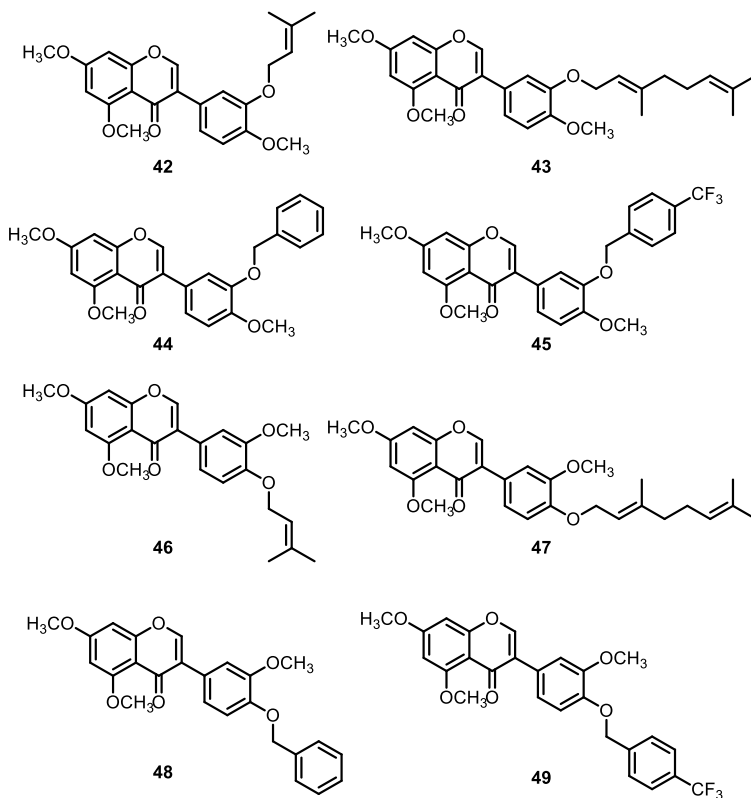


Figure 24: GlaB derivatives. Chemical structure of GlaB analogues bearing modification to the substituents on ring B.

2.7. Conclusions and Outlook

In conclusion, two different total syntheses of GlaB (**13**) have been successfully developed: the first one comprising 7 steps and an overall yield of 7%, while the second approach relies on 3 steps only with an excellent overall yield of 15%.

With the provided material, the Glab-Gli1 interaction has been first demonstrated via NMR, and then through *in vitro* studies. Furthermore, allograft *in vivo* studies proved the efficacy of GlaB (**13**) to inhibit the cell growth of Gli-dependent-Hh-dependent tumors, like MB and BCC.

SAR studies demonstrated the importance of ring B-prenyl chains for Glab-Gli1 interaction and the still ongoing biological studies on the second generation of derivatives will help to understand the role played by prenyl chains and to find a GlaB derivative, which is optimal in terms of selectivity and potency as Gli1 inhibitor.

3. Microtubules: a Successful Target in Cancer Therapy

3.1. Microtubules: a Successful Target against Cancers

Microtubules are intracellular structures and the third principal component of the cytoskeleton, together with microfilaments and intermediate filaments. Microtubules are involved in many processes, such as intracellular transport, chromosome separation, and the maintenance of the cellular shape. Structurally, microtubules are heterodimers of α - and β -tubulin, globular proteins with a molecular weight of approximately 55 kDa (Figure 25). Tubulin heterodimers polymerize to form first head-to-tail assembled linear protofilaments. Parallel nucleation of 13 linear protofilaments around a central core lead to the formation of a microtubule (Figure 25). Therefore, microtubules are cylindrical tubes 50 μm long with an external and internal diameter of 24 and 12 nm respectively. Since the end to end polymerization, microtubules are polar structures with two ends:^[69] a fast-growing (+) end, exposing β -tubulin, and a slow-growing (-) end, exposing α -tubulin (Figure 25).

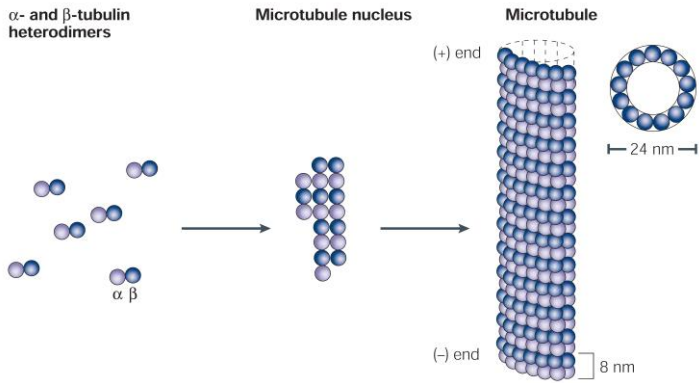


Figure 25: Microtubule assembly (Reproduced with permission)^[70]

The functional properties of microtubules are regulated by polymerization and depolymerization processes. Microtubules are dynamic structures and they possess two dynamic behaviors, so called *dynamic instability* and *treadmilling*.^[69] The dynamic instability consists in stochastic long periods of slow lengthening, brief periods of rapid shortening, and periods of pause, when lengthening and shortening are not detected.^[69] On the other hand, in treadmilling a microtubule loses tubulin subunits from the (-) end and simultaneously gets tubulin subunits at the (+) end, without changing in mass.^[69] Both behaviors can occur in a population of microtubules. Polymerization and depolymerization processes are controlled by the energy provided by the hydrolysis of GTP in GDP and inorganic phosphate (Pi) (Figure 26). Both α - and β -tubulin bind GTP. The site in α -tubulin is able to bind GTP irreversibly and it does not have hydrolytic properties. On the other hand, the site on β -tubulin only binds GTP reversibly and is able

to hydrolyze it. GTP bound to β -tubulin occurs shortly after polymerization. In the “treadmilling” phase, microtubules lose tubulin-GDP molecules at the (-) end and gain tubulin-GTP molecules at the (+) end. If new tubulin-GTP molecules are added more rapidly than the hydrolysis of GTP, the microtubule maintain a GTP cap at the (+) end and the microtubule is stable against depolymerization (Figure 26).^[69] In fact, GTP hydrolysis weakens the binding affinity of tubulin heterodimers, promoting a conformational change. In contrary, when the addition of new GTP-tubulin units is slower that the GDP hydrolysis, then GDP-tubulin dissociates from the microtubule leading to microtubule’s depolymerization and shrinkage. This event is also known as microtubule catastrophe (Figure 26).^[69]

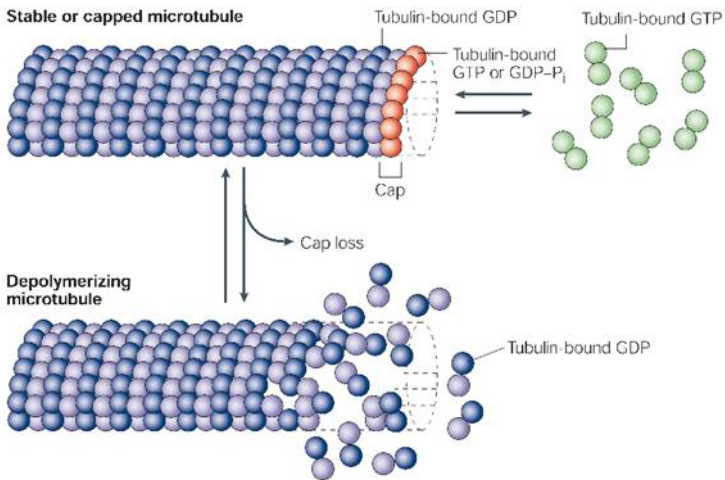


Figure 26: Tubulin polymerization (above) and tubulin depolymerization (below) (Reproduced with permission).^[70]

As mentioned before, the microtubule dynamics control various important processes in living cells (cell shape-maintenance, intracellular transportation, signal transduction, cell division, and mitosis). The rapid turnover of microtubules is particularly critical during mitosis. Any interference in the microtubule dynamics may cause cell cycle arrest and lead to apoptosis or necrosis. For that reason, microtubules are an important target for anticancer drugs. Due to their crucial roles in dividing cells, microtubules have been considered the most successful target in cancer therapy.

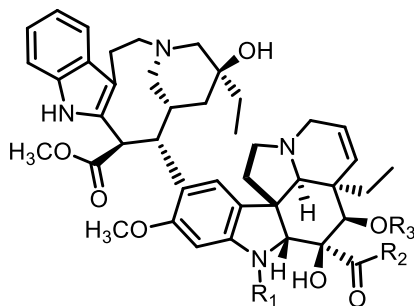
3.2. Microtubule-Targeting Agents

Based on their mechanism of action, microtubule-targeting agents (MTAs) are classified in: microtubule-destabilizing agents (MDAs) and microtubule-stabilizing agents (MSAs). The former prevent the polymerization of tubulin and promote the depolymerization of microtubules. In contrast, the latter act in the opposite way by depolymerization of microtubules and promoting the polymerization of tubulin to microtubules.

3.2.1. Microtubule-Destabilizing Agents

3.2.1.1. *Vinca* alkaloids

The *Vinca* alkaloids have been the first successful drugs used for the treatment of childhood leukemia since 1960s. Vinblastine (Velban®) (50) and vincristine (Oncovin®) (51) (Figure 27) are the most representative molecules of this class and they were isolated from the leaves of periwinkle plant *Catharanthus roseus* (L.) G. Don (also known as *Vinca rosea*). Semi-synthetic compounds related to vinblastine were developed for the treatment of a variety of cancers,^[71,72] such as vindesine (Eldisine®) (52) (Figure 27).^[73]



Vinblastine $R_1 = \text{CH}_3$, $R_2 = \text{OCH}_3$, $R_3 = \text{COCH}_3$ (**50**)
Vincristine $R_1 = \text{CHO}$, $R_2 = \text{OCH}_3$, $R_3 = \text{COCH}_3$ (**51**)
Vindesine $R_1 = \text{CH}_3$, $R_2 = \text{NH}_2$, $R_3 = \text{H}$ (**52**)

Figure 27: *Vinca* alkaloids.

The binding site of the *Vinca* alkaloids is located at the exposed (+) end of the microtubules in β -tubulin, near to the GTP-binding site^[74], and they are able to suppress microtubule dynamics (Figure 28).^[75] At sufficiently high *Vinca* alkaloid concentration in the cell, binding to the soluble β -tubulin^[76] occurs, causing microtubule destabilization.

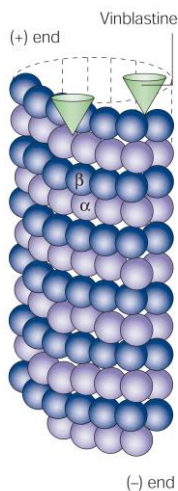


Figure 28: Vinblastine-binding site (Reproduced with permission).^[70]

3.2.1.2. Colchicine and combrestatins

Colchicine (53) (Figure 29) was isolated in 1820 from *Colchicum autumnale* and successfully used for the treatment of gout, an inflammatory arthritis due to high levels of uric acid in the blood.^[77] Colchicine, as *Vinca* alkaloids, depolymerizes microtubules, binding β -tubulin in the colchicine-site (Figure 30).^[70] Nevertheless, colchicine has never been used for cancer treatment because of its dose-related severe toxicities.^[72]

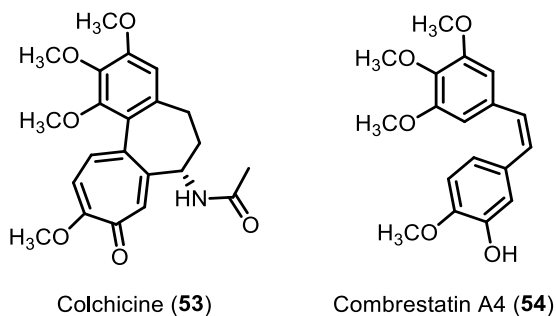


Figure 29: Structures of colchicine (**53**) and combrestatin A-4 (**54**).

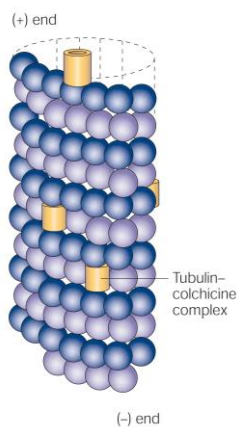


Figure 30: Colchicine-binding site (Reproduced with permission).^[70]

Combretastatins are natural cis-stilbenes, structurally related to colchicine, isolated from *Combretum caffrum*. Combretastatins are able to bind the colchicine binding-site (Figure 30) and combrestatin A-4 (**54**)

(Figure 29) is successfully used to disrupt the blood vessels of cancers.^[78]

3.2.2. Microtubule Stabilizing Agents

3.2.2.1. Molecules targeting taxol-binding site

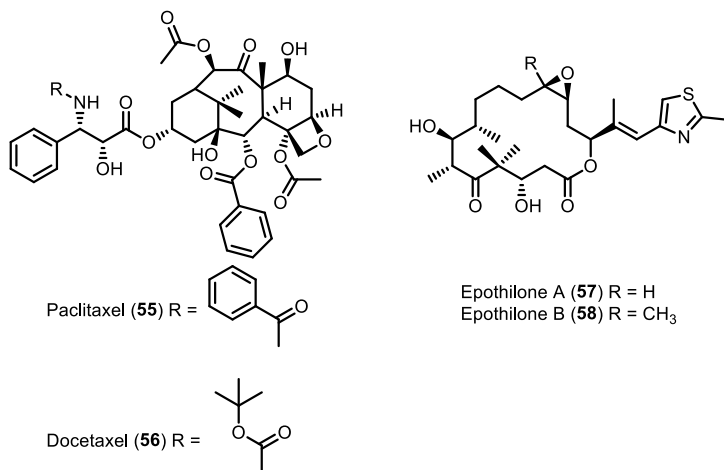


Figure 31: Structure of taxols and epothilones.

Taxols. Paclitaxel (Taxol[®]) (55) (Figure 31) was discovered during the NCI screening program, as alluded to above. Paclitaxel (55) is a natural compound, extracted from the stem bark of the tree *Taxus brevifolia*. Among the years, several semi-synthetic paclitaxel derivatives, like docetaxel (Taxotere[®]) (56) and cabazitaxel (Taxotere[®]),

have been successfully used in cancer therapy.^[72] The taxanes bind to the β -tubulin subunit and promote microtubule stabilization.^[79]

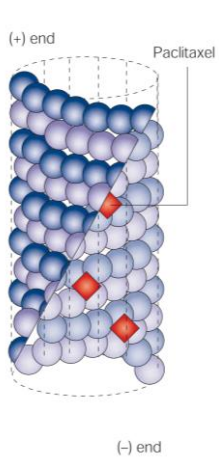


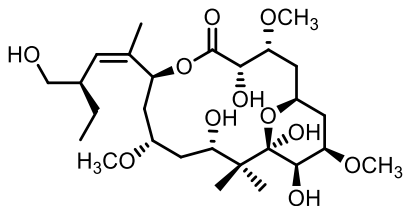
Figure 32: Taxol-binding site (Reproduced with permission).^[70]

Epothilones. Epothilones A (57) and B (58) (Figure 31) were isolated by Gerth and co-workers from the soil bacterium *Sorangium cellulosus*.^[80] These compounds bind β -tubulin to the taxane-binding site and they act in a paclitaxel-like manner and promote microtubule assembly.^[81] Clinical evaluation of epothilones or epothilone-derivatives is still ongoing.^[82]

3.2.2.2. Molecules with different binding sites

Laulimalide^[83,84] and peloruside A (59)^[85] (Figure 33) are marine macrolides with potent cytotoxic activity. These agents bind to a pocket close to the taxol-binding site on β -tubulin at the surface of the

microtubule.^[86] Peloruside A (**59**) has shown great efficacy *in vivo* against lung and MDR-breast tumor, while the development of laulimalide was stopped because of its severe toxicity and mortality.^[87]



Peruloside A (**59**)

Figure 33: Structures of peruloside A (**59**).

3.3. Limitations of the MTAs

MTAs have been considered the most successful drugs against cancers.^[70] One of the most important limitation of using these agents is the occurrence of dose-related side effects, caused by DNA-damage and apoptosis. Neurologic (loss of tendon reflex, numbness, motor weakness, constipation, urinary retention, headache, mental depression, dizziness) and hematologic (myelosuppression, neutropenia) toxicities are the most important, together with nausea, vomiting and diarrhea.^[87]

Another limitation is the emergence of drug resistance mechanisms.^[70] It has been shown that tumors can become resistant to paclitaxel (**55**) or *Vinca* alkaloids because of the overexpression of the P-glycoprotein 1 (P-gp) effluxing pump, a transmembrane ATP-binding cassette (ABC) protein able to decrease the intracellular drug-levels.^[70] The overexpression of different tubulin isotypes, and specifically the β III-tubulin isotype, can also impair the drug-tubulin binding.^[70]

To this end, the research of new MTAs, which are active also in multi-drug resistance (MDR) contexts, is crucial for the success of anticancer therapy.

3.4. Marine Macrolides (-)-Zampanolide and (+)-Dactylolide: new MSAs

3.4.1. Isolation and Structure Elucidation

(-)-Zampanolide (**60**) is able to inhibit cell growth in leukemia (HL60) and ovarian (1A9; A2780 and A2780AD) cancer cell lines.^[88,89] Closer investigations identified **60** as a new MSA with comparable mechanism of action as the antitumor drug paclitaxel (**55**).^[89]

Structurally, **60** is a 20-membered macrolide (Figure 34) with two reported isolations from sponges: first in 1996 from *Fasciospongia ramosa* (Cape Zampa, Okinawa) by Tanaka and Higa,^[88] and later in 2009 from *Cacospongia mycofijiensis* by Northcote, Miller and co-workers.^[89] The earlier work by Tanaka and Higa succeeded in the structure determination of **60** using HR-FABMS and 2D-NMR. However, the analysis of the stereochemistry was partial: the relative configuration of the three chiral centers at C11, C15 and C19 was confirmed, while leaving the relative configuration of C20 along with the absolute configuration of **60** unassigned.^[88] Finally, in 2001 the synthesis of the unnatural antipode of **60**, (+)-zampanolide (**61**) (Figure 34) by Smith and co-workers established the complete stereochemistry of **60**.^[90,91]

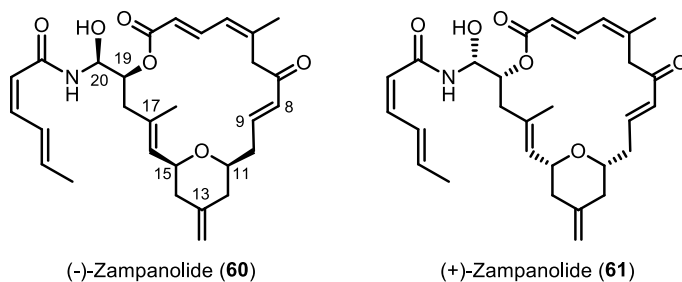


Figure 34: Structures of (-)-zampanolide (**60**) and synthetic non-natural (+)-zampanolide (**61**).

Earlier in 2001, (+)-dactylolide (**62**) (Figure 35) was isolated by Riccio and co-workers as a minor metabolite from a *Dactylospongia* sponge (Vanuatu islands in South Pacific Ocean).^[92] In the work of Riccio and co-workers, 1D and 2D NMR experiments along with mass spectrometry served to identify the structure, while the relative configuration at C19 as well as the absolute configuration of their isolated product was left undetermined.^[92]

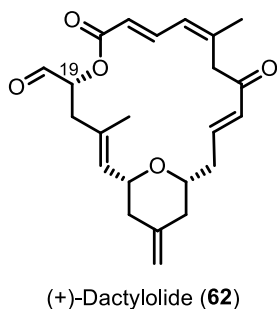
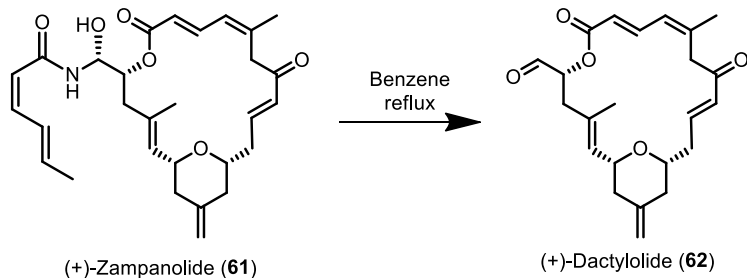


Figure 35: Structure of (+)-dactylolide (**62**).

Meanwhile, Smith and co-workers reported, that they obtained (+)-dactylolide (**62**) (Figure 35) by thermolytic degradation of their synthetic **60** (Scheme 9), and determined the relative and absolute configuration of **62**.^[90,91]



Scheme 9: Thermolytic degradation of synthetic (+)-zampanolide (**60**) into (+)-dactylolide (**62**).

Both, the natural and synthetic **62** were characterized as dextrorotatory, i.e. having a sign (+) for the respective specific rotation. However, at comparable concentrations in MeOH the absolute values of their specific rotations differ strongly in magnitude, with $+30^\circ$ for natural compound and $+235^\circ$ for synthetic **62**. The order of magnitude for the latter was later confirmed by two total syntheses of **62**, where the synthetic materials have been found having specific rotation values of $+134^\circ$ ^[93] and $+163^\circ$.^[94] Recent attempts to rationalize the observed deviation of the specific rotation value for the natural compound in comparison to the three synthetic **62** compounds, has led mainly to two hypotheses. First, Sanchez and Keck reason that variations were due to the enolization equilibria in the respective solutions. This in turn would

lead to different specific rotation values.^[93] A second and more recent hypothesis by Chen and Kingston^[95] suggests that the small specific rotation observed by Riccio and co-workers points to the fact that their isolated compound corresponds to (-)-dactylolide (**63**) (Figure 36).^[96-101] This second hypothesis is based on the argument that enolization and/or hemiacetal formation leads to the observed (+) sign of the natural product.^[95] In fact, formation of the hemiacetal or acetal species in MeOH does occur under slightly acid conditions. Furthermore, Chen and Kingston's argument can be supported by further two points. On the one hand, nature seldomly produces two such complex structures, as **60** and **62**, as enantiomers. On the other hand, **63** has not been derived from natural sources so far, even though it is reasonable to consider **63** a precursor for the biosynthesis of **60**.^[83] Finally, the conditions employed by Riccio and co-workers for the extraction could have potentially lead to a degradation product of **60** by cleaving the C-N bond of the hemiaminal moiety to afford **63**,^[83] in analogy to the observations in synthetic **61**.^[90,91] Due to the lack of experimental data and scarcity of the natural material supporting the presented theories, it is impossible to draw a final conclusion on the validity of these speculations. Moreover, all specific rotations for both **62** and **63** have been repeatedly and independently determined in MeOH. Setting the variation in absolute value aside (possibly arising from differences in experimental conditions such as solvent quality and/or sample history), synthetic **62** was always characterized as dextrorotatory (three independent total syntheses) and levorotatory in case of synthetic **63** (seven independent total syntheses).

In conclusion, the deviation of absolute specific rotation values of the natural product with respect to the synthetic materials implies that the absolute configuration of the natural product cannot be considered established. In addition, discrepancies between the ^{13}C -NMR spectra of synthetic and natural (+)-dactylolide (**62**)^[90,91] also leave open the possibility that the configuration of C19 in natural (+)-dactylolide is *R* and not *S* (**64**) (Figure 36).

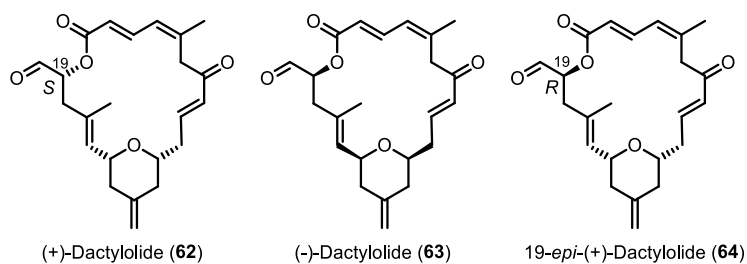


Figure 36: Structures of (+)-dactylolide (**62**), (-)-dactylolide (**63**) and 19-epi-(+)-dactylolide (**64**).

3.4.2. Biological Activity

3.4.2.1. (-)-Zampanolide: biological activity, mechanism of action and binding to tubulin

As alluded to before, Tanaka and Higa have found that (-)-zampanolide (**60**) exhibits a potent cytotoxic activity ($\text{IC}_{50} = 2\text{-}10\text{ nM}$) against a multitude of cancer cell lines, like leukemia (P388), lung carcinoma (A549), colon adenocarcinoma (HT29), and skin melanoma (MEL28) cell lines.^[88] Northcote, Miller and co-workers confirmed the

high cytotoxicity of **60**, performing MTT-cell proliferation assays on leukemia (HL60, $IC_{50} = 4.3$ nM) and ovarian (1A9, $IC_{50} = 14.3$ nM) cancer cell lines.^[89] Furthermore, they also investigated the mechanism of action of **60**. They treated HL60 cells with 2-10 nM concentrations of **60** for 16 hours and they showed that (-)-zampanolide (**60**) was able to arrest the cell cycle in the G₂/M phase of the cell cycle and to induce apoptosis or necrosis of the cells. These findings suggest that (-)-zampanolide (**60**) is a possible antimitotic compound. In order to demonstrate that **60** targets the microtubules, 1A9 cells were treated with (-)-zampanolide (**60**) at 10 nM concentration for 12 hours. (-)-Zampanolide (**60**) was able to induce microtubule bundle formation in interphase cells and to promote the formation of asters (microtubule formations, which control the separation of the cells during mitosis process).^[89] Moreover, 1A9 cells exposed to various concentrations of (-)-zampanolide (**60**) for 16 hours showed a dose-dependent shift of soluble tubulin to the particulate fraction, similar to what paclitaxel (**55**) do.^[89] Northcote, Miller and co-workers checked the MDR susceptibility of **60**, and no significant variations in terms of IC_{50} (7.1 nM and 7.5 nM, respectively) values was observed when (-)-zampanolide (**60**) was tested against the ovarian cancer cell line A2780 and its MDR isoform, A2780AD, which overexpresses the P-gp effluxing pump.^[89] They concluded that (-)-zampanolide (**60**) was a novel and very potent MSA, with a taxol-like mechanism of action, which, in contrast to the latter, maintains its cytotoxic activity against both drug-sensitive and MDR cancer cell lines.^[89] The capability of (-)-zampanolide (**60**) to maintain its anticancer activity in MDR-contests

has been confirmed in a study performed by Cerchietti and co-workers.^[102] **60** was tested against the acute myeloid leukemia (AML), acute lymphoblastic leukemia (ALL), and their taxol-resistant, P-gp overexpressing isoforms (KG-1a and CCRF-CEM/VBL respectively) and showed GI₅₀ values below 1 nM against the whole set of cells.^[102]

In 2012, Díaz and co-workers, in collaboration with the groups of Northcote and Miller, and Altmann, demonstrated the mode of binding of (-)-zampanolide (**60**).^[103] The study discovered that **60** is able to bind irreversibly the taxol-binding site on β -tubulin.^[103] In fact, the displacement of (-)-zampanolide (**60**) by the fluorescent taxol derivative Flutax-2 was completely abrogated when microtubules were incubated with **60** for a short period of time (less than 30 min).^[103] MS/MS analysis of the tryptic digests of the zampanolide-modified tubulin adduct showed that the side chains of the aminoacidic residues N228 and H229 act as nucleophiles.^[103] The electrophilic site on (-)-zampanolide (**60**) could not be elucidated at the time, but, in 2013, Steinmetz and co-workers, using synthetic material provided by Altmann group,^[104] were able to solve and crystallize the complex between α/β -tubulin, protein RB3, tubulin tyrosine ligase and (-)-zampanolide (**60**) at 1.8 Å resolution.^[104]

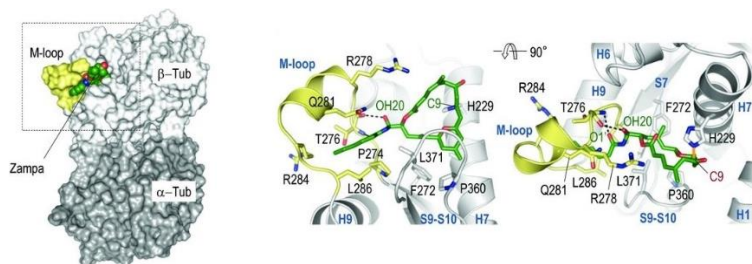


Figure 37: Crystal structure of **60** in complex with $\alpha\beta$ -tubulin. Complex between $\alpha\beta$ -tubulin and (-)-zampanolide (**60**) (left). (-)-Zampanolide in the taxane binding site (centre). H229 covalent binding at (-)-zampanolide C9 (right) (Reproduced with permission).^[104]

As shown in Figure 37, the Michael-acceptor at C9 in the enone moiety of **60** binds the imidazole side chain of the β -tubulin residue H229,^[104] as previously supposed by Díaz and co-workers.^[103] Furthermore, from the crystal structure H-bonding can be observed between OH20 and O1 of (-)-zampanolide (**60**) and the carbonyl oxygen and the NH group of T276.^[103] The latter interactions appears to be essential. In fact, it is known from a number of studies that the lack of the hemiaminal-linked dienamide side chain in (-)-zampanolide derivatives is related to a reduced biological activity (see below).

3.4.2.2. (+)-Dactylolide: biological activity

Intriguingly, while (-)-zampanolide (**60**) is a nM inhibitor of cancer cell growth *in vitro*, natural (+)-dactylolide (**62**) is substantially less active, although the available data set is limited to two cell lines, investigated in the isolation paper. Riccio and co-workers reported that

(+)-dactylolide (**62**) inhibited the growth of lymphocytic leukemia (L1210) and ovarian carcinoma (SKOV-3) cells.^[92] At the outset of this dissertation, no other data on the biological activity of (+)-dactylolide (**62**) have been published. On the other hand, data on the biological activity of synthetic (-)-dactylolide (**63**) are available from a number of studies. **63** exhibits sub- μM IC_{50} values against a multitude of cancer cell lines, although (-)-zampanolide (**60**) is still 100- to 300-fold more potent.^[95] The latter data are in accordance with what Uenishi and co-workers^[99] as well as Field *et al*^[103] have already pointed out. In fact, the hemiaminal-linked dienamide side chain in (-)-zampanolide (**60**) is crucial for its biological activity.

Note, that not even synthetic (+)-zampanolide (**61**) has ever been tested, and in this context the importance of the macrocycle configuration for the biological activity remains unclear.

3.5. Aims and Scope

The continuous evaluation of the antitumor potential of new cytotoxic natural products is essential to overcome the MDR problem.^[105] Marine macrolide (-)-zampanolide (**60**) showed high IC₅₀ values against drug-sensitive and MDR cancer cell lines.^[95] (+)-Dactylolide (**62**), a structurally related marine macrolide, has been found substantially less active.^[92] At the outset of this PhD thesis no further biological data were available for synthetic (+)-dactylolide (**62**) and (+)-zampanolide (**61**). Our goal was to synthesize (+)-dactylolide (**62**) and (+)-zampanolide (**61**), in order to investigate how the macrocycle configuration could influence the biological activity.

Furthermore, we designed a synthesis of the C19 epimer of (+)-dactylolide (**62**), in order to definitively clear the discrepancies observed in the specific rotation values and the ¹³C-NMR spectra of synthetic and natural materials and, finally, establish the absolute configuration of natural (+)-dactylolide (**62**).

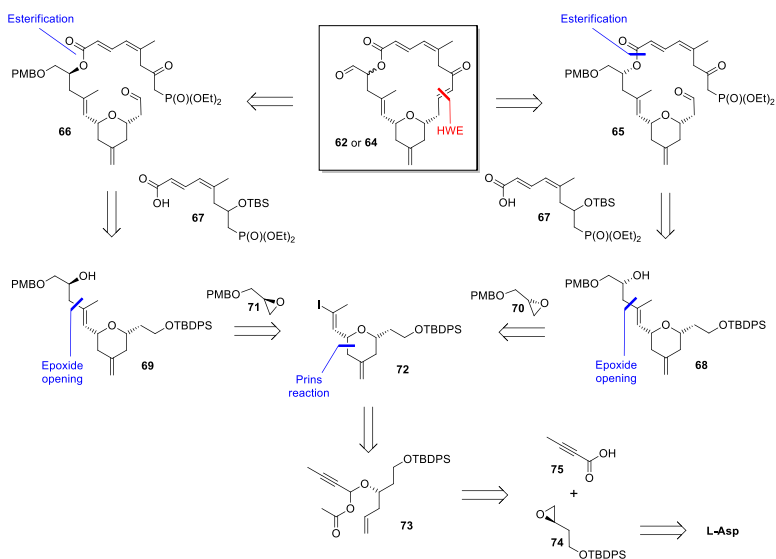
4. (+)-Dactylolide, 19-*epi*-(+)- Dactylolide and (+)- Zampanolide: Synthesis and Biological Evaluation⁴

4.1. Retrosynthesis

The strategy to be followed for the synthesis of **62** and **64** was analogous to the one that had been developed previously by Altmann and co-workers for the synthesis of **63**.^[101,106] This strategy entails macrocyclic ring-closure by an highly efficient intramolecular *Horner-Wittig-Emmons* (HWE) reaction of ω -dialkylphosphono β -keto aldehydes **65** and **66**, respectively (Scheme 10). The ω -dialkylphosphono β -keto aldehydes as the crucial precursors for the macrocyclization reaction were to be obtained by esterification of acid **67**^[101,106] with protected alcohols **68** and **69**, respectively, followed by protecting group manipulations and oxidation. The construction of the tetrahydropyran (THP) ring was envisioned to be achieved through

⁴ This part of my PhD research was carried out in the laboratories of Prof. Karl-Heinz Altmann, ETH-Zürich (Switzerland).

Prins cyclization of the acetylated acetal **73**; the alkyne moiety of the resulting THP derivative was then to be converted into vinyl iodide **72**, which would be a precursor for both target structures. Metalation of **72** and reaction of the metal vinyl species with PMB-protected (*S*)-glycidol (**70**) or (*R*)-glycidol (**71**) was envisaged to produce alcohols **68** and **69**, respectively. The synthesis of acetylated acetal **73** from *L*-aspartic acid in a 7-step sequence *via* epoxide **74** had been described previously.^[101,106] In total, the longest linear sequence from *L*-aspartic acid to **62** or **64** would thus comprise 20 discrete steps. As alluded to above, this sequence had been successfully implemented in the synthesis of **63** as described by Zurwerra *et al.*^[101,106]

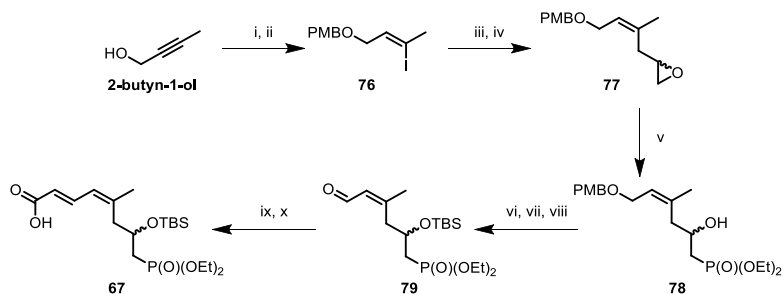


Scheme 10: Retrosynthetic analysis for the synthesis of **62** and **64**.

4.2. Synthesis of (+)-Dactylolide and 19-*epi*-(+)-Dactylolide

4.2.1. Synthesis of Acid **67**

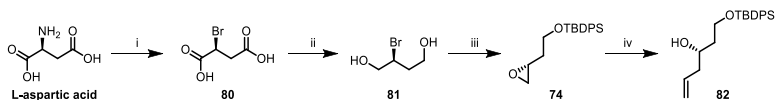
Since the acid **67** is the same used for the synthesis of **63**,^[101,106] the synthesis will not be discussed in details. As shown in Scheme 11, the synthesis starts from commercially available 2-butyn-1-ol, which was converted into (Z)-vinyl iodide via Corey's reductive alumination/iodination sequence.^[107] The resulting vinyl alcohol was protected using PMB-trichloroacetimidate^[108,109] and then homologated with epichlorohydrin. The resulting chlorohydrin was converted to the epoxide **77**, followed by the regioselective epoxide opening reaction to afford the β -hydroxy phosphonate **78** in 70% yield. TBS protection of the resulting secondary alcohol and PMB removal with DDQ,^[110] followed by Swern^[111] oxidation gave **79**. HWE olefination and hydrolysis of the ethyl ester then completed the synthesis of the acid **67**. As previously described by Zurwerra *et al*,^[101,106] the synthesis provided **67** in high quantities (up to 10 grams).



Scheme 11: Synthesis of the acid **67**. i) Red-Al, I₂; ii) PMBOC(NH)CCl₃, PPTS, 87% over two steps; iii) (±)-Epichlorohydrin, *n*-BuLi, BF₃·Et₂O; iv) KOH, 49% over two steps; v) Diethyl phosphite, *n*-BuLi, BF₃·Et₂O, 70%; vi) ImH, DMAP, TBSCl; vii) DDQ; viii) (COCl)₂, DMSO, Et₃N, 75% over three steps; ix) Triethyl phosphonoacetate, *n*-BuLi, x) NaOH 1M, 96% over two steps.

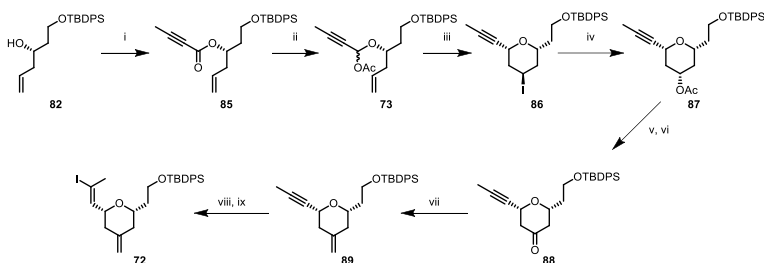
4.2.2. Synthesis of THP-vinyl Iodide 72

We next addressed the synthesis of the common fragment of **62** and **64**: the THP-vinyl iodide **72**. Starting from commercially available *L*-(+)-aspartic acid (Scheme 12) and following a previously reported 3-steps procedure,^[149] we were able to synthesize the epoxide **74** in multigram quantities. The corresponding homoallylic alcohol **82** was then obtained via regioselective copper-mediated epoxide opening, using vinylmagnesium bromide (Scheme 12).^[112]



Scheme 12: Synthesis of the homoallylic alcohol **82**. i) H₂SO₄, KBr, NaNO₂, 92%; ii) BH₃, 83%; iii) NaH, TBDPSCl, 65%; iv) Vinylmagnesium bromide, CuI, 96%.

82 was esterified with 2-butynoic acid **75**,^[113] affording the ester **85**. Reductive acylation reaction of **85** produced the acid-labile species **73** in high yields. As reported by Zurwerra *et al.*,^[101,106] TMSI^[114] successfully promoted the *Prins*-type cyclization of the acylated acetal **73**, affording **86** in high and reproducible yields. Also in this case, the use of 2,6-dimethylpyridine was found to be necessary, in order to suppress the non-selective HI-mediated cyclization.^[114]



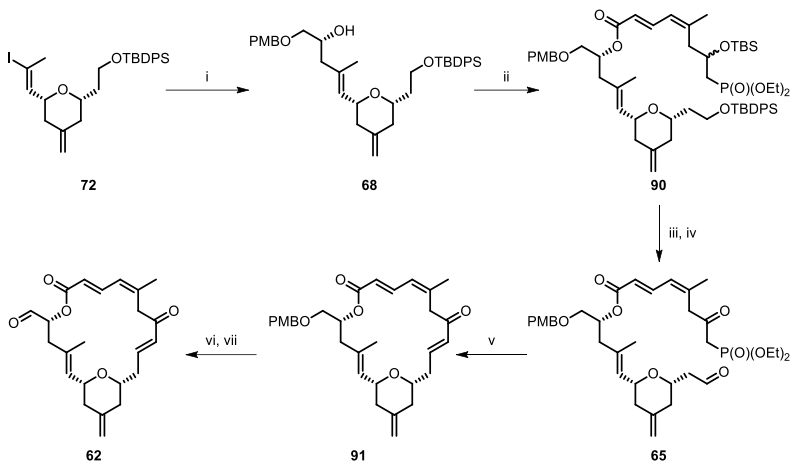
Scheme 13: Synthesis of the THP-vinyl iodide **72**. i) **75**, DCC, DMAP, 74%; ii) DIBAL-H, pyridine, DMAP, Ac₂O, 91%; iii) TMSI, 2,6-lutidine, 73%; iv) CsOAc, 18-crown-6, 75%; v) K₂CO₃; vi) DMP, 78% over two steps; vii) Methyltriphenylphosphonium bromide, *n*-BuLi, 77%; viii) CuCN, *n*-BuLi, Bu₃SnH, MeOH; ix) NIS, 95% over two steps.

At this point of the synthesis, we had to install the C13 *exo*-methylene group. The first step involved a cesium-mediated acetate substitution.^[115] The acetate ester of **87** was then hydrolysed under basic conditions and the resulting secondary alcohol oxidated to the ketone **88** with DMP. *Wittig* olefination using methyltriphenylphosphonium bromide as carbon source provided **89** in good yields. The last step to accomplish the synthesis of the southern fragment was the reduction of the internal alkyne in **89** to the (*E*)-vinyl iodide **72** via stannylation-

, using $\text{Bu}_3\text{Sn}(\text{Bu})\text{CuCNLi}_2$,^[116,117] iodination sequence, which gave the desired vinyl iodide **72** in high yields.

4.2.3. Completion of the Synthesis of (+)-Dactylolide (**64**)

With the two fragments in hand, we were able to complete the synthesis of the (+)-dactylolide (**62**). The first reaction involved the epoxide opening of the PMB-protected (*S*)-glycidol (**70**). The reaction was promoted by the vinyl lithium species of **72**, produced *in situ* by treatment of **72** with $t\text{BuLi}$. The corresponding alcohol **68** was then esterified with the acid **67** under *Yamaguchi*'s conditions,^[118] providing the fully protected ester **90** (Scheme 14).



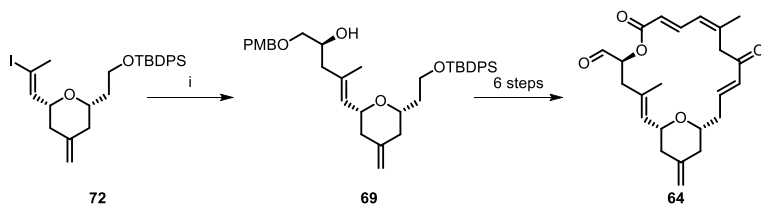
Scheme 14: Completion of the synthesis of (+)-dactylolide (**62**). i) **70**, ^tBuLi, BF₃·Et₂O, 59%; ii) **67**, 2,4,6-trichlorobenzoyl chloride, Et₃N, DMAP, 65%; iii) HF-pyridine; iv) DMP; v) Ba(OH)₂, 65% over three steps; vi) DDQ; vii) DMP, 66% over two steps.

HF-py was used to promote global silyl removal and the resulting free diol was then oxidized with DMP to the β-ketophosphonate aldehyde **65**, the crucial precursor for the intramolecular *HWE* reaction. Since compound **65** has been found to be unstable upon overnight storage at -20 °C, the latter was used without any further purification. As described for the synthesis of (-)-dactylolide (**63**),^[101,106] the use of freshly activated Ba(OH)₂^[119,120] afforded the macrocycle **91** in reproducible yields. PMB removal using DDQ and oxidation with DMP^[121] then completed the total synthesis of (+)-dactylolide (**62**), with an overall yield of 1.4%. The spectral data for synthetic **62** proved to be identical in all respects with the spectral data derived from the natural product.^[92] However, also in our case we found that the synthetic

materials have a higher value of the specific rotation: +163° instead of +30°.

4.2.4. Completion of the Synthesis of 19-epi-(+)-Dactylolide (64)

For the synthesis of **64**, the epoxide opening reaction was performed using the PMB-protected (*R*)-glycidol **71**, provided by the synthesis of the (-)-dactylolide (**63**),^[101,106] giving **69** (Scheme 15). Same procedures were used to synthesize **64** and the yields were reproducible.



Scheme 15: Completion of the synthesis of 19-epi-(+)-dactylolide (**64**). i) **71**, ^tBuLi, BF₃·Et₂O, 52%.

Surprisingly, the value of the specific rotation for **64** was found to be similar to the natural dactylolide (+29°), but only the spectra of synthetic **62** correspond to the spectra of natural (+)-dactylolide.

4.3. Synthesis of (+)-Zampanolide⁵

With **62** in hand, in order to complete the total synthesis of (+)-zampanolide **61**, we had to install the hemiaminal-linked dienamide side chain.

Thanks to the work of a former PhD student in Altmann's laboratories, a stereoselective procedure for the aza-aldol reaction has been found. Previous to his discovery, in none of the former syntheses of (+)- or (-)-zampanolide the side chain could be introduced stereoselectively. DIBAL-H (**92**) proved to be the best reducing agent in terms of conversion percentage, but not in terms of diastereoselectivity. Based on the protocol used by Ghosh and co-workers,^[122] using (*S*)-TRIP (**93**) (Figure 38), the idea was to create a chiral variant of DIBAL-H (Figure 38): BINAL-H (**94**). The latter can be easily prepared starting from lithium aluminium hydride, ethanol and the corresponding (*R*)- or (*S*)-1,1'-bi-2-naphthol (Figure 38) and has been used for the enantioselective reduction of ketones.^[123]

⁵ The stereoselective version of the aza-aldol reaction was developed by Tobias Brüttsch and explained in details in his PhD thesis entitled: Total Synthesis of Mandelalide A and Synthesis of (-)-Zampanolide Analogs for Structure-Activity Relationship Studies (DISS. ETH NO. 23856).

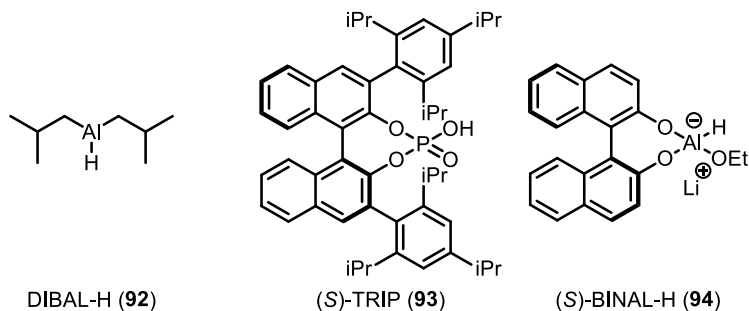
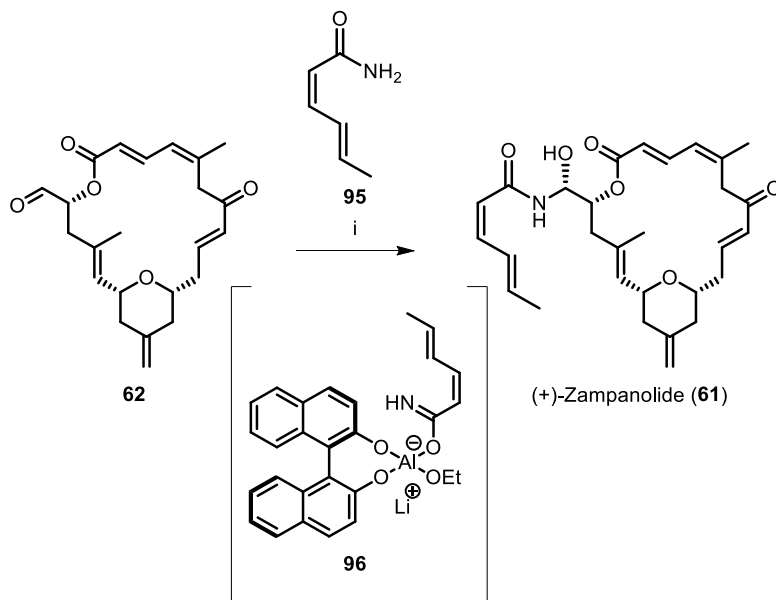


Figure 38: Reagents and catalyst for aza-aldol addition

When a solution of (*R*)-BINAL-H and sorbamide (**95**) (Scheme 16) was added to a (+)-dactylolide (**62**) solution at room temperature, full conversion of the latter was observed after 10-15 min. The reaction afforded (+)-zampanolide (**61**) in an excellent diastereomeric ratio (*dr*) of 93:7. Normal phase semi-preparative HPLC purification allowed the isolation of the desired C20 isomer in 74% yield.

Our example is the first diastereoselective synthesis of (+)-zampanolide (**61**) and the second synthesis of this compound. The successful application of this procedure to this substrate indicates that the stereoselective formation of the hemiaminal centre at C20, using the chiral BINAL-amide complex **96**, is not substrate-controlled, but represents a new stereoselective aza-aldol process.



Scheme 16: Synthesis of (+)-zampanolide (61). i) LAH, EtOH, (R)-BINOL, 74%.

4.4. Biological Evaluation of Zampanolide Analogs⁶

4.4.1. *In Vitro* Antiproliferative Activity

The compounds **60-64** were tested against ovarian cancer cell line A2780 and its MDR isoform, A2780AD (Table 2).

Table 2: Antiproliferative activity of **60**, **61**, **62**, **63** and **64**. Taxol was used as control. IC₅₀ values are reported in nM.

	60	61	62	63	64	Taxol
A2780 (ovarian)	0.802 ± 0.01	10500 ± 1138	15382 ± 1790	1254 ± 139	9488 ± 2431	0.48 ± 0.36
A2780AD (ovarian)^a	2.68 ± 0.21	11445 ± 70	11399 ± 194	1252 ± 567	12848 ± 743	5870 ± 382

^aMultidrug-resistant cell line overexpressing the P-gp effluxing pump.

None of them showed IC₅₀ value comparable to the corresponding levorotatory conformation and the compounds were at least 1000-fold less potent.

In addition, Flutax-2 displacement test proved the inability of the latter compounds to interact with tubulin.

⁶ These experiments were carried out in collaboration with Dr. Fernando Diaz, CISC, Madrid, Spain.

4.5. Conclusions and Outlook

In conclusion, (+)-dactylolide (**62**), 19-*epi*-(+)-dactylolide (**64**) and (+)-zampanolide (**61**) have been successfully synthesized, confirming that the synthetic procedures previously developed for the synthesis of (-)-dactylolide (**63**) and (-)-zampanolide (**60**) are highly reproducible.

We have proven that the lower absolute value of specific rotation observed for natural (+)-dactylolide (**62**) is not caused by a C19 epimer. This means that the absolute configuration of (+)-dactylolide (**62**) cannot be considered established.

The new methodology for the stereoselective aza-aldol reaction has been employed for the synthesis of (+)-zampanolide (**61**), providing high values of diastereoselectivity and high yields.

The biological data of the dextrorotatory compounds have shown low values of cytotoxicity. This means that the absolute configuration of the macrocycle plays a pivotal role in drug-protein binding process.

5. Experimental Section

5.1. General Methods for Sapienza project

All non-aqueous reactions were performed under an argon atmosphere using flame-dried glassware and standard syringe/septa techniques.

All absolute solvents were purchased as anhydrous grade from Sigma Aldrich and used without further purification unless otherwise stated. Solvents for extractions, flash column chromatography (FC) and thin layer chromatography (TLC) were purchased as commercial grade from Sigma Aldrich and used without further purification unless otherwise stated. Reactions were magnetically stirred and monitored by TLC performed on Merck TLC aluminum sheets (silica gel 60 F254). Spots were visualized with UV light ($\lambda = 254$ nm). Chromatographic purification of products (FC) was performed using Sigma Aldrich silica gel 60 for preparative column chromatography (particle size 40-63 μm).

Melting points (Mp) were obtained in open capillary tubes using a Büchi melting point apparatus B-545 and are uncorrected.

^1H - and ^{13}C -NMR spectra were recorded in CDCl_3 , acetone- d_6 , DMSO- d_6 or methanol- d_4 on a Bruker AV-400 400 MHz spectrometer

(operating at 400 MHz for ^1H and 100 MHz for ^{13}C) at room temperature and tetramethylsilane (TMS) as internal standard. Chemical shifts (δ) are reported in parts per million (ppm) and are referenced to CHCl_3 ($\delta = 7.26$ ppm for ^1H , $\delta = 77.16$ ppm for ^{13}C), acetone ($\delta = 2.05$ ppm for ^1H , $\delta = 29.84$ ppm for ^{13}C) DMSO ($\delta = 2.50$ ppm for ^1H , $\delta 39.52$ ppm for ^{13}C), or MeOH ($\delta = 3.31$ ppm for ^1H , $\delta 49.00$ ppm for ^{13}C). All ^{13}C -NMR spectra were measured with complete proton decoupling. Data for NMR spectra are reported as follows: s = singlet, d = doublet, t = triplet, q = quartet, m = multiplet, br = broad signal, J = coupling constant in Hz.

High-resolution mass spectra (HRMS) were recorded on Bruker BioApex Fourier transform ion cyclotron resonance (FT-ICR) mass spectrometer.

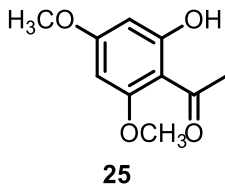
HPLC analysis was performed on a Waters 2690 Separation Module, equipped with a Rheodyne Model 8125 20- μL injector and a Model M486 programmable multi-wavelength detector (PDA). Chromatographic data were collected and processed using the Empower Chromatography Manager software. Column: Phenomenex Luna C18, 5 μm (250 \times 4.6 mm); eluent A) $\text{H}_2\text{O}/\text{CH}_3\text{CN}$, 95:5 v/v, eluent B) $\text{H}_2\text{O}/\text{CH}_3\text{CN}$, 5:95 v/v; gradient elution: for 0-5 min A:B = 50:50; 5-20 min up to 100% B; 20-25 min to 100% B; Flow rate: 1.0 ml/min; UV detection at 295 nm. The purity of the compounds was always higher than 95 %.

The compounds are referred to by increasing numbers **X**, following the sequential references in the main text.

Analytics of compounds **40** and **41** were identical to samples previously synthesized.^[124]

5.2. First Total Synthesis of GlaB (13)

1-(2-hydroxy-4,6-dimethoxyphenyl)ethanone (**25**)



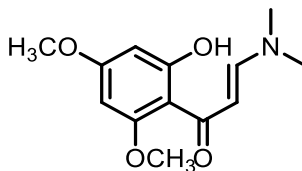
In a two-neck round-bottom flask, 2',4',6'-trimethoxyacetophenone (**24**) (5 g, 23.8 mmol, 1.00 equiv.) was dissolved in dry DCM (75 mL) under argon. BBr_3 (15 mL, 87.3 mmol, 3.50 equiv.) was added drop wise. The resulting solution was stirred at room temperature for 2 h before quenching with 4.0 M NaOH aqueous solution (90 mL) and stirred for 30 min. The organic phase was separated and the aqueous solution was then extracted with DCM (3 x 100 mL) and combined organic layers were washed once with brine (100 mL), dried over Na_2SO_4 and concentrated *in vacuo*. The resulting solid was recrystallized from EtOH, providing **25** (4.43 g, 22.8 mmol, 98%) as white crystals.

Mp: 81–82°C. $^1\text{H-NMR}$ (400 MHz, acetone- d_6): δ = 13.8 (s, 1H, OH), 5.94 (d, J = 2.4 Hz, 1H, ArH), 5.91 (d, J = 2.4 Hz, 1H, ArH), 3.80 (s, 3H, OCH_3), 3.72 (s, 3H, OCH_3), 2.43 (s, 3H, CH_3). $^{13}\text{C-NMR}$ (100 MHz,

acetone-*d*₆): δ = 202.5, 167.4, 166.3, 163.2, 105.5, 93.4, 90.4, 55.2, 55.0, 31.9.

HRMS (ESI): calcd. for C₁₀H₁₃O⁺ [(M+H)⁺]: 197.080800; found: 197.080848.

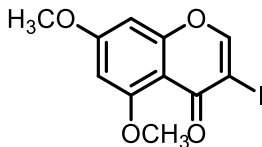
(*E*)-3-(dimethylamino)-1-(2-hydroxy-4,6-dimethoxyphenyl)prop-2-en-1-one
(26)



26

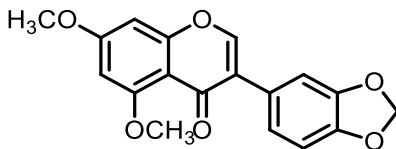
A mixture of **25** (4.5 g, 22.9 mmol, 1.00 equiv.) and DMF-DMA (13 mL, 97.1 mmol, 4.00 equiv.) was stirred at 95 °C for 3 h. Later on, the solvent was removed *in vacuo* and the obtained red solid product **26** (5.8 g, 22.9 mmol, quantitative crude) was used without any further purification

Mp: 145–147°C. **¹H-NMR** (400 MHz, CDCl₃): δ = 15.65 (s, 1H, OH), 7.92 (d, *J* = 12 Hz, 1H, =CH–N), 6.25 (d, *J* = 12.0 Hz, 1H, =CH–(CO)), 6.07 (d, *J* = 2.4 Hz, 1H, ArH), 5.91 (d, *J* = 2.4 Hz, 1H, ArH), 3.84 (s, 3H, OCH₃), 3.80 (s, 3H, OCH₃), 3.15 (s, 3H, NCH₃), 2.92 (s, 3H, NCH₃); **¹³C-NMR** (100 MHz, CDCl₃): δ = 191.6, 169.0, 165.5, 162.9, 155.8, 106.6, 96.3, 95.6, 92.1, 57.1, 56.6. **MS** (ESI): calcd. for C₁₃H₁₈O₄N [(M+H)⁺]: 252.1; found, 252.3.

3-iodo-5,7-dimethoxy-4H-chromen-4-one (**22**)**22**

To a solution of **26** (5.8 g, 22.9 mmol, 1.00 equiv.) in MeOH (450 mL), I₂ (11.7 g, 46.2 mmol, 2.00 equiv.) was added. The brown mixture was stirred at room temperature for 1 h, then the solvent was evaporated *in vacuo*. To remove residual I₂, the crude was treated with a saturated aqueous Na₂S₂O₃ until the mixture became clear. The mixture was then extracted with CHCl₃ (3 x 150 mL), and the combined organic layers were dried over Na₂SO₄ and concentrated *in vacuo*. The residue was purified by FC (EtOAc/hexane 1:3) to obtain **22** (2.5 g, 7.5 mmol, 33%) as a white powder.

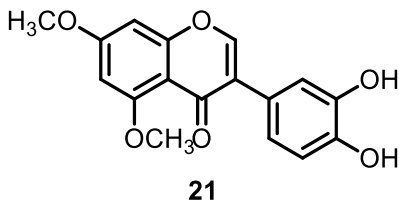
Mp: 156–157°C. ¹H-NMR (400 MHz, CDCl₃): δ = 8.02 (s, 1H, H-2), 6.37 (d, *J* = 2.0 Hz, 1H, ArH), 6.32 (d, *J* = 2.0 Hz, 1H, ArH), 3.87 (s, 3H, OCH₃), 3.82 (s, 3H, OCH₃). ¹³C-NMR (100 MHz, CDCl₃): δ = 183.4, 164.3, 161.0, 159.8, 155.3, 107.5, 96.6, 92.4, 89.7, 56.4, 55.8. **HRMS** (ESI): calcd. for C₁₁H₁₀O₄I [(M+H)⁺]: 332.961800; found, 332.961633.

3-(benzo[d][1,3]dioxol-5-yl)-5,7-dimethoxy-4H-chromen-4-one (**27**)**27**

To a solution of **22** (2.5 g, 7.5 mmol, 1.00 equiv.) in a mixture of degassed DME/H₂O = 1:1 (150 mL) Na₂CO₃ (3.18 g, 30 mmol, 4.00 equiv.), **23** (1.8 g, 11 mmol, 1.50 equiv.) and Pd EnCat™40 (937 mg, 5% mol) were consecutively added. The resulting mixture was stirred at 45 °C for 2 h and then filtered through a Celite pad. The residue was washed first with H₂O (50 mL) and then with DCM (50 mL). The organic phase was separated and the aqueous layer was extracted with DCM (3 x 50mL). The combined organic layers were dried over Na₂SO₄ and concentrated *in vacuo*. The crude residue was purified by FC (EtOAc/hexane 1:2) to give **27** (1.4 g, 4.3 mmol, 57%) as a gray powder.

Mp: 155–156°C. **¹H-NMR** (400 MHz, CDCl₃): δ = 7.75 (s, 1H, H-2), 7.1 (d, *J* = 2.0 Hz, 1H, H-2'), 6.94 (dd, *J* = 8.0 and 2.0 Hz, 1H, H-6'), 6.83 (d, *J* = 8.0 Hz, 1H, H-5'), 6.44 (d, *J* = 2.2 Hz, 1H, H-6), 6.37 (d, *J* = 2.2 Hz, 1H, H-8), 5.97 (brs, 2H, O–CH₂–O), 3.94 (s, 3H, OCH₃), 3.89 (s, 3H, OCH₃). **¹³C-NMR** (100 MHz, CDCl₃): δ = 175.1, 164.0, 161.5, 160.3, 150.1, 147.6, 147.1, 126.5, 126.0, 122.8, 110.5, 110.0, 108.4, 101.3, 96.7, 92.7, 56.4,

55.8. **HRMS** (ESI): calcd. for $C_{18}H_{15}O_6$ [(M+H)⁺]: 327.086300; found, 327.086206.

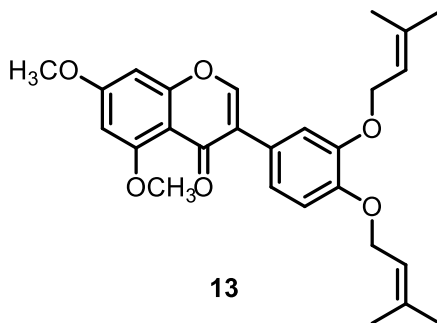
3-(3,4-dihydroxyphenyl)-5,7-dimethoxy-4H-chromen-4-one (**21**)

In a two-neck round-bottom flask, **27** (1.4 g, 4.3 mmol, 1.00 equiv.) and $\text{Pb}(\text{OAc})_4$ (freshly recrystallized from degassed AcOH, 7.5 g, 17 mmol, 4.00 equiv.) in dry benzene (100 mL) was stirred at reflux under argon overnight. After, cooling to room temperature, the reaction mixture was filtered through a pad of Celite, the residue was washed with DCM (50 mL) and the filtrate was concentrated *in vacuo*.

The crude product was diluted with a mixture of THF/ H_2O = 5:1 (50 mL) and AcOH (50 mL), and the resulting solution was stirred at room temperature for 6 h. Then, saturated aqueous NaHCO_3 was added until pH = 8 and extracted with EtOAc (3 × 100 mL). The combined organic layers were dried over Na_2SO_4 and concentrated *in vacuo* to obtain **21** (570 mg, 1.8 mmol, 42%) as a yellow solid.

Mp: 127–129°C. $^1\text{H-NMR}$ (400 MHz, methanol- d_4): δ = 7.86 (s, 1H, H-2), 6.88 (brs, 1H, H-2'), 6.70 (brs, 2H, H-5' and H-6'), 6.50 (d, J = 2.0 Hz, 1H, H-6), 6.40 (d, J = 2.0 Hz, 1H, H-8), 3.80 (s, 3H, OCH_3), 3.79 (s,

3H, OCH₃). **¹³C-NMR** (100 MHz, methanol-*d*₄): 175.0, 165.1, 161.1, 159.9, 151.3, 145.1, 145.0, 126.5, 123.1, 120.5, 117.0, 110.0, 114.5, 95.9, 92.8, 55.1.
HRMS (ESI): calcd. for C₁₇H₁₅O₆ [(M+H)⁺]: 315.086300; found, 315.086363.

Glabrescione B (**13**)

To a solution of **21** (570 mg, 1.3 mmol, 1.00 equiv.) in acetone (100 mL) K_2CO_3 (7.4 g, 5.4 mmol, 4.50 equiv.) was added. After 10 min 3,3-dimethylallyl bromide (968 mg, 6.5 mmol, 5.00 equiv.) was added and the mixture was stirred at reflux overnight. Afterward, the solvent was evaporated and the resulting solid was dissolved in EtOAc (25 mL) and H_2O (25 mL). The aqueous layer was then extracted with EtOAc (3 x 25 mL). The combined organic layers were dried over Na_2SO_4 and finally concentrated *in vacuo*. The crude was purified by FC (EtOAc/hexane 1:5) to obtain GlaB (**13**) as white powder. The powder was recrystallized from hexane resulting with white crystals.

The spectral data were identical to an authentic sample of GlaB.

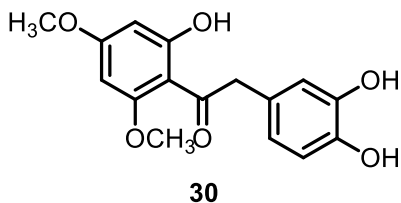
Mp: 102–104°C. **¹H-NMR** (400 MHz, acetone-*d*₆): δ = 7.94 (s, 1H, H-8), 7.16 (d, *J* = 1.6 Hz, 1H, H-15), 6.99 (dd, *J* = 8.0 Hz and 1.6 Hz, 1H, H-11), 6.89 (d, *J* = 8.0 Hz, 1H, H-12), 6.50 (d, *J* = 2.0 Hz, 1H, H-1), 6.42 (d, *J* = 2.0 Hz, 1H, H-3), 5.43 (m, 2H, 2 x =CH), 4.51 (d, *J* = 6.8 Hz, 4H, OCH₂), 3.86 (s, 3H, OCH₃), 3.81 (s, 3H, OCH₃), 1.70 (s, 6H, 2 CH₃), 1.67 (s, 6H, 2 CH₃). **¹³C-NMR** (400 MHz, CDCl₃): δ = 175.6, 164.0, 161.2, 159.7, 150.2, 148.9, 148.5, 136.9, 126.5, 125.0, 121.4, 120.7, 115.5, 110.0, 114.0, 96.5, 92.6, 66.0, 56.4, 55.9, 25.6, 18.1. **HRMS** (ESI): calcd. for C₂₇H₃₁O₆ [(M+H)⁺]: 451.211500; found, 451.211495.

5.3. Second Total Synthesis of GlaB and GlaB Ring-B Derivatives

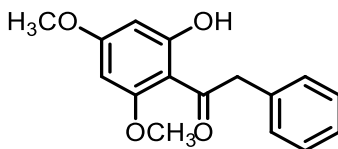
5.3.1. General procedure for the preparation of deoxybenzoines (30, 34-36)

In a two-neck round-bottom flask a mixture of 3,5-dimethoxyphenol (6 mmol, 1.00 equiv.), 3,4-disubstituted-phenylacetic acid (6 mmol, 1.00 equiv.) and $\text{BF}_3 \cdot \text{Et}_2\text{O}$ (48 mmol, 8.00 equiv.) was stirred at 90 °C for 90 min under argon. The reaction mixture was poured into 10% aqueous NaOAc (100 mL) and allowed to stir at room temperature for 24 h, forming a brown precipitate. The precipitate was filtered and washed with H_2O (2 x 20 mL). The precipitate was resuspended with EtOAc, dried over Na_2SO_4 and finally concentrated *in vacuo*. The residue was purified by FC using a mixture of Petroleum Ether/EtOAc as eluent, to obtain the corresponding deoxybenzoin.

2-(3,4-dihydroxyphenyl)-1-(2-hydroxy-4,6-dimethoxyphenyl)ethanone
(30)

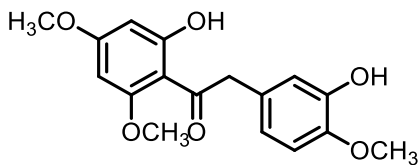


Pale Brown solid (Yield 50%). **Mp**: 130-132 °C. **TLC** R_f = 0.30 (EtOAc/PE 7:3, UV). **¹H-NMR** (400 MHz, acetone- d_6): δ = 13.90 (s, 1H, C2-OH), 7.76 (brs, 2H, OH), 6.75-6.73 (m, 2H, H-2' and H-5'), 6.58 (dd, J = 8.0 Hz, J = 1.2 Hz, 1H, H-6'), 6.06 (d, J = 2.0 Hz, 1H, H-5), 6.04 (d, J = 2.8 Hz, 1H, H-3), 4.16 (s, 2H, CH₂), 3.93 (s, 3H, OCH₃), 3.84 (s, 3H, OCH₃). **¹³C-NMR** (100 MHz, acetone- d_6): δ = 204.3, 168.7, 167.3, 163.7, 145.6, 144.6, 128.2, 121.8, 117.4, 115.8, 106.1, 94.6, 91.5, 56.2, 56.0, 50.0. **HRMS** (ESI): calcd. for C₁₆H₁₇O₆ [(M+H)⁺]: 305.10196; found, 305.10178.

1-(2-hydroxy-4,6-dimethoxyphenyl)-2-phenylethanone (**34**)**34**

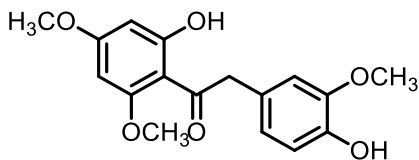
Pale Yellow solid (Yield 65%). **Mp**: 111.6-112.65 °C. **TLC** R_f = 0.30 (EtOAc/PE 7:3, UV). **¹H-NMR** (400 MHz, acetone-*d*₆): δ = 13.83 (s, 1H, OH), 7.32-7.19 (m, 5H, H-2', H-3', H-4', H-5' and H-6'), 6.07 (d, J = 2.4 Hz, 1H, H-5), 6.06 (d, J = 2.4 Hz, 1H, H-3), 4.33 (s, 2H, CH₂), 3.92 (s, 3H, OCH₃), 3.85 (s, 3H, OCH₃). **¹³C-NMR** (100 MHz, acetone-*d*₆): δ = 203.8, 168.7, 167.5, 163.8, 136.8, 130.4, 129.0, 127.2, 106.2, 94.6, 91.5, 56.2, 56.1, 50.7. **HRMS** (ESI): calcd. for C₁₆H₁₇O₄ [(M+H)⁺]: 273.11213; found, 273.11203.

1-(2-hydroxy-4,6-dimethoxyphenyl)-2-(3-hydroxy-4-methoxyphenyl)ethanone (35)

**35**

Pale Yellow solid (Yield 55%). **Mp**: 114.2-115.3 °C. **TLC** R_f = 0.33 (EtOAc/PE 7:3, UV). **¹H-NMR** (400 MHz, acetone- d_6): δ = 13.88 (s, 1H, C2-OH), 7.51 (brs, 1H, OH), 6.84 (d, J = 8.4 Hz, 1H, H-5'), 6.76 (d, J = 2.4Hz, 1H, H-2'), 6.67 (dd, J = 8 Hz, J = 2 Hz, 1H, H-6'), 6.06 (d, J = 2 Hz, 1H, H-5), 6.04 (d, J = 2.4 Hz, 1H, H-3), 4.20 (s, 2H, CH₂), 3.93 (s, 3H, OCH₃), 3.84 (s, 3H, OCH₃), 3.80 (s, 3H, OCH₃). **¹³C-NMR** (100 MHz, acetone- d_6): δ = 204.2, 168.7, 167.4, 163.8, 147.2, 147.1, 129.5, 121.3, 117.3, 112.3, 106.1, 94.6, 91.5, 56.2, 56.2, 56.0, 50.0. **HRMS** (ESI): calcd. for C₁₇H₁₉O₆ [(M+H)⁺]: 319.11761; found, 319.11767.

2-(4-hydroxy-3-methoxyphenyl)-1-(2-hydroxy-4,6-dimethoxyphenyl)ethanone (**36**)



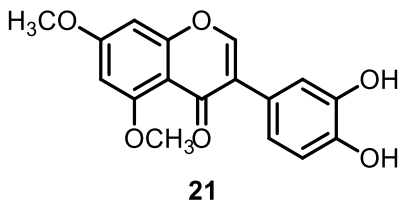
36

Pale Yellow solid (Yield 55%). **Mp**: 133-135 °C. **TLC** R_f = 0.33 (EtOAc/PE 7:3, UV). **¹H-NMR** (400 MHz, acetone- d_6): δ = 13.87 (s, 1H, C2-OH), 7.42 (brs, 1H, OH), 6.86 (d, J = 1.6 Hz, 1H, H-2'), 6.74 (d, J = 8 Hz, 1H, H-5'), 6.69 (dd, J = 8 Hz, J = 1.6 Hz, 1H, H-6'), 6.07 (d, J = 2,4 Hz, 1H, H-5), 6.05 (d J = 2,4 Hz, 1H, H-3), 4.23 (s, 2H, CH₂), 3.95 (s, 3H, OCH₃), 3.84 (s, 3H, OCH₃), 3.81 (s, 3H, OCH₃). **¹³C-NMR** (100 MHz, acetone- d_6): δ = 203.4, 167.8, 166.5, 162.9, 147.2, 145.3, 127.0, 122.1, 114.7, 113.2, 105.3, 93.7, 90.6, 55.3, 55.2, 49.3. **HRMS** (ESI): calcd. for C₁₇H₁₉O₆ [(M+H)⁺]: 319.11761; found, 319.11794.

5.3.2. General procedure for the Vilsmeier-Haack reaction for the preparation of isoflavones (21, 37-39)

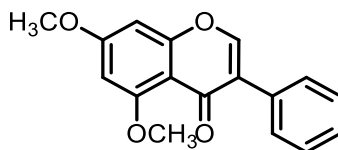
In a two-neck round-bottom flask a solution of deoxybenzoin (3 mmol, 1.00 equiv.) in DMF (5 mL) was cooled to 0 °C and $\text{BF}_3 \cdot \text{Et}_2\text{O}$ (9 mmol, 3.00 equiv.) was added drop wise under argon. In another flask, DMF (8 mL) was cooled to 0 °C and PCl_5 (4.5 mmol, 1.50 equiv.) was added. The mixture was then allowed to stir at 55 °C for 20 min. The light yellow colored solution containing *N,N'*-dimethyl(chloromethylene)ammonium chloride was then added to the above reaction mixture at 0 °C. The mixture was stirred at room temperature for 2 h under argon and then poured into 0.1 N methanolic HCl (70 mL) and allowed to stir at 70 °C for 2 h. After removing the solvents *in vacuo*, H_2O (50 mL) and EtOAc (50 mL) were added and the aqueous phase was extracted with EtOAc (3 x 100 mL). The combined organic layers were washed once with brine (100 mL), dried over Na_2SO_4 , and finally concentrated under reduced pressure. The residue was purified by FC using Petroleum Ether/EtOAc as eluent, to give the corresponding isoflavone.

3-(3,4-dihydroxyphenyl)-5,7-dimethoxy-4H-chromen-4-one (**21**)



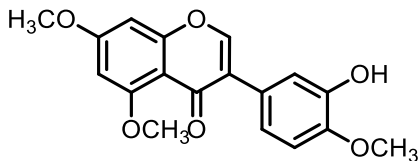
White solid (Yield 30%). See spectral data above.

5,7-dimethoxy-3-phenyl-4H-chromen-4-one (37)

**37**

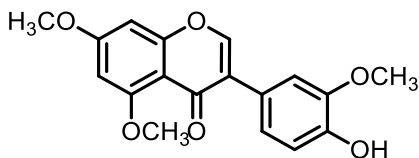
Pale Pink solid (Yield 35%). **Mp**: 96-97 °C. **TLC** R_f = 0.35 (EtOAc/PE 7:3, UV). **¹H-NMR** (400 MHz, CDCl₃): δ = 7.78 (s, 1H, H-2), 7.53 (d, 2H, H-2' and H-6'), 7.41-7.34 (m, 3H, H-3', H-4' and H-5'), 6.44 (brd, 1H, H-8), 6.37 (brd, 1H, H-6), 3.93 (s, 3H, OCH₃), 3.88 (s, 3H, OCH₃). **¹³C-NMR** (100 MHz, acetone-*d*₆): δ = 175.3, 164.1, 161.6, 160.0, 150.7, 132.2, 129.3, 128.3, 128.0, 126.5, 110.1, 96.3, 92.7, 56.5, 55.9. **HRMS** (ESI): calcd. for C₁₆H₁₅O₄ [(M+H)⁺]: 283.09649; found, 283.09672.

3-(3-hydroxy-4-methoxyphenyl)-5,7-dimethoxy-4H-chromen-4-one (38)

**38**

Brown solid (Yield 32%). **Mp**: 175-177 °C. **TLC** R_f = 0.30 (EtOAc/PE 7:3, UV). **$^1\text{H-NMR}$** (400 MHz, $\text{DMSO-}d_6$): δ = 8.97 (s, 1H, OH), 8.14 (s, 1H, H-2), 6.98 (d, J = 2 Hz, 1H, H-2'), 6.93 (d, J = 8 Hz, 1H, H-5'), 6.87 (dd, J = 8 Hz, J = 2 Hz, 1H, H-6'), 6.65 (d, J = 2 Hz, 1H, H-6), 6.50 (d, J = 2.4 Hz, 1H, H-8), 3.88 (s, 3H, OCH_3), 3.82 (s, 3H, OCH_3), 3.78 (s, 3H, OCH_3). **$^{13}\text{C-NMR}$** (100 MHz, $\text{DMSO-}d_6$): δ = 173.7, 163.6, 160.8, 159.2, 150.9, 147.4, 145.9, 145.8, 124.8, 119.9, 116.6, 116.5, 111.8, 109.0, 96.2, 92.9, 56.1, 55.9, 55.6. **HRMS** (ESI): calcd. for $\text{C}_{18}\text{H}_{17}\text{O}_6$ [(M+H) $^+$]: 329.10196; found, 329.10203.

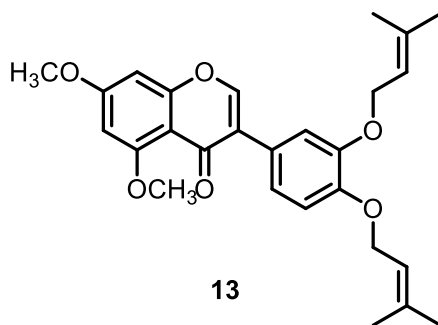
3-(4-hydroxy-3-methoxyphenyl)-5,7-dimethoxy-4H-chromen-4-one (39)

**39**

Brown Solid (Yield 31%). **Mp**: 223-224 °C. **TLC** R_f = 0.29 (EtOAc/PE 7:3) (UV). **¹H-NMR** (400 MHz, CDCl₃): δ = 8.01 (s, 1H, OH), 7.77 (s, 1H, H-2), 7.28 (s, 1H, H-2'), 6.91 (d, J = 8 Hz, 1H, H-5'), 6.87 (d, J = 8 Hz, 1H, H-6'), 6.44 (brd, 1H, H-6), 6.37 (brd, 1H, H-8), 3.93 (s, 3H, OCH₃), 3.90 (s, 3H, OCH₃), 3.88 (s, 3H, OCH₃). **¹³C-NMR** (100 MHz, CDCl₃): δ = 175.6, 164.0, 161.6, 160.0, 150.3, 146.3, 145.8, 126.1, 124.3, 121.7, 114.2, 112.7, 110.0, 96.3, 92.7, 56.5, 56.2, 55.9. **HRMS** (ESI): calcd. for C₁₈H₁₇O₆ [(M+H)⁺]: 329.10196; found, 329.10171.

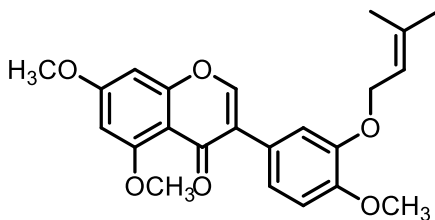
5.3.3. General procedure for the alkylation/benzylation reaction (13, 40-49)

To a solution of the isoflavone (0.18 mmol, 1.00 equiv.) in acetone (5 mL), K_2CO_3 (1.8 mmol, 10.00 equiv.) was added. After stirring for 15 min the corresponding alky/benzyl bromide (0.9 mmol, 5.00 equiv.) was added drop wise to the mixture and stirred at 45 °C overnight. After removing the acetone *in vacuo*, H_2O (10 mL) and EtOAc (20 mL) were added and the aqueous phase was extracted with EtOAc (3 x 20 mL). The combined organic layers were dried over Na_2SO_4 , and finally concentrated under reduced pressure. The residue was purified by FC using Petroleum Ether/EtOAc as eluent to give the corresponding substituted-isoflavone.

Glabrescione B (13)

White solid (Yield 90%). See spectral data above.

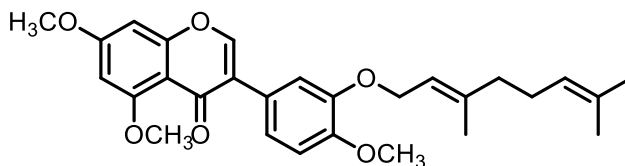
5,7-dimethoxy-3-(4-methoxy-3-((3-methylbut-2-en-1-yl)oxy)phenyl)-4H-chromen-4-one (42)



42

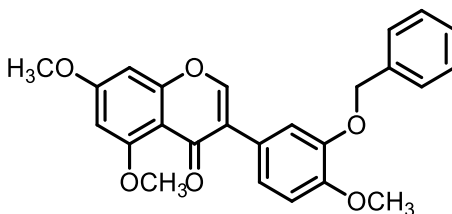
White Solid (Yield 95%). **Mp**: 113-113.2 °C. **TLC** R_f = 0.50 (EtOAc/PE 7:3, UV). **$^1\text{H-NMR}$** (400 MHz, CDCl_3): δ = 7.76 (s, 1H, H-2), 7.22 (d, J = 2 Hz, 1H, H-2'), 7.01 (dd, J = 8.0 Hz, J = 1.6 Hz, 1H, H-6'), 6.88 (d, J = 8 Hz, 1H, H-5'), 6.44 (d, J = 1.2 Hz, 1H, H-6), 6.37 (d, J = 2.4 Hz, 1H, H-8), 5.55 (t, J = 6.8 Hz, 1H, CH), 4.59 (d, J = 8 Hz, 2H, CH_2), 3.94 (s, 3H, OCH_3), 3.88 (s, 3H, OCH_3), 3.87 (s, 3H, OCH_3), 1.76 (s, 3H, CH_3), 1.71 (s, 3H, CH_3). **$^{13}\text{C-NMR}$** (100 MHz, CDCl_3): δ = 175.5, 164.0, 161.6, 160.0, 150.3, 149.5, 148.0, 137.8, 126.1, 124.8, 121.5, 120.0, 114.6, 111.2, 110.1, 96.3, 92.6, 65.9, 56.5, 56.0, 55.8, 26.0, 18.4. **HRMS** (ESI): calcd. for $\text{C}_{23}\text{H}_{25}\text{O}_6$ [(M+H) $^+$]: 397.16456; found, 397.16441.

(*E*)-3-(3-((3,7-dimethylocta-2,6-dien-1-yl)oxy)-4-methoxyphenyl)-5,7-dimethoxy-4*H*-chromen-4-one (**43**)

**43**

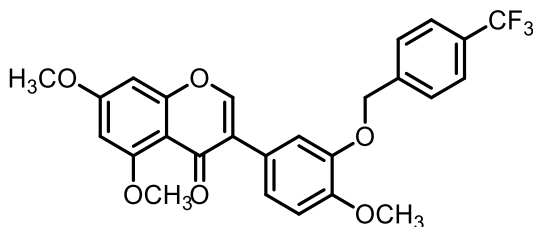
Pale White Solid (Yield 88%). **Mp**: 92-93.3 °C. **TLC** R_f = 0.58 (EtOAc/PE 7:3, UV). **¹H-NMR** (400 MHz, CDCl₃): δ = 7.76 (s, 1H, H-2), 7.22 (d, J = 2 Hz, 1H, H-2'), 7.02 (dd, J = 8 Hz, J = 2 Hz, 1H, H-6'), 6.88 (d, J = 8 Hz, 1H, H-5'), 6.43 (d, J = 2 Hz, 1H, H-6), 6.36 (d, J = 2 Hz, 1H, H-8), 5.55 (t, J = 6.0 Hz, 1H, CH), 5.09 (t, J = 6.0 Hz, 1H, CH), 4.62 (d, J = 6.0 Hz, 2H, CH₂), 3.94 (s, 3H, OCH₃), 3.88 (s, 6H, OCH₃), 2.10-2.04 (m, 4H, CH₂), 1.71 (s, 3H, CH₃), 1.66 (s, 3H, CH₃), 1.59 (s, 3H, CH₃). **¹³C-NMR** (100 MHz, CDCl₃): δ = 175.5, 164.0, 161.6, 160.0, 150.3, 149.5, 148.0, 140.80, 131.78, 126.14, 124.79, 124.09, 121.51, 119.78, 114.70, 111.24, 110.07, 96.28, 92.64, 66.08, 56.50, 56.03, 55.84, 39.72, 26.44, 25.78, 17.79, 16.85. **HRMS** (ESI): calcd. for C₂₈H₃₃O₆ [(M+H)⁺]: 465.22717; found, 465.22743.

3-(3-(benzyloxy)-4-methoxyphenyl)-5,7-dimethoxy-4H-chromen-4-one
(44)

**44**

Light Brown Solid (Yield 95%). **Mp**: 128-129 °C. **TLC** R_f = 0.42 (EtOAc/PE 7:3, UV). **$^1\text{H-NMR}$** (400 MHz, CDCl_3): δ = 7.45 (s, 1H, H-2), 7.37-7.26 (m, 3H, H-3'', H-4'' and H-5''), 7.06 (d, J = 8 Hz, 1H, H-6''), 6.91 (d, J = 8 Hz, 1H, H-2''), 6.44 (brd, 1H, H-6), 6.37 (brd, 1H, H-8), 5.17 (s, 2H, CH_2), 3.95 (s, 3H, OCH_3), 3.90 (s, 3H, OCH_3), 3.89 (s, 3H, OCH_3). **$^{13}\text{C-NMR}$** (100 MHz, CDCl_3): δ = 175.6, 164.0, 160.0, 150.4, 148.0, 137.3, 128.6, 127.9, 127.7, 124.9, 122.1, 115.6, 111.8, 96.4, 92.7, 71.3, 56.6, 56.2, 55.9. **HRMS** (ESI): calcd. for $\text{C}_{25}\text{H}_{23}\text{O}_6$ [$\text{M}+\text{H}$] $^+$: 419.15891; found, 419.14871.

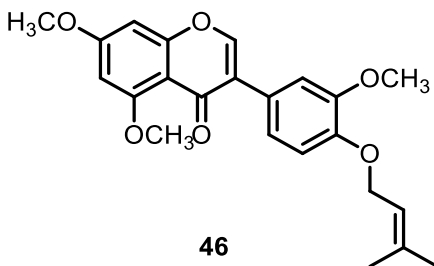
5,7-dimethoxy-3-(4-methoxy-3-((4-(trifluoromethyl)benzyl)oxy)phenyl)-4H-chromen-4-one (**45**)



45

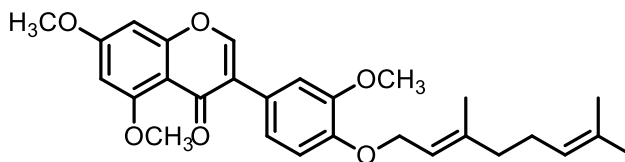
Pale White Solid (Yield 92%). **Mp**: 131-134 °C. **TLC** R_f = 0.42 (EtOAc/PE 7:3, UV). **¹H-NMR** (400 MHz, CDCl₃): δ = 7.73 (s, 1H, H-2), 7.63-7.57 (m, 4H, H-2'', H-3'', H-5'' and H-6''), 7.29 (d, J = 1.6 Hz, 1H, H-2'), 7.05 (dd, J = 8 Hz, J = 2 Hz, 1H, H-6'), 6.92 (d, J = 8 Hz, 1H, H-5'), 6.43 (d, J = 2 Hz, 1H, H-6), 6.37 (d, J = 1.6 Hz, 1H, H-8), 5.22 (s, 2H, CH₂) 3.94 (s, 3H, OCH₃), 3.90 (s, 3H, OCH₃), 3.88 (s, 3H, OCH₃). **¹³C-NMR** (100 MHz, CDCl₃): δ = 175.5, 164.1, 161.6, 160.0, 150.3, 149.8, 147.6, 141.4, 127.6, 125.8, 125.6, 125.6, 125.0, 122.3, 115.7, 111.8, 110.0, 96.4, 92.7, 70.4, 56.5, 56.2, 55.9. **HRMS** (ESI): calcd. for C₂₆H₂₂F₃O₆ [(M+H)⁺]: 487.13630; found, 487.13656.

5,7-dimethoxy-3-(3-methoxy-4-((3-methylbut-2-en-1-yl)oxy)phenyl)-4H-chromen-4-one (**46**)



White Solid (Yield 95%). **Mp**: 130.9-132.6 °C. **TLC** R_f = 0.50 (EtOAc/PE 7:3, UV). **¹H-NMR** (400 MHz, CDCl₃): δ = 7.77 (s, 1H, H-2), 7.23 (s, 1H, H-2'), 6.95 (dd, J = 8 Hz, J = 2 Hz, 1H, H-6'), 6.87 (d, J = 8 Hz, 1H, H-5'), 6.43 (d, J = 1.6 Hz, 1H, H-6), 6.36 (d, J = 1.6 Hz, 1H, H-8), 5.52 (t, J = 6.4 Hz, 1H, CH), 4.59 (d, J = 7.8 Hz, 1H, CH₂), 3.93 (s, 3H, OCH₃), 3.89 (s, 3H, OCH₃), 3.88 (s, 3H, OCH₃), 1.76 (s, 3H, CH₃), 1.72 (s, 3H, CH₃). **¹³C-NMR** (100 MHz, CDCl₃): δ = 175.64, 163.96, 161.59, 159.96, 150.30, 149.12, 148.29, 137.63, 126.11, 124.94, 121.12, 120.14, 113.18, 112.84, 110.06, 96.28, 92.64, 65.86, 56.50, 56.11, 55.83, 25.93, 18.34. **HRMS** (ESI): calcd. for C₂₃H₂₅O₆ [(M+H)⁺]: 397.16456; found, 397.16490.

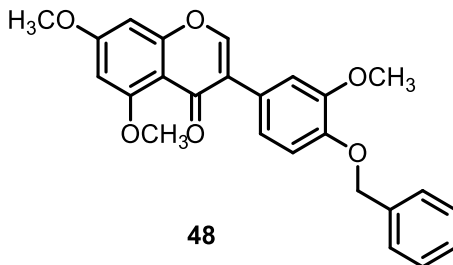
(E)-3-(4-((3,7-dimethylocta-2,6-dien-1-yl)oxy)-3-methoxyphenyl)-5,7-dimethoxy-4H-chromen-4-one (**47**)



47

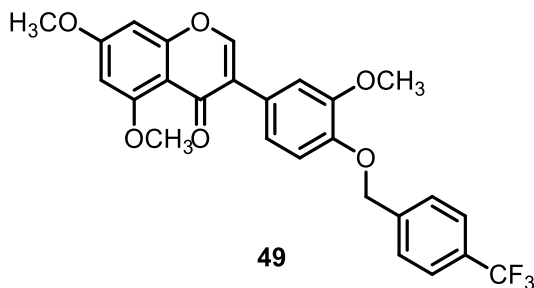
Pale White Solid (Yield 89%). **Mp**: 93.5-95.3 °C. **TLC** R_f = 0.58 (EtOAc/PE 7:3, UV). **¹H-NMR** (400 MHz, CDCl₃): δ = 7.79 (s, 1H, H-2), 7.23 (s, 1H, H-2'), 6.95 (d, J = 8 Hz, 1H, H-6'), 6.88 (d, J = 8 Hz, 1H, H-5'), 6.43 (d, J = 2 Hz, 1H, H-6), 6.37 (d, J = 2 Hz, 1H, H-8), 5.52 (t, J = 6 Hz, 1H, CH), 5.07 (t, J = 6 Hz, 1H, CH), 4.63 (d, J = 8 Hz, 2H, CH₂), 3.93 (s, 3H, OCH₃), 3.89 (s, 3H, OCH₃), 3.88 (s, 3H, OCH₃), 2.09 (d, J = 6 Hz, 2H, CH₂), 2.06 (d, J = 5.6 Hz, 2H, CH₂), 1.72 (s, 3H, CH₃), 1.67 (s, 3H, CH₃), 1.59 (s, 3H, CH₃). **¹³C-NMR** (100 MHz, CDCl₃): δ = 175.5, 164.0, 161.6, 160.0, 150.3, 149.1, 148.3, 140.6, 131.8, 126.1, 125.0, 124.0, 121.1, 120.0, 113.2, 112.9, 110.0, 96.3, 92.6, 66.0, 56.5, 56.1, 55.8, 39.7, 26.4, 25.8, 17.8, 16.8. **HRMS** (ESI): calcd. for C₂₈H₃₃O₆ [(M+H)⁺]: 465.22717; found, 465.22715.

3-(4-(benzyloxy)-3-methoxyphenyl)-5,7-dimethoxy-4H-chromen-4-one
(48)



Pale White solid (Yield 95%). **Mp**: 148.5-149 °C. **TLC** R_f = 0.42 (EtOAc/PE 7:3, UV). **¹H-NMR** (400 MHz, CDCl₃): δ = 7.75 (s, 1H, H-2), 7.43 (d, J = 8 Hz, 2H, H-2'', H-6''), 7.35 (t, J = 8 Hz, 1H, H-3'', H-5''), 7.29 (d, J = 7.2 Hz, 1H, H-4''), 7.25 (s, 1H, H-2'), 6.89 (d, J = 8 Hz, 1H, H-6), 6.86 (d, J = 8 Hz, 1H, H-8), 6.42 (brd, 1H, H-6), 6.36 (brd, 1H, H-8), 5.17 (s, 2H, CH₂), 3.93 (s, 3H, OCH₃), 3.91 (s, 3H, OCH₃), 3.87 (s, 3H, OCH₃). **¹³C-NMR** (100 MHz, CDCl₃): δ = 175.5, 164.0, 161.6, 160.0, 150.4, 149.4, 148.2, 137.3, 128.7, 127.9, 127.4, 125.5, 121.2, 113.8, 113.6, 110.1, 96.3, 92.7, 71.1, 56.5, 56.3, 55.9. **HRMS** (ESI): calcd. for C₂₅H₂₃O₆ [(M+H)⁺]: 419.15891; found, 419.14962.

5,7-dimethoxy-3-(3-methoxy-4-(4-(trifluoromethyl)benzyl)oxy)phenyl)-4H-chromen-4-one (**49**)



White Solid (Yield 94%). **Mp**: 136.8-137.9 °C. **TLC** R_f = 0.42 (EtOAc/PE 7:3, UV). **¹H-NMR** (400 MHz, CDCl₃): δ = 8.02 (d, J = 8 Hz, 2H, H-5'' and H-3''), 7.71 (s, 1H, H-2), 7.52 (d, J = 8 Hz, 2H, H-2'' and H-6''), 7.06 (s, 1H, H-2'), 7.04 (dd, J = 8 Hz, J = 1.6 Hz, 1H, H-6'), 6.92 (d, J = 1.6 Hz, 1H, H-5'), 6.43 (d, J = 2 Hz, 1H, H-6), 6.37 (d, J = 1.6 Hz, 1H, H-8), 5.22 (s, 2H, CH₂), 3.93 (s, 3H, OCH₃), 3.90 (s, 3H, OCH₃), 3.88 (s, 3H, OCH₃). **¹³C-NMR** (100 MHz, CDCl₃): δ = 175.4, 167.1, 164.0, 161.6, 160.0, 150.3, 149.8, 147.6, 142.6, 129.9, 129.6, 127.1, 125.9, 124.9, 122.3, 115.7, 111.7, 110.0, 96.3, 92.7, 70.6, 56.5, 56.2, 55.9, 52.2, 29.8. **HRMS** (ESI): calcd. for C₂₆H₂₂F₃O₆ [(M+H)⁺]: 487.13630; found, 487.13647.

5.4. General Methods for ETH project

All non-aqueous reactions were performed under an argon atmosphere using flame-dried glassware and standard syringe/septa techniques.

DCM, THF and Et₂O used for reactions were distilled under argon before using (DCM from CaH₂, THF and Et₂O from Na/benzophenone). All other solvents were purchased as anhydrous grade from Acros (dried over molecular sieves) and used without further purification unless otherwise stated. Solvents for extractions, flash column chromatography (FC) and thin layer chromatography (TLC) were purchased as commercial grade and distilled prior to use. Reactions were magnetically stirred and monitored by TLC performed on Merck TLC aluminum sheets (silica gel 60 F254). Spots were visualized with UV light ($\lambda = 254 \text{ nm}$) or through staining with Ce₂(SO₄)₃/phosphomolybdic acid/H₂SO₄ (CPS) or KMnO₄/K₂CO₃. Chromatographic purification of products (FC) was performed using Fluka silica gel 60 for preparative column chromatography (particle size 40-63 μm).

Melting points (Mp) were obtained in open capillary tubes using a Büchi melting point apparatus B-540 and are uncorrected.

¹H- and ¹³C-NMR spectra were recorded in CDCl₃ and DMSO-*d*₆ on a Bruker AV-400 400 MHz or on a Bruker AV-500 500 MHz spectrometer at room temperature. Chemical shifts (δ) are reported in ppm and are referenced to CHCl₃ ($\delta = 7.26 \text{ ppm}$ for ¹H, $\delta = 77.16 \text{ ppm}$

for ^{13}C), or DMSO ($\delta = 2.50$ ppm for ^1H , $\delta = 39.52$ ppm for ^{13}C). All ^{13}C -NMR spectra were measured with complete proton decoupling. Data for NMR spectra are reported as follows: s = singlet, d = doublet, t = triplet, q = quartet, m = multiplet, br = broad signal, J = coupling constant in Hz.

Infrared spectra (IR) were recorded on a Jasco FT/IR-6200 instrument. Resonance frequencies are given as wavenumbers in cm^{-1} .

Optical rotations were measured on a Anton Paar MCP-300 modular circular polarimeter, operating at the sodium D line with a 10 or 100 mm path length cell and are reported as follows: $[\alpha]_{\text{D}}^{24}$: (concentration (g/100 mL), and solvent).

High-resolution mass spectra (HRMS) were recorded on a Bruker maXis (ESI) or on a Micromass (Waters) AutoSpec Ultima spectrometer (EI), respectively, by the ETH Zürich MS service.

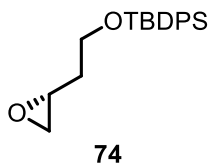
HPLC analysis were performed using the following combination of devices by VWR HITACHI: column oven L-2350, PDA detector L-2455, autosampler L-2200, and pump L-2130.

The compounds are referred to by increasing numbers **X**, following the sequential references in the main text. Moreover, **Xa** names correspond to the intermediate compounds which do not have a number in the main text, while compounds of the synthesis of 19-epi-(+)-dactylolide not shown in the main text are referred to by **Xb**.

Compounds **67**, **71**, **80**, **81** and **95** were prepared according to procedures already described.^[101,125]

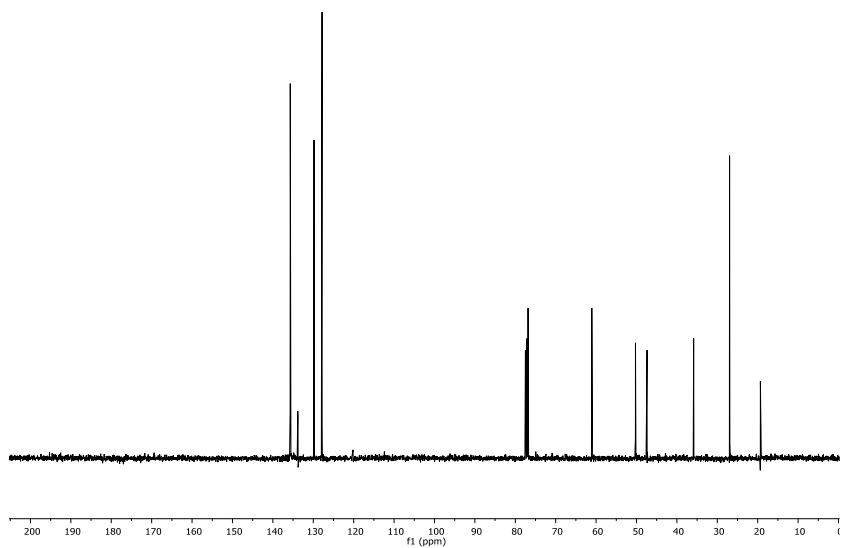
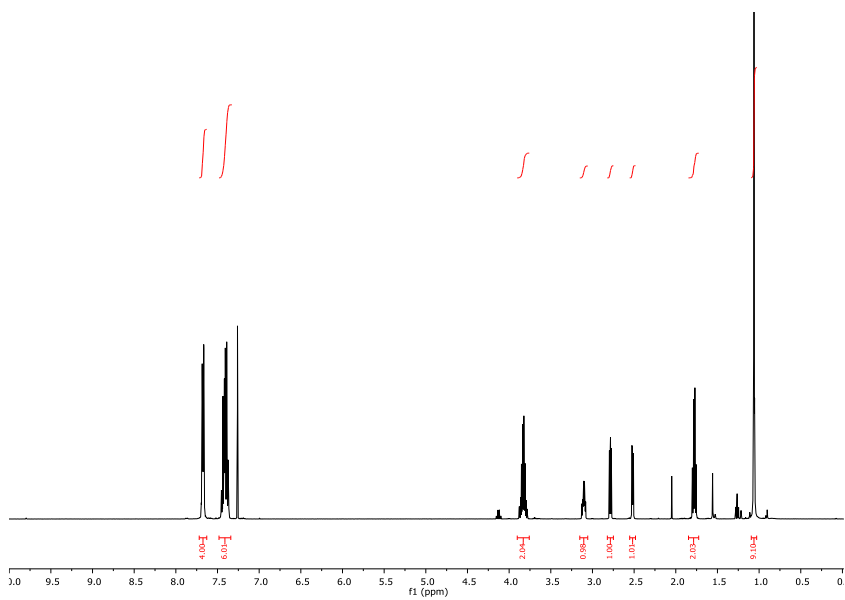
5.5. Synthesis of (+)-dactylolide (**62**)

(*R*)-*tert*-Butyl-(2-(oxiran-2-yl)ethoxy)diphenylsilane (**64**)

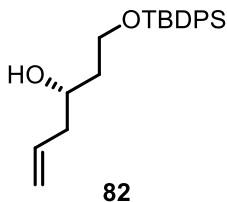


In a two-neck round-bottom flask, to a suspension of NaH (60% in mineral oil, 8.24 g, 343.27 mmol, 3.00 equiv., previously washed with hexane) in THF (150 mL) at $-16\text{ }^{\circ}\text{C}$ was added a solution of **81** (19.34 g, 114.42 mmol, 1.00 equiv.) in THF (100 mL) drop wise over a 15 min period under argon, keeping the temperature below $-10\text{ }^{\circ}\text{C}$ during the addition. A solution of TBDPSCl (33.02 g, 120.15 mmol, 1.05 equiv) in THF (75 mL) was added at that temperature after 30 min and the cooling bath was removed and allowed to reach room temperature. After 45 min, H_2O (100 mL) was added carefully at $0\text{ }^{\circ}\text{C}$ followed by saturated aqueous NH_4Cl (100 mL). The phases were separated and the aqueous phase was extracted with EtOAc (3 x 150 mL). The combined organic extracts were dried over MgSO_4 and concentrated *in vacuo*. The residue was purified by FC (EtOAc/Hex 1:30 \rightarrow 1:25) to give **64** (24.28 g, 74.37 mmol, 65%) as a colorless oil.

TLC: $R_f = 0.51$ (EtOAc/Hex 1:10, UV, CPS). **$^1\text{H-NMR}$** (400 MHz, CDCl_3): $\delta = 7.68\text{-}7.65$ (m, 4 H), $7.45\text{-}7.36$ (m, 6 H), $3.87\text{-}3.78$ (m, 2 H), $3.12\text{-}3.07$ (m, 1 H), 2.78 (dd, $J = 5.1, 4.1$, 1 H), 2.51 (dd, $J = 5.1, 2.8$, 1 H), $1.80\text{-}1.75$ (m, 2 H), 1.06 (s, 9 H). **$^{13}\text{C-NMR}$** (100 MHz, CDCl_3): $\delta = 135.7, 135.7, 133.8, 133.8, 129.8, 127.8, 61.0, 50.2, 47.4, 35.8, 26.9, 19.3$. **IR** (thin film): $\tilde{\nu} = 3070, 2956, 2930, 2857, 1472, 1427, 1389, 1110, 823, 738, 701\text{ cm}^{-1}$. **HRMS** (ESI): calcd for $\text{C}_{20}\text{H}_{26}\text{NaO}_2\text{Si}$ [(M+Na) $^+$]: 349.1594; found: 349.1587. **$[\alpha]_D^{24}$** : $+5.19^\circ$ ($c = 0.95, \text{CHCl}_3$).



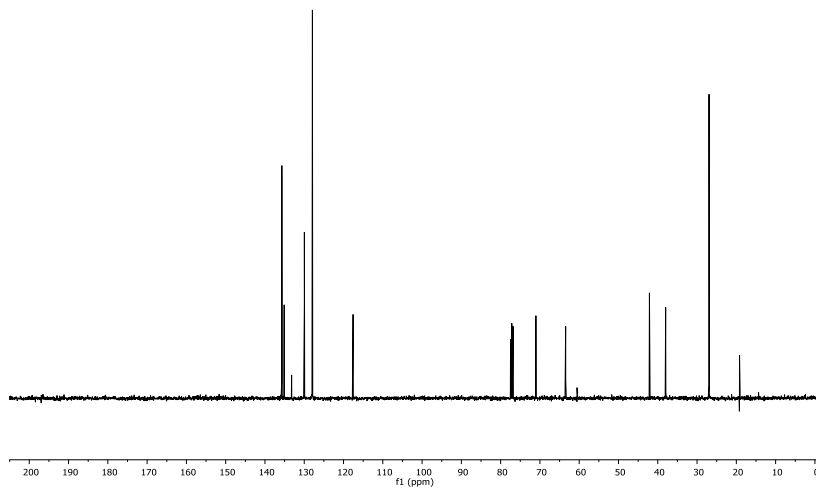
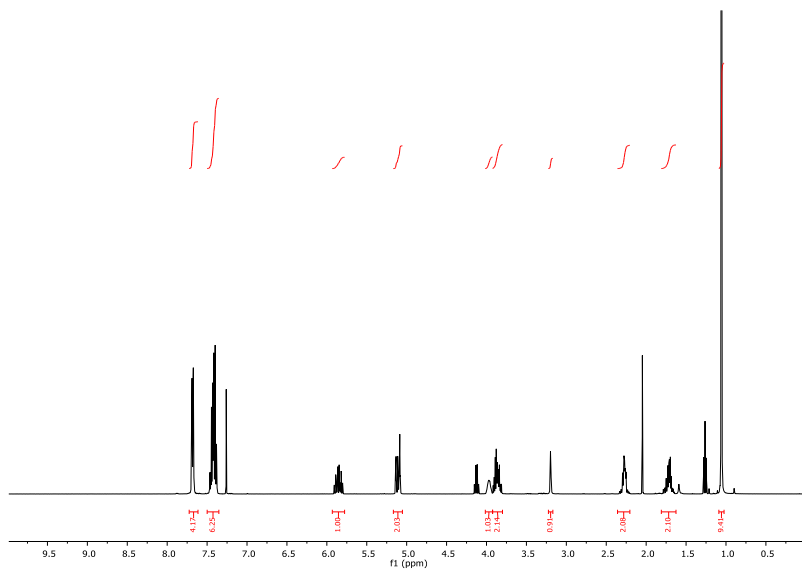
(*S*)-1-((*tert*-butyldiphenylsilyl)oxy)hex-5-en-3-ol (**82**)



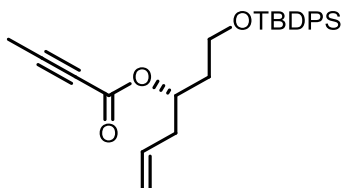
In a two-neck round-bottom flask, to a solution of vinylmagnesium bromide (1 M in THF, 70.50 mL, 70.50 mmol, 2.00 equiv.) was added CuI (671 mg, 3.52 mmol, 0.10 equiv.) at $-60\text{ }^{\circ}\text{C}$ under argon. After 5 min a solution of **74** (11.51 g, 35.25 mmol, 1.00 equiv.) in THF (45 mL) was added and the internal temperature was kept below $-55\text{ }^{\circ}\text{C}$ during the addition. The reaction was then allowed to rise slowly to $-30\text{ }^{\circ}\text{C}$ over a period of 1.5 h; then saturated aqueous NH_4Cl (90 mL) was added slowly, followed by H_2O (35 mL). The cooling bath was removed, the mixture was stirred for 15 min, 25% aqueous NH_4OH (18 mL) was added and stirred for additional 10 min. The phases were separated, the blue aqueous phase was extracted with EtOAc (3 x 50 mL), and the combined organic phases were dried over MgSO_4 . The organic layers were concentrated *in vacuo* and the residue was purified by FC (EtOAc/Hex 1:10 \rightarrow 1:5) afforded **82** (11.94 g, 33.67 mmol, 96%) as a pale-yellow, viscous oil.

TLC: $R_f = 0.40$ (EtOAc/Hex 1:5, UV, CPS). **$^1\text{H-NMR}$** (400 MHz, CDCl_3): $\delta = 7.69\text{--}7.67$ (m, 4 H), $7.46\text{--}7.38$ (m, 6 H), 5.85 (ddt, $J = 17.1, 10.2,$

7.2, 1 H), 5.14-5.08 (m, 2 H), 4.00-3.93 (m, 1 H), 3.91-3.81 (m, 2 H), 3.15 (d, $J = 2.6$, 1 H), 2.33-2.21 (m, 2 H), 1.78-1.65 (m, 2 H), 1.06 (s, 9 H). $^{13}\text{C-NMR}$ (100 MHz, CDCl_3): $\delta = 135.7, 135.7, 135.1, 133.2, 133.1, 129.9, 127.9, 117.5, 71.0, 63.5, 42.1, 38.0, 27.0, 19.2$. **IR** (thin film): $\tilde{\nu} = 3446, 3071, 2953, 2930, 2857, 1472, 1427, 1390, 1361, 1108, 1077, 997, 914, 822, 737, 700, 613, 503, 487 \text{ cm}^{-1}$. **HRMS** (ESI): calcd for $\text{C}_{22}\text{H}_{30}\text{NaO}_2\text{Si}$ [(M+Na) $^+$]: 377.1907; found: 377.1913. $[\alpha]_D^{24}$: -4.05° ($c = 1.21, \text{CHCl}_3$).



(S)-1-((tert-butyl)diphenylsilyloxy)hex-5-en-3-yl but-2-ynoate (**85**)

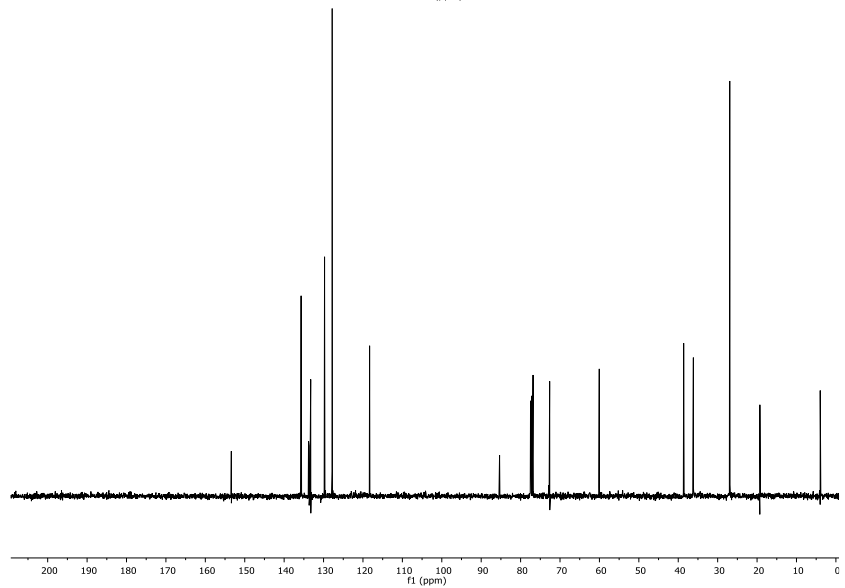
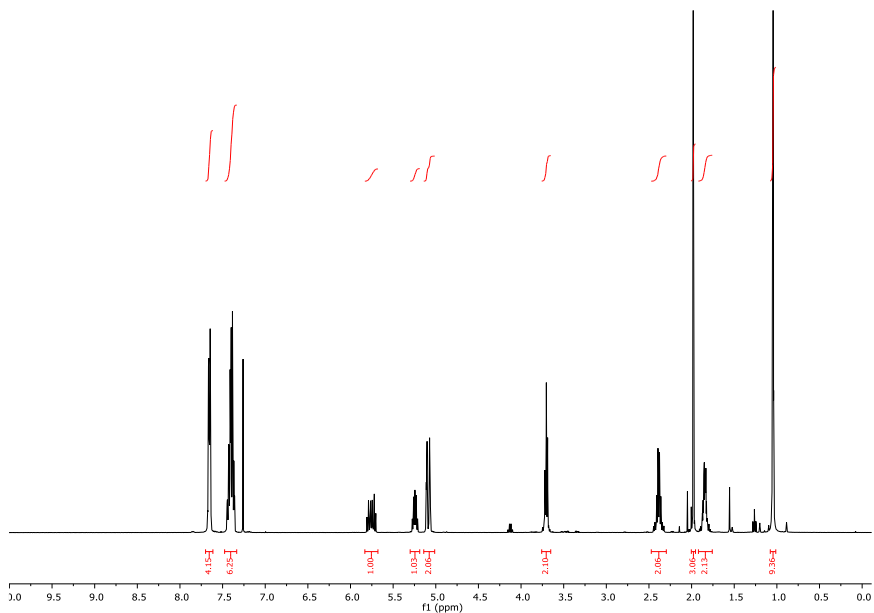


85

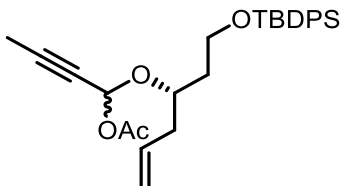
In a two-neck round-bottom flask, to a solution of **82** (11.94 g, 33.67 mmol, 1.00 equiv.) in dry DCM (100 mL) were added sequentially DMAP (0.41 g, 3.37 mmol, 0.10 equiv.), 2-butynoic acid (**75**) (3.11 g, 37.04 mmol, 1.10 equiv.), and a solution of DCC (8.34 g, 40.41 mmol, 1.20 equiv.) in DCM (100 mL) at 0 °C under argon. The resulting suspension was allowed to warm to room temperature and stirring was continued for 16 h. After the addition of Et₂O (650 mL), a precipitate was formed and the mixture was filtered. The filter cake was washed with Et₂O (300 mL) and the filtrate concentrated *in vacuo* to give a brown-red oil which was purified by FC (EtOAc/Hex 1:30), to give **85** (10.51 g, 24.99 mmol, 74%) as a colorless oil.

TLC: R_f = 0.44 (EtOAc/Hex 1:10, UV, CPS). ¹H-NMR (400 MHz, CDCl₃): δ = 7.67- 7.65 (m, 4 H), 7.46-7.37 (m, 6 H), 5.77 (ddt, J = 17.4, 9.7, 7.0, 1 H), 5.29-5.23 (m, 1 H), 5.13-5.07 (m, 2 H), 3.77-3.68 (m, 2 H), 2.46-2.34 (m, 2 H), 1.98 (s, 3 H), 1.89-1.83 (m, 2 H), 1.07 (s, 9 H). ¹³C-NMR (100 MHz, CDCl₃): δ = 153.3, 135.7, 135.6, 133.8, 133.6, 133.2, 129.7, 127.8,

118.2, 85.3, 72.8, 72.6, 60.0, 38.6, 36.1, 26.9, 19.2, 3.9. **IR** (thin film): $\tilde{\nu}$ = 3071, 3050, 2957, 2359, 2342, 2243, 1706, 1472, 1428, 1389, 1249, 1110, 1063, 700 cm^{-1} . **HRMS** (ESI): calcd for $\text{C}_{26}\text{H}_{32}\text{O}_3\text{Si}$ [(M+Na)⁺]: 443.2013; found: 443.2016. $[\alpha]_D^{24}$: +17.76° (c = 1.16, CHCl_3).



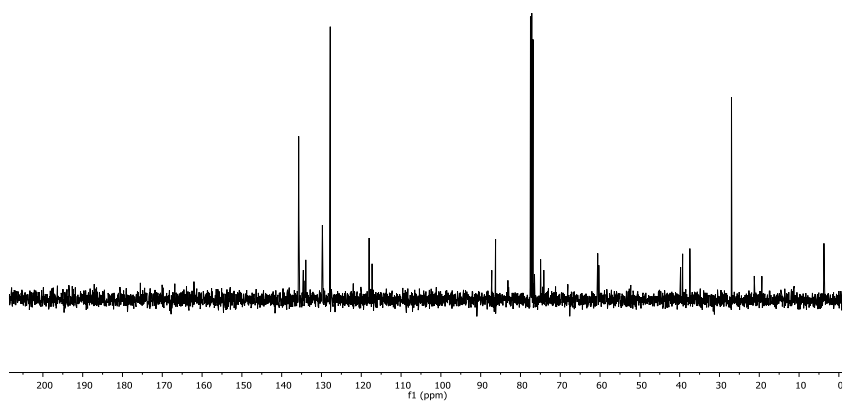
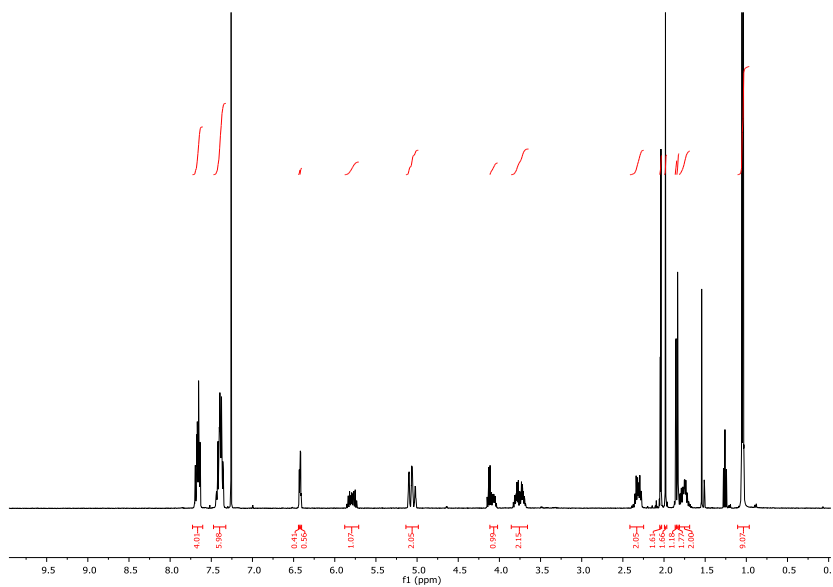
1-(((S)-1-((tert-butyl)diphenylsilyloxy)hex-5-en-3-yl)oxy)but-2-yn-1-yl acetate (**73**)

**73**

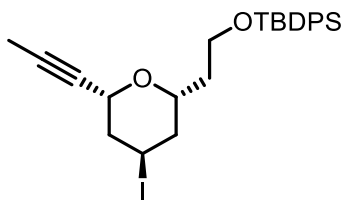
In a two-neck round-bottom flask, to a solution of **85** (10.51 g, 24.99 mmol, 1.00 equiv.) in DCM (200 mL) at $-78\text{ }^{\circ}\text{C}$ was added slowly DIBAL-H (1.2M in toluene, 42 mL, 49.97 mmol, 2.00 equiv.) under argon. After 30 min pyridine (6.06 mL, 74.96 mmol, 3.00 equiv.), DMAP (9.16 g, 74.96 mmol, 3.00 equiv.), and Ac_2O (14.17 mL, 149.92 mmol, 6.00 equiv.) were added sequentially at $-78\text{ }^{\circ}\text{C}$ and the mixture was stirred at that temperature for 22 h. Saturated aqueous NH_4Cl (120 mL) and saturated aqueous Rochelle salt (240 mL) were then added at $-78\text{ }^{\circ}\text{C}$ and the mixture was allowed to warm to room temperature and stirring was continued until the formation of two clear phases (about 90 min). The aqueous phase was extracted with DCM (3 x 200 mL) and the combined organic phases were washed with saturated aqueous NaHCO_3 (2 x 100 mL) and brine (50 mL, once), and then dried over MgSO_4 . Concentration of the solution *in vacuo* and purification of the residue by FC on deactivated stationary silica phase (EtOAc/Hex 1:30,

2% NEt₃ (v/v) afforded **73** (10.55 g, 22.70 mmol, 91%) as a 1.37:1 mixture of diastereomers as a colorless, viscous oil.

TLC: R_f = 0.40 (EtOAc/Hex 1:10, UV, CPS). **¹H-NMR** (400 MHz, CDCl₃): δ = 7.72- 7.66 (m, 4 H), 7.45-7.36 (m, 6 H), 6.45 (q, *J* = 1.8, 0.37 H), 6.44 (q, *J* = 1.8, 0.63 H), 5.87- 5.75 (m, 1 H), 5.12-5.02 (m, 2 H), 4.17-4.06 (m, 1 H), 3.85-3.71 (m, 2 H), 2.41-2.30 (m, 2 H), 2.05 (s, 1.12 H), 1.99 (s, 1.88 H), 1.86 (d, *J* = 1.8, 1.15 H), 1.84 (d, *J* = 1.8, 1.85 H), 1.83-1.71 (m, 2 H), 1.07 (s, 3.38 H), 1.06 (s, 5.62 H). **¹³C-NMR** (100 MHz, CDCl₃): δ = 169.9, 169.7, 135.7, 135.7, 135.6, 135.6, 134.5, 134.1, 134.0, 133.9, 133.9, 129.7, 129.7, 129.7, 127.8, 127.8, 118.0, 117.2, 87.2, 86.2, 83.1, 82.9, 76.4, 74.9, 74.4, 74.1, 60.6, 60.3, 39.7, 39.2, 37.4, 37.4, 27.0, 26.9, 21.2, 21.2, 19.3, 19.3, 3.7, 3.7. **IR** (thin film): $\tilde{\nu}$ = 3072, 2956, 2857, 2259, 1740, 1472, 1370, 1228, 1082, 903, 822, 701 cm⁻¹. **HRMS** (ESI): calcd for C₂₈H₃₆NaO₄Si [(M+Na)⁺]: 487.2275; found: 487.2272. **[α]_D²⁴**: +19.58° (c = 1.42, CHCl₃).



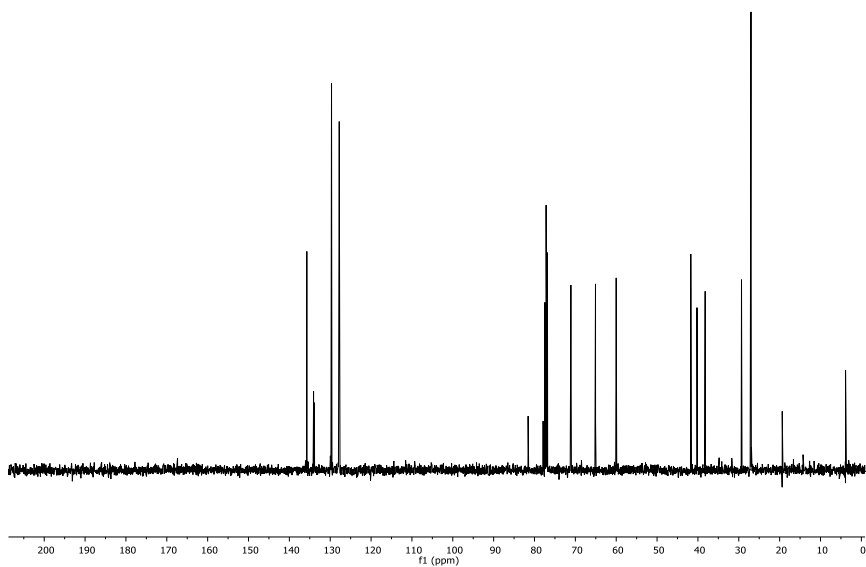
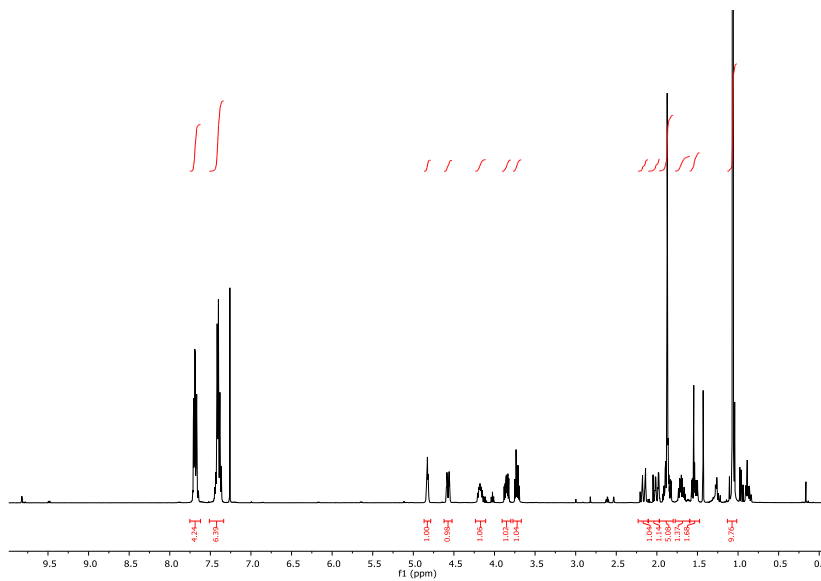
tert-butyl(2-((2*R*,4*R*,6*R*)-4-iodo-6-(prop-1-yn-1-yl)tetrahydro-2*H*-pyran-2-yl)ethoxy)diphenylsilane (**86**)

**86**

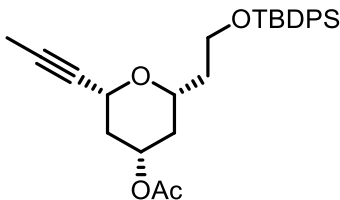
In a two-neck round-bottom flask, to a solution of **73** (9.00 g, 19.36 mmol, 1.00 equiv.) in DCM (200 mL) at $-19\text{ }^{\circ}\text{C}$ was added 2,6-lutidine (0.45 mL, 3.87 mmol, 0.20 equiv.) followed by slow addition of TMSI (6.89 mL, 48.42 mmol, 2.50 equiv.) under argon. The cooling bath was removed after 10 min and the yellow solution was allowed to warm to room temperature. After 45 min saturated aqueous NaHCO_3 (80 mL) was carefully added, the phases were separated, and the aqueous layer was extracted with DCM (3 x 50 mL). The combined organic phases were dried over MgSO_4 and concentrated under reduced pressure. Purification of the residue by FC (EtOAc/Hex 1:40 \rightarrow 1:15) afforded **86** (7.57 g, 14.21 mmol, 73%) as a pale-yellow, viscous oil.

TLC: $R_f = 0.45$ (EtOAc/Hex 1:10, UV, CPS). **$^1\text{H-NMR}$** (400 MHz, CDCl_3) $\delta = 7.71\text{--}7.67$ (m, 4 H), 7.44–7.36 (m, 6 H), 4.83 (quin, $J = 3.1$, 1 H), 4.57 (br. dquin, $J = 10.8$, 2.1, 1 H), 4.21–4.15 (m, 1 H), 3.86 (ddd, $J = 10.5$,

8.2, 4.9, 1 H), 3.73 (dt, $J = 10.3, 5.4$, 1 H), 2.16 (dq, $J = 14.8, 2.3$, 1 H), 1.99 (ddd, $J = 14.7, 2.4, 2.1$, 1 H), 1.93-1.82 (m, 2 H), 1.87 (d, $J = 2.1$, 3 H), 1.69 (ddt, $J = 13.7, 8.3, 5.3$, 1 H), 1.57-1.50 (m, 1 H), 1.07 (s, 9 H). **$^{13}\text{C-NMR}$** (100 MHz, CDCl_3): $\delta = 135.7, 135.7, 134.1, 133.9, 129.7, 127.8, 127.8, 81.5, 77.9, 71.1, 65.1, 60.1, 41.8, 40.3, 38.3, 29.3, 27.0, 19.4, 3.8$. **IR** (thin film): $\tilde{\nu} = 3070, 2953, 2856, 2360, 2341, 1472, 1427, 1389, 1232, 1107, 1095, 1049, 822, 737, 702 \text{ cm}^{-1}$. **HRMS** (EI): calcd for $\text{C}_{26}\text{H}_{34}\text{IO}_2\text{Si}$ [(M+H) $^+$]: 533.1367; found: 533.1357. **$[\alpha]_D^{24}$** : $+2.03^\circ$ (c = 1.23, CHCl_3).



(2*R*,4*S*,6*R*)-2-(2-((*tert*-butyldiphenylsilyl)oxy)ethyl)-6-(prop-1-yn-1-yl)tetrahydro-2*H*-pyran-4-yl acetate (**87**)

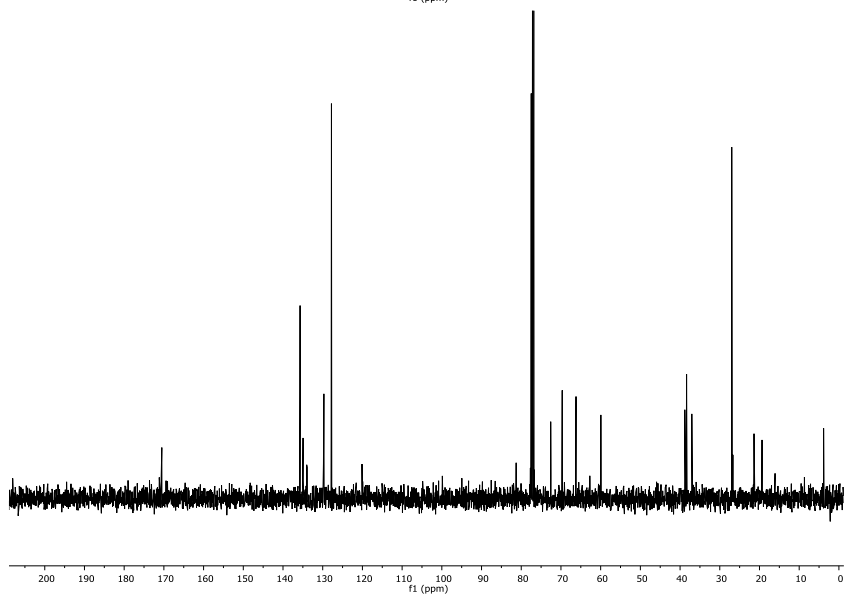
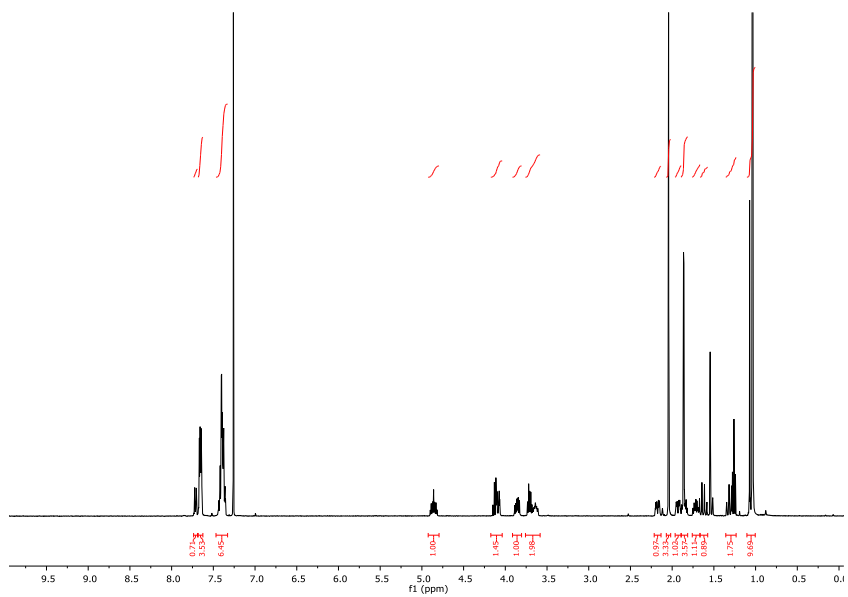


87

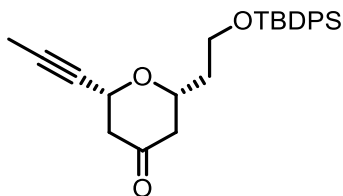
To a solution of **86** (7.42 g, 13.93 mmol, 1.00 equiv.) in toluene (600 mL), a solution of 18-crown-6 (14.73 g, 55.73 mmol, 4.00 equiv.) in toluene (100 mL) was added, followed by CsOAc (26.74 g, 139.33 mmol, 10.00 equiv.) at room temperature and the mixture was heated to 55 °C for 4 d. The reaction was cooled to room temperature and H₂O (200 mL) and EtOAc (200 mL) were added. The phases were separated and the aqueous layer was extracted with EtOAc (3 x 150 mL). The combined organic extracts were washed with brine (200 mL, once), dried over MgSO₄ and concentrated *in vacuo*. Purification of the residue by FC (EtOAc/Hex 1:25→1:10) afforded **87** (4.83 g, 10.39 mmol, 75%) as a colorless, viscous oil.

TLC: *R*_f = 0.29 (EtOAc/Hex 1:10, UV, CPS or KMnO₄). **¹H-NMR** (400 MHz, CDCl₃): δ = 7.67-7.64 (m, 4 H), 7.44-7.36 (m, 6 H), 4.86 (tt, *J* = 11.3, 4.8, 1 H), 4.09 (dquin, *J* = 11.6, 2.1, 1 H), 3.87 (ddd, *J* = 10.3, 8.3, 4.9, 1 H), 3.72 (dt, *J* = 10.3, 5.4, 1 H), 3.67-3.61 (m, 1 H), 2.18 (dddd, *J* = 12.6,

4.9, 2.4, 2.1, 1 H), 2.04 (s, 3 H), 1.94 (dddd, $J = 12.3, 4.8, 2.4, 1.8, 1 \text{ H}$), 1.89-1.82 (m, 1 H), 1.86 (d, $J = 2.1, 3 \text{ H}$), 1.72 (ddt, $J = 14.1, 8.4, 5.4, 1 \text{ H}$), 1.64 (dd, $J = 23.9, 11.5, 1 \text{ H}$), 1.31 (dd, $J = 23.6, 11.5, 1 \text{ H}$), 1.05 (s, 9 H). $^{13}\text{C-NMR}$ (100 MHz, CDCl_3): $\delta = 170.5, 135.7, 135.7, 134.9, 134.1, 133.9, 129.7, 129.7, 127.8, 81.2, 77.7, 72.6, 69.7, 66.2, 60.0, 38.8, 38.4, 37.1, 27.0, 21.3, 19.3, 3.8$. **IR** (thin film): $\tilde{\nu} = 3071, 2956, 2856, 2360, 2342, 1740, 1472, 1428, 1389, 1237, 1109, 1063, 1031, 907, 822 \text{ cm}^{-1}$. **HRMS** (ESI): calcd for $\text{C}_{28}\text{H}_{37}\text{O}_4\text{Si}$ [(M+H) $^+$]: 465.2456; found: 465.2461. $[\alpha]_D^{24}$: $+12.36^\circ$ ($c = 0.72, \text{CHCl}_3$).



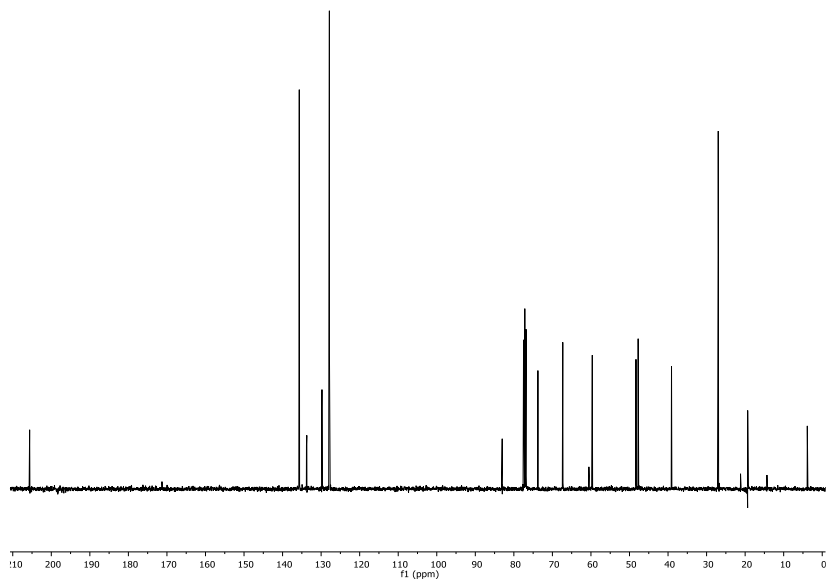
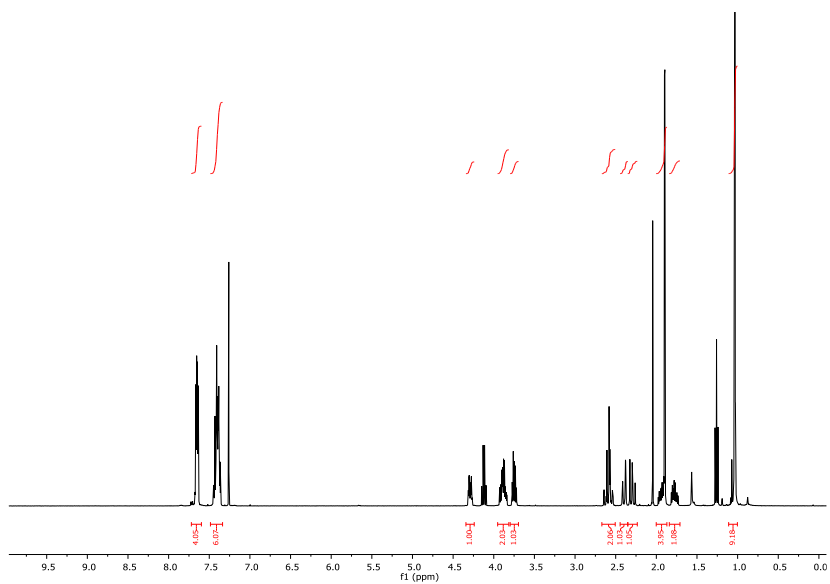
(2R,6R)-2-(2-((tert-butylidiphenylsilyl)oxy)ethyl)-6-(prop-1-yn-1-yl)dihydro-2H-pyran-4(3H)-one (**88**)

**88**

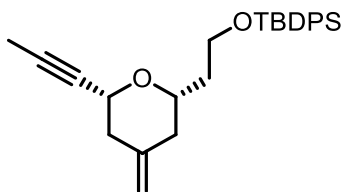
To a stirred solution of **87** (4.83 g, 10.39 mmol, 1.00 equiv.) in MeOH (200 mL) K_2CO_3 (14.37 g, 103.94 mmol, 10.00 equiv.) and H_2O (10 mL) were added and the mixture was stirred for 3 h at room temperature. Brine (100 mL) and EtOAc (100 mL) were then added and the phases separated. The aqueous phase was extracted with EtOAc (3 x 50 mL) and the combined organic extracts were dried over $MgSO_4$ and concentrated *in vacuo*.

The crude product was dissolved in DCM (100 mL) and DMP (6.61 g, 15.59 mmol, 1.50 equiv.) was added under argon and the mixture was stirred for 2 h. A mixture of saturated aqueous $Na_2S_2O_3$ (50 mL) and saturated aqueous $NaHCO_3$ (50 mL) was then added and stirring was continued for 10 min. The phases were separated, the aqueous phase was extracted with DCM (3 x 100 mL), and the combined organic extracts were dried over $MgSO_4$ and concentrated *in vacuo*. Purification of the residue by FC (EtOAc/Hex 1:10→1:5) gave **88** (3.40 g, 8.08 mmol, 78% over two steps) as a colorless oil.

TLC: $R_f = 0.33$ (EtOAc/Hex 1:5, UV, CPS or KMnO_4). **$^1\text{H-NMR}$** (400 MHz, CDCl_3): $\delta = 7.67\text{-}7.63$ (m, 4 H), $7.45\text{-}7.36$ (m, 6 H), 4.29 (ddq, $J = 10.3, 4.1, 2.1, 1$ H), $3.93\text{-}3.83$ (m, 2 H), 3.75 (dt, $J = 10.4, 5.3, 1$ H), 2.61 (dd, $J = 15.0, 10.5, 1$ H), 2.56 (ddd, $J = 15.0, 4.0, 1.6, 1$ H), 2.39 (ddd, $J = 14.6, 2.6, 1.6, 1$ H), 2.29 (dd, $J = 14.6, 11.6, 1$ H), 1.97- 1.88 (m, 1 H), 1.89 (d, $J = 2.1, 3$ H), 1.82-1.73 (m, 1 H), 1.04 (s, 9 H). **$^{13}\text{C-NMR}$** (100 MHz, CDCl_3): $\delta = 205.6, 135.7, 135.7, 133.8, 133.8, 129.8, 129.8, 127.9, 83.0, 77.0, 73.8, 67.3, 59.7, 48.3, 47.8, 39.1, 27.0, 19.3, 3.9$. **IR** (thin film): $\tilde{\nu} = 2955, 2927, 2856, 1722, 1473, 1427, 1337, 1227, 1109, 1086, 702$ cm^{-1} . **HRMS** (ESI): calcd for $\text{C}_{26}\text{H}_{32}\text{NaO}_3\text{Si}$ $[(\text{M}+\text{Na})^+]$: 443.2013; found: 443.2018. **$[\alpha]_D^{24}$** : $+22.36^\circ$ ($c = 0.89, \text{CHCl}_3$).

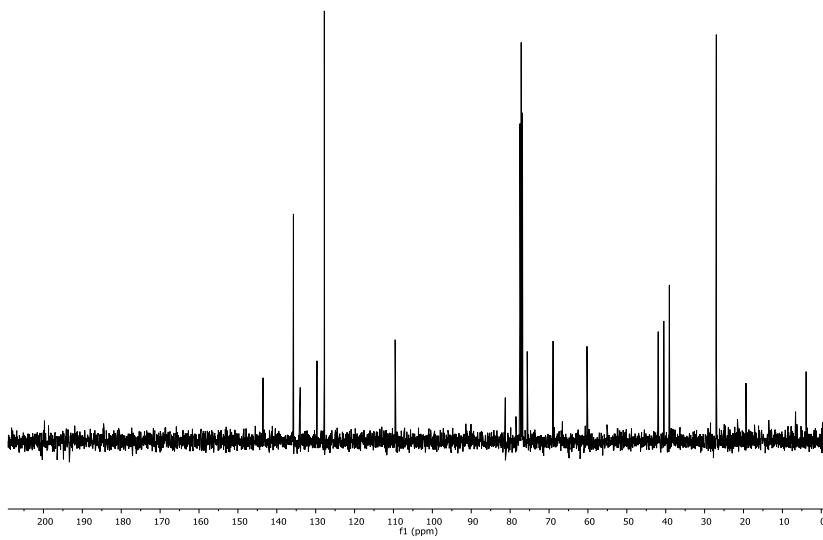
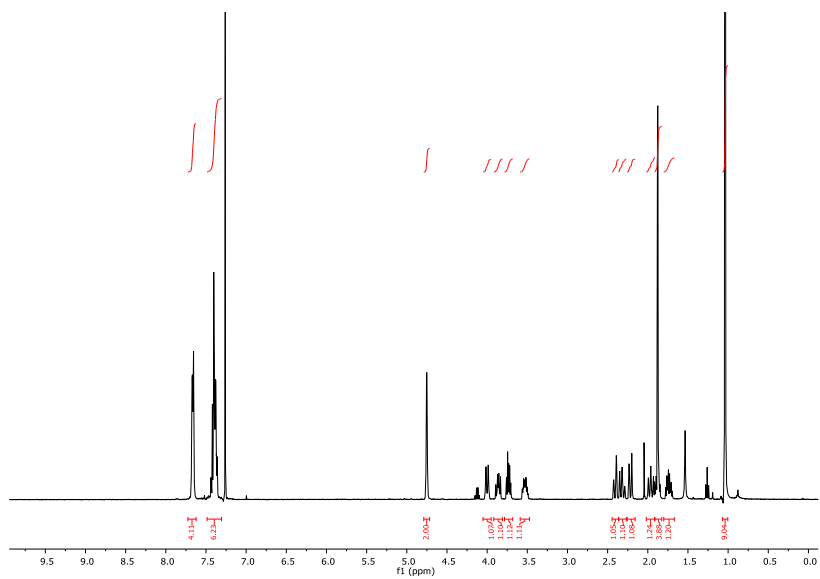


tert-butyl(2-((2*S*,6*R*)-4-methylene-6-(prop-1-yn-1-yl)tetrahydro-2*H*-pyran-2-yl)ethoxy)diphenylsilane (**89**)

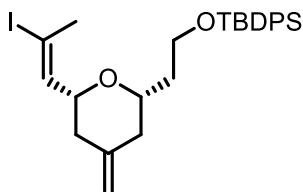
**89**

In a two-neck round-bottom flask, to a solution of MePh₃PBr (5.78 g, 16.17 mmol, 2.00 equiv.) in THF (45 mL) *n*-BuLi (1.6M in hexane, 9.60 mL, 15.36 mmol, 1.90 equiv.) was added at -78 °C under argon. After stirring for 15 min at -78 °C the temperature was allowed to rise to 0 °C and stirring was continued for 30 min. Then a solution of **78** (3.40 g, 8.08 mmol, 1.00 equiv.) in THF (25 mL) was added at that temperature and the mixture was then heated to 50 °C for 90 min. After cooling to room temperature H₂O (25 mL) and EtOAc (25 mL) were added, the phases were separated, and the aqueous phase was extracted with EtOAc (3 x 25 mL). The organic extracts were dried over MgSO₄ and the solution was concentrated *in vacuo*. Purification of the residue by FC (EtOAc/Hex 1:100→1:50) gave **89** (2.62 g, 6.23 mmol, 77%) as a colorless oil.

TLC: $R_f = 0.62$ (EtOAc/Hex 1:10, UV, CPS). **$^1\text{H-NMR}$** (400 MHz, CDCl_3): $\delta = 7.68-7.65$ (m, 4 H), 7.44-7.35 (m, 6 H), 4.76-4.74 (m, 2 H), 4.00 (ddq, $J = 11.0, 2.4, 2.1, 1$ H), 3.87 (ddd, $J = 10.2, 8.1, 5.0, 1$ H), 3.74 (dt, $J = 10.2, 5.5, 1$ H), 3.56-3.50 (m, 1 H), 2.43-2.39 (m, 1 H), 2.36-2.29 (m, 1 H), 2.24-2.20 (m, 1 H), 2.00-1.93 (m, 1 H), 1.92-1.85 (m, 1 H), 1.88 (d, $J = 2.1, 3$ H), 1.78-1.70 (m, 1 H), 1.04 (s, 9 H). **$^{13}\text{C-NMR}$** (100 MHz, CDCl_3): $\delta = 143.5, 135.7, 135.7, 134.1, 134.0, 129.7, 129.7, 127.8, 109.6, 81.2, 78.5, 75.6, 69.0, 60.3, 42.0, 40.5, 39.1, 27.0, 19.3, 3.9$. **IR** (thin film): $\tilde{\nu} = 3071, 2944, 2931, 2857, 2360, 2342, 1651, 1472, 1427, 1389, 1345, 1110, 1089, 1060, 998, 894, 823, 702$ cm^{-1} . **HRMS** (ESI): calcd for $\text{C}_{27}\text{H}_{34}\text{O}_2\text{NaSi}$ $[(\text{M}+\text{Na})^+]$: 441.2220; found: 441.2230. **$[\alpha]_D^{24}$** : $+4.29^\circ$ ($c = 1.19, \text{CHCl}_3$).



tert-butyl(2-((2*S*,6*R*)-6-((*E*)-2-iodoprop-1-en-1-yl)-4-methylenetetrahydro-2*H*-pyran-2-yl)ethoxy)diphenylsilane (**72**)

**72**

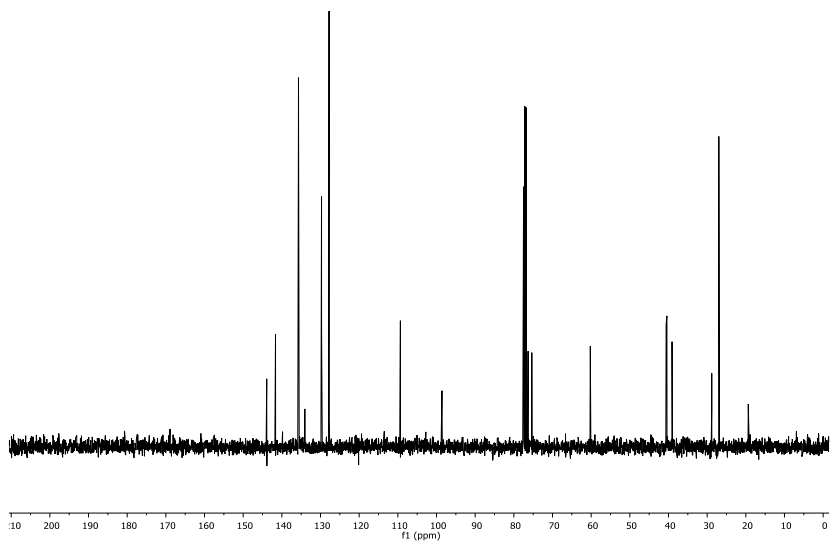
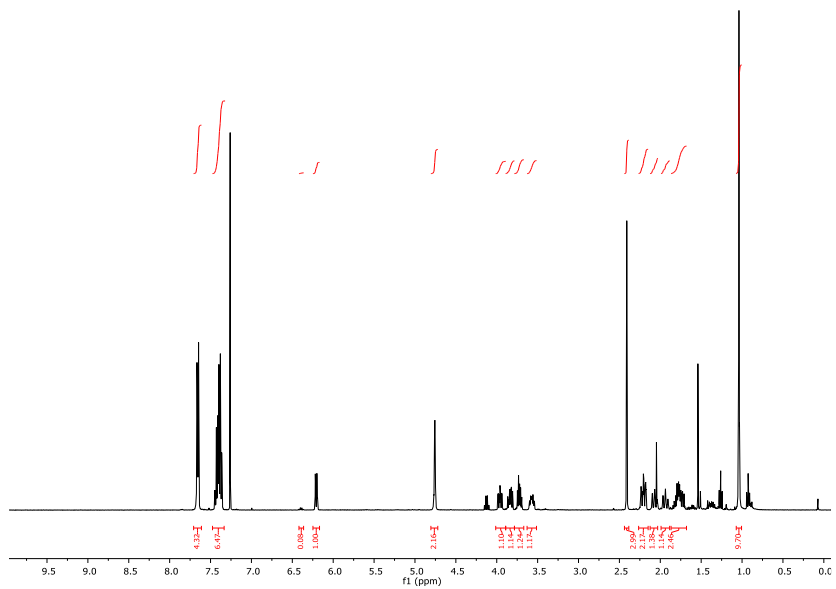
In a two-neck round-bottom flask, to a suspension of CuCN (2.14 g, 23.89 mmol, 5.00 equiv.) in THF (50 mL) at $-78\text{ }^{\circ}\text{C}$, a solution of *n*-BuLi (1.6M in hexane, 29.9 mL, 47.77 mmol, 10.00 equiv.) was added under argon. After 5 min the flask was immersed in a cooling bath at $-40\text{ }^{\circ}\text{C}$, resulting in the formation of a clear pale-yellow solution. The mixture was cooled back to $-78\text{ }^{\circ}\text{C}$ after 10 min and the mixture became heterogeneous. Neat Bu₃SnH (12.85 mL, 47.77 mmol, 10.00 equiv.) was then added dropwise, leading to a turbid yellow solution with development of gas. After 20 min at $-78\text{ }^{\circ}\text{C}$ the mixture was stirred for 5 min at $-40\text{ }^{\circ}\text{C}$, giving an almost clear golden-yellow solution. After 10 min at $-40\text{ }^{\circ}\text{C}$ the solution was cooled to $-78\text{ }^{\circ}\text{C}$ and MeOH (21.31 mL, 525.50 mmol, 110.00 equiv.) was added. After 10 min at $-78\text{ }^{\circ}\text{C}$ the flask was immersed in a cooling bath at $-40\text{ }^{\circ}\text{C}$ and the reaction mixture turned into a clear red solution. After 10 min at $-40\text{ }^{\circ}\text{C}$ this solution was

cooled back to $-78\text{ }^{\circ}\text{C}$ and a solution of **79** (2.00 g, 4.78 mmol, 1.00 equiv.) in THF (32 mL) was added. The mixture was then kept into the freezer at $-20\text{ }^{\circ}\text{C}$ for 15 h. A mixture of saturated aqueous NH_4Cl (100 mL) and 25% aqueous NH_4OH (20 mL) and EtOAc (50 mL) were added to the reaction mixture and kept stirring for 30 min. The two almost clear phases were separated, and the aqueous phase was extracted with EtOAc (3 x 50 mL). The organic extracts were dried over MgSO_4 , the solution was concentrated *in vacuo*. Purification of the residue by FC on deactivated silica (Hex \rightarrow EtOAc/Hex 1:100 \rightarrow 1:50, 1% (v/v) NEt_3) gave the vinylstannane as a pale-yellow oil which was used immediately.

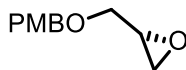
A solution of the vinylstannane in THF (35 mL) was cooled to $-17\text{ }^{\circ}\text{C}$ followed by addition of NIS (1.61 g, 7.17 mmol, 1.50 equiv.) in THF (7 mL) under argon, to give an almost clear yellow solution. After 10 min a mixture of saturated aqueous $\text{Na}_2\text{S}_2\text{O}_3$ (20 mL) and saturated aqueous NaHCO_3 (20 mL) was added followed by EtOAc (20 mL). Stirring was continued until two clear, colorless phases were formed. The phases were separated and the aqueous phase was extracted with EtOAc (3 x 20 mL). The combined organic extracts were dried over MgSO_4 and then concentrated *in vacuo*. The residue was purified by FC (EtOAc/Hex 1:50 \rightarrow 1:25) to afford the desired product **72** (2.35 g, 4.30 mmol, 90% over two steps) as a pale yellow oil.

TLC: $R_f = 0.64$ (EtOAc/Hex 1:20, UV, CPS). $^1\text{H-NMR}$ (400 MHz, CDCl_3): $\delta = 7.70\text{--}7.67$ (m, 4 H), $7.47\text{--}7.38$ (m, 6 H), 6.24 (dq, $J = 7.7, 1.5, 1$ H), 4.81-4.77 (m, 2 H), 3.99 (ddd, $J = 10.8, 7.7, 2.6, 1$ H), 3.87 (ddd, $J = 10.1, 8.1, 5.4, 1$ H), 3.76 (dt, $J = 10.1, 5.6, 1$ H), 3.64-3.57 (m, 1 H), 2.44 (d, $J =$

1.5, 3 H), 2.27-2.20 (m, 2 H), 2.13-2.06 (m, 1 H), 2.00-1.94 (m, 1 H), 1.87-1.73 (m, 2 H), 1.08 (s, 9 H). $^{13}\text{C-NMR}$ (100 MHz, CDCl_3): δ = 141.6, 135.6, 135.6, 134.0, 133.9, 129.7, 127.7, 109.3, 98.5, 76.3, 75.3, 60.2, 40.6, 40.4, 39.0, 28.8, 26.9, 19.3. **IR** (thin film): $\tilde{\nu}$ = 3070, 2931, 2890, 2856, 1651, 1472, 1427, 1360, 1105, 1087, 998, 858, 700 cm^{-1} . **HRMS** (ESI): calcd for $\text{C}_{27}\text{H}_{36}\text{IO}_2\text{Si}$ [(M+H) $^+$]: 547.1524; found: 547.1521. $[\alpha]_D^{24}$: -1.53° (c = 0.85, CHCl_3).



(R)-2-(((4-methoxybenzyl)oxy)methyl)oxirane (**70**)

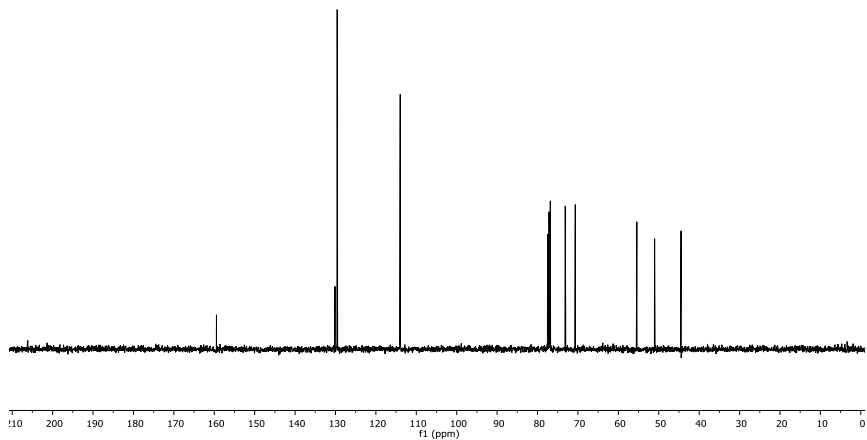
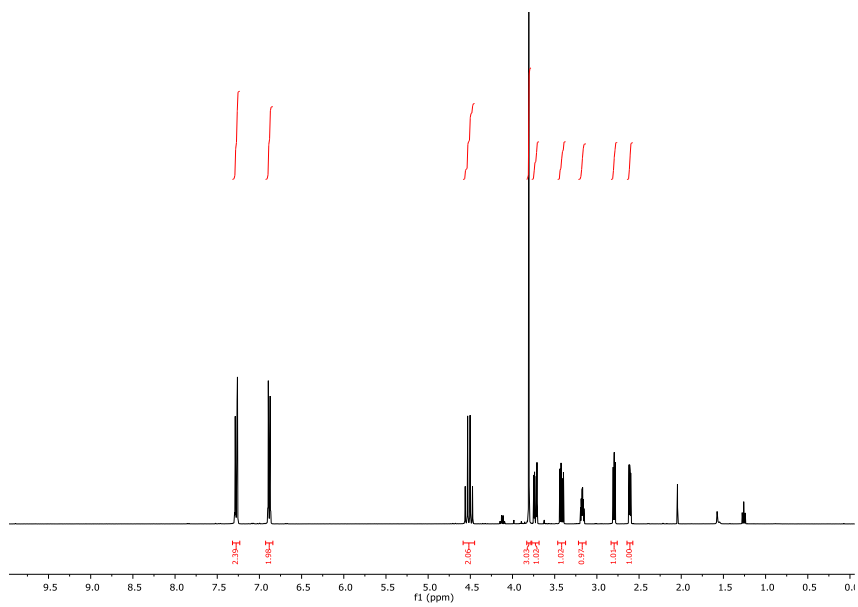


70

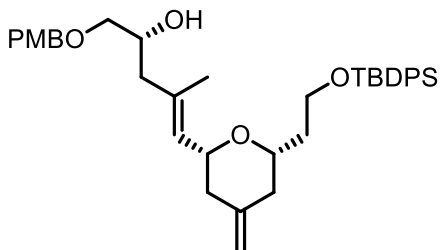
In a two-neck round-bottom flask, to a suspension of NaH (60% in mineral oil, 3.23 g, 80.99 mmol, 1.20 equiv., previously washed with hexane) in dry DMF (70 mL) at 0 °C a solution of (S)-glycidol (4.48 g, 67.49 mmol, 1.00 equiv.) in DMF (9 mL) was added under argon. After stirring for 30 min at 0 °C 4-methoxybenzyl chloride (12.68 g, 80.99 mmol, 1.20 equiv.) was slowly added followed by a spatula tip of TBAI. The mixture was allowed to warm to room temperature and stirred for 20 h. H₂O (90 mL) was then added carefully followed by EtOAc (45 mL); the phases were separated and the aqueous phase was extracted with Et₂O (3 x 100 mL). The combined organic extracts were dried over MgSO₄, concentrated *in vacuo*, and the residue was purified by FC (EtOAc/Hex 1:10→1:5→1:3) to give **70** (6.84 g, 35.22 mmol, 52.2%) as a colorless oil.

TLC: R_f = 0.31 (EtOAc/Hex 1:3, UV, CPS). ¹H-NMR (400 MHz, CDCl₃): δ = 7.29-7.26 (m, 2 H), 6.90-6.86 (m, 2 H), 4.54 (d, J = 11.6, 1 H), 4.49 (d, J = 11.6, 1 H), 3.81 (s, 3 H), 3.73 (dd, J = 11.4, 3.1, 1 H), 3.42 (dd, J = 11.4, 5.8, 1 H), 3.19-3.15 (m, 1 H), 2.79 (dd, J = 5.0, 4.2, 1 H), 2.60 (dd, J

= 5.1, 2.7, 1 H). $^{13}\text{C-NMR}$ (100 MHz, CDCl_3): δ = 159.5, 130.1, 129.6, 114.0, 73.1, 70.7, 55.4, 51.0, 44.5. **IR** (thin film): $\tilde{\nu}$ = 2999, 2934, 2836, 1731, 1612, 1512, 1464, 1384, 1301, 1244, 1174, 1086, 1031, 818 cm^{-1} . **HRMS** (ESI): calcd for $\text{C}_{11}\text{H}_{14}\text{NaO}_3$ $[(\text{M}+\text{Na})^+]$: 217.0835; found: 217.0840. $[\alpha]_D^{24}$: +3.68° (c = 0.98, CHCl_3).



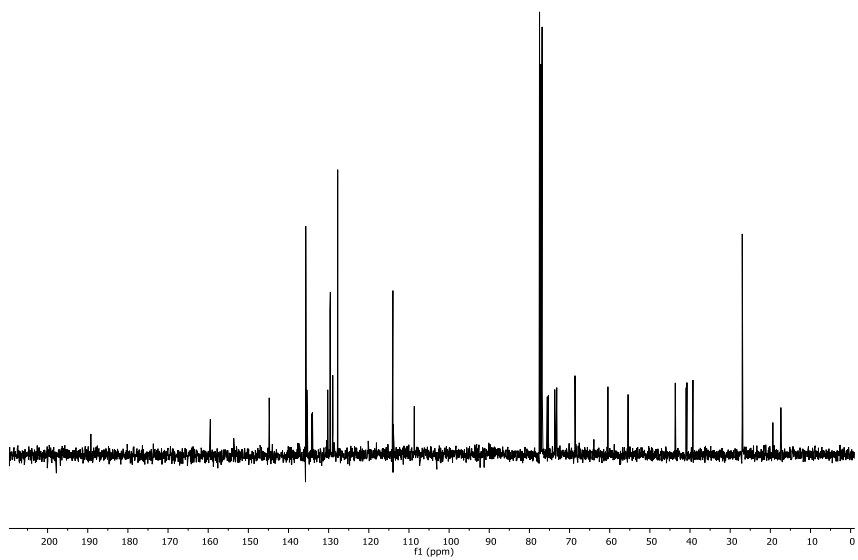
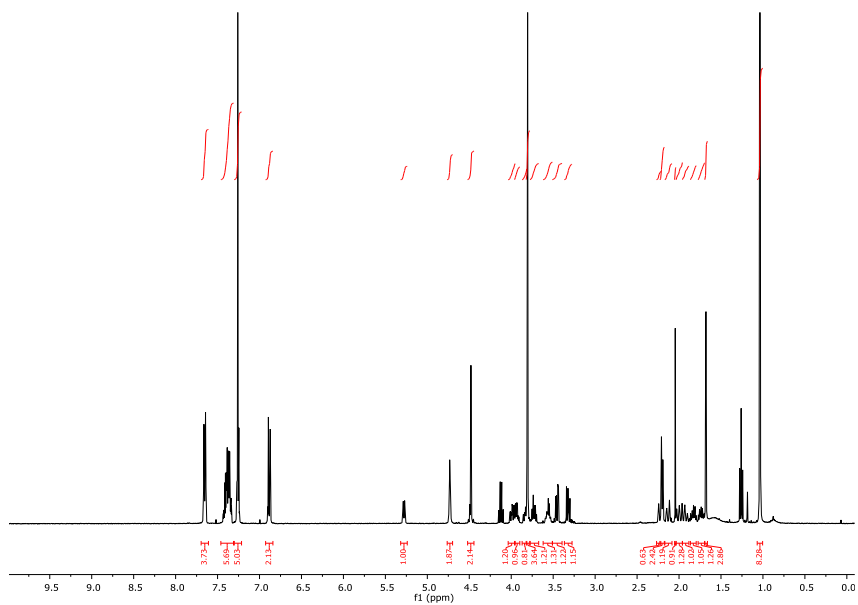
(*R,E*)-5-((2*R,6S*)-6-(2-((*tert*-butyldiphenylsilyl)oxy)ethyl)-4-methylenetetrahydro-2*H*-pyran-2-yl)-1-((4-methoxybenzyl)oxy)-4-methylpent-4-en-2-ol (**68**)

**68**

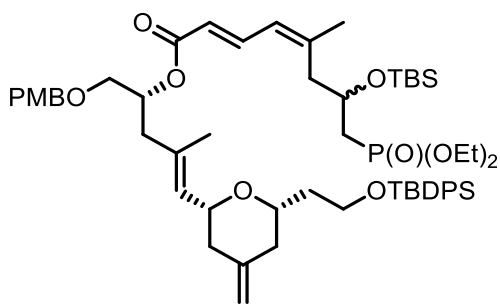
In a two-neck round-bottom flask, vinyl iodide **72** (490 mg, 0.90 mmol, 1.00 equiv., azeotropically dried twice with 2 mL of toluene right before use) was dissolved in dry toluene (9 mL) and the solution was cooled to $-78\text{ }^{\circ}\text{C}$ under argon. $t\text{BuLi}$ (1.6M in pentane, 1.10 mL, 1.79 mmol, 2.00 equiv.) was then added and the colorless solution was stirred for 30 min. The reaction mixture was then cooled to around -85 to $-90\text{ }^{\circ}\text{C}$ and a solution of **70** (435 mg, 2.24 mmol, 2.50 equiv., azeotropically dried twice with 2 mL of toluene right before use) in dry toluene (2.6 mL) was added followed by $\text{BF}_3 \cdot \text{OEt}_2$ (0.28 mL, 2.24 mmol, 2.50 equiv.; addition ca. 1 min after the addition of **70**) giving a pale yellow solution. The reaction was stirred at $-78\text{ }^{\circ}\text{C}$ for 1 h. The cooling bath was removed and saturated aqueous NaHCO_3 (13 mL) and EtOAc

(13 mL) were added. The phases were separated and the aqueous phase was extracted with EtOAc (3 x 6 mL). The combined organic extracts were dried over MgSO₄, concentrated *in vacuo*, and the residue purified by FC (EtOAc/Hex 1:5) to give **68** (323 mg, 0.53 mmol, 59%) as a colorless oil.

TLC: R_f = 0.17 (EtOAc/Hex 1:5, UV, CPS). **¹H-NMR** (400 MHz, CDCl₃): δ = 7.68-7.65 (m, 4 H), 7.44-7.34 (m, 6 H), 7.28-7.24 (m, 2 H), 6.90-6.87 (m, 2 H), 5.29 (dq, J = 7.7, 1.2, 1 H), 4.75-4.73 (m, 2 H), 4.49 (s, 2 H), 3.99 (ddd, J = 10.9, 7.7, 2.7, 1 H), 3.98-3.91 (m, 1 H), 3.84 (ddd, J = 10.1, 8.0, 5.5, 1 H), 3.80 (s, 3 H), 3.74 (dt, J = 10.1, 5.7, 1 H), 3.60-3.54 (m, 1 H), 3.46 (dd, J = 9.5, 3.5, 1 H), 3.33 (dd, J = 9.5, 7.1, 1 H), 2.31 (d, J = 3.5, 1 H), 2.25-2.22 (m, 1 H), 2.20 (d, J = 6.8, 2 H), 2.16-2.12 (m, 1 H), 2.04-2.00 (m, 1 H), 1.97-1.90 (m, 1 H), 1.89-1.80 (m, 1 H), 1.77-1.71 (m, 1 H), 1.69 (d, J = 1.2, 3 H), 1.05 (s, 9 H). **¹³C-NMR** (100 MHz, CDCl₃): δ = 159.4, 144.7, 135.7, 135.7, 135.4, 134.1, 134.0, 130.2, 129.7, 129.5, 129.0, 127.7, 127.7, 114.0, 108.7, 75.5, 75.3, 73.7, 73.2, 68.6, 60.4, 55.4, 43.7, 41.0, 40.7, 39.2, 27.0, 19.4, 17.3. **IR** (thin film): $\tilde{\nu}$ = 3070, 2932, 2857, 1612, 1513, 1471, 1427, 1247, 1106, 1087, 1058, 1036, 998, 821, 702 cm⁻¹. **HRMS** (ESI): calcd for C₃₈H₅₁O₅Si [(M+Na)⁺]: 615.3500; found: 615.3494. **[α]_D²⁴**: -7.21° (c = 0.86, CHCl₃).



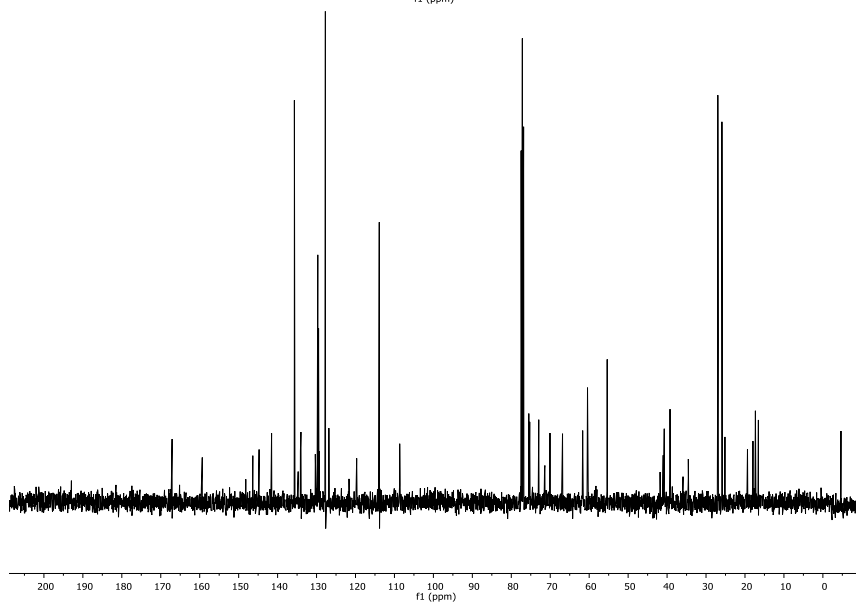
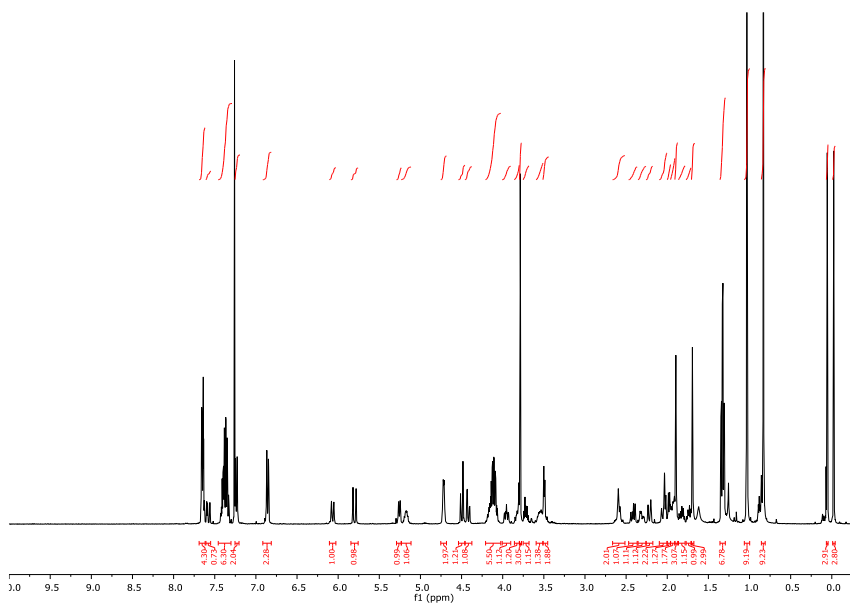
(2*E*,4*Z*)-(*R*,*E*)-5-((2*R*,6*S*)-6-(2-((*tert*-butyldiphenylsilyl)oxy)ethyl)-4-methylenetetrahydro-2*H*-pyran-2-yl)-1-((4-methoxybenzyl)oxy)-4-methylpent-4-en-2-yl 7-((*tert*-butyldimethylsilyl)oxy)-8-(diethoxyphosphoryl)-5-methylocta-2,4-dienoate (**90**)

**90**

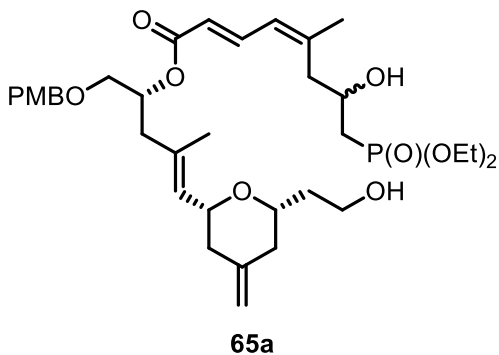
In a two-neck round bottom flask, to a solution of **67** (231 mg, 0.59 mmol, 1.20 equiv., co-evaporated twice with 2 mL of toluene immediately before use) in toluene (3.5 mL) NEt₃ (0.20 mL, 1.27 mmol, 2.60 equiv.) was added under argon, followed by 2,4,6-trichlorobenzoyl chloride (0.11 mL, 0.73 mmol, 1.5 equiv.) giving a pale yellow mixture. After 1.5 h at room temperature, a solution of **68** (300 mg, 0.49 mmol, 1.00 equiv., co-evaporated twice with 2 mL of toluene) and DMAP (60 mg, 0.49 mmol, 1.00 equiv., mixture sonicated to produce a clear solution) in toluene (1.2 mL; plus additional 1.7 mL for rinsing) was added, immediately leading to a yellow suspension. After stirring at room temperature for 18 h saturated aqueous NaHCO₃ (6 mL), H₂O (6 mL), and EtOAc (6 mL) were added, the phases were separated and the

aqueous phase was extracted with EtOAc (3 x 6 mL). The combined organic extracts were dried over MgSO₄, concentrated *in vacuo*, and the residue was purified by FC (EtOAc/Hex 1:3→1:2→1:1) to give **90** (321 mg, 0.32 mmol, 65%) as a pale yellow, viscous oil.

TLC: *R*_f = 0.54 (EtOAc/Hex 1:1, UV, CPS). **¹H-NMR** (400 MHz, CDCl₃): δ = 7.67-7.64 (m, 4 H), 7.59 (dd, *J* = 15.3, 11.9, 1 H), 7.43-7.32 (m, 6 H), 7.25-7.22 (m, 2 H), 6.87- 6.84 (m, 2 H), 6.07 (d, *J* = 11.8, 1 H), 5.80 (d, *J* = 15.2, 1 H), 5.26 (d, *J* = 7.8, 1 H), 5.21- 5.14 (m, 1 H), 4.73-4.71 (m, 2 H), 4.50 (d, *J* = 11.8, 1 H), 4.42 (dd, *J* = 11.8, 2.6, 1 H), 4.19-4.07 (m, 5 H), 3.96 (ddd, *J* = 10.9, 7.8, 2.6, 1 H), 3.85-3.80 (m, 1 H), 3.78 (s, br, 3 H), 3.72 (dt, 10.2, 5.5, 1 H), 3.60-3.51 (m, 1 H), 3.51-3.46 (m, 2 H), 2.64-2.54 (m, 2 H), 2.42 (dd, *J* = 13.7, 7.8, 1 H), 2.31 (ddd, *J* = 13.7, 5.7, 2.2, 1 H), 2.22 (d, *J* = 13.1, 1 H), 2.05 (d, *J* = 13.1, 1 H), 2.03-2.02 (m, 1 H), 1.99-1.97 (m, 1 H), 1.97-1.91 (m, 2 H), 1.89 (s, 3 H), 1.87-1.79 (m, 1 H), 1.76-1.71 (m, 1 H), 1.70 (s, 3 H), 1.32 (dt, *J* = 7.1, 3.0, 6 H), 1.03 (s, 9 H), 0.83 (s, 9 H), 0.06 (s, 3 H), -0.02 (s, 3 H). **¹³C-NMR** (100 MHz, CDCl₃) δ 167.09, 159.34, 146.36, 144.75, 141.54, 135.69, 134.14, 134.01, 130.32, 129.68, 129.48, 129.30, 127.74, 126.84, 119.72, 113.90, 108.65, 77.48, 77.16, 76.84, 75.50, 75.27, 72.95, 71.37, 70.07, 66.85, 61.67, 60.43, 55.37, 41.79, 41.00, 40.85, 40.73, 39.25, 34.55, 26.97, 25.92, 25.15, 19.36, 17.95, 17.33, 16.62, 16.56, -4.56, -4.65. **IR** (thin film): $\tilde{\nu}$ = 2952, 2930, 2893, 2857, 1710, 1636, 1612, 1514, 1248, 1146, 1111, 1089, 1049, 1024, 823, 703 cm⁻¹. **HRMS** (ESI): calcd for C₅₇H₈₆O₁₀PSi₂ [(M+H)⁺]: 1017.5492; found: 1017.5489. [α]_D²⁴: -0.67° (c = 0.75, CHCl₃).



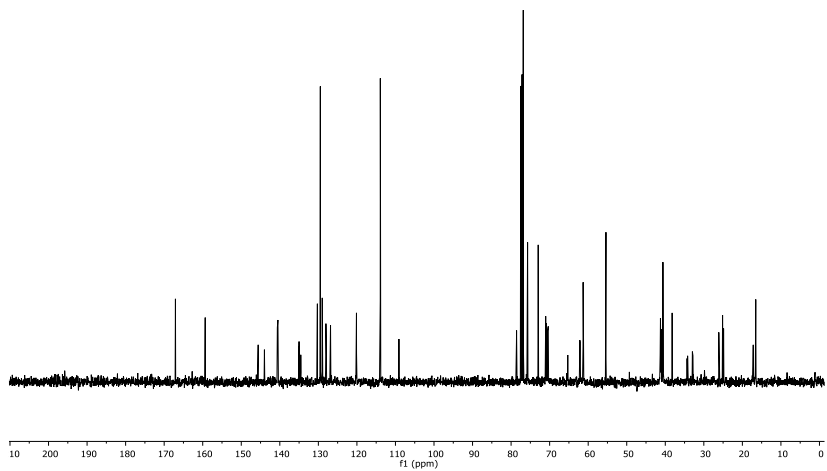
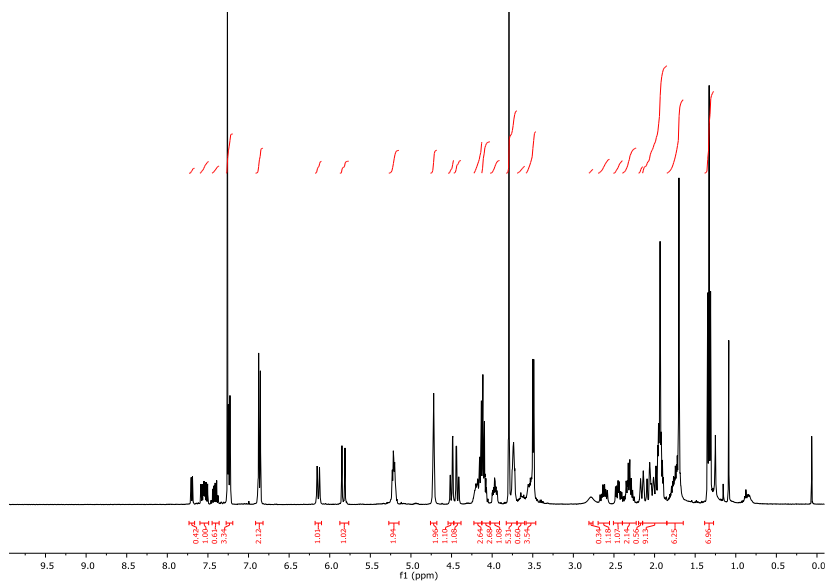
(2E,4Z)-(R,E)-5-((2R,6S)-6-(2-hydroxyethyl)-4-methylenetetrahydro-2H-pyran-2-yl)-1-((4-methoxybenzyl)oxy)-4-methylpent-4-en-2-yl 8-(diethoxyphosphoryl)-7-hydroxy-5-methylocta-2,4-dienoate (**65a**)



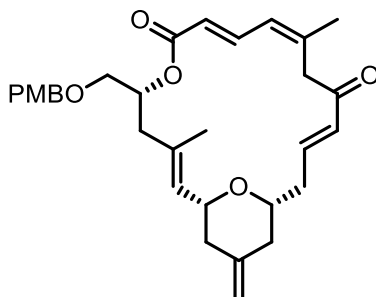
In a falcon tube, to a stirred solution of **90** (300 mg, 0.29 mmol, 1.00 equiv.) in THF (11 mL) 70% HF•py (2.9 mL) was added at 0 °C. The cooling bath was removed after 5 min and the reaction was stirred at room temperature for 14 h. The solution was then carefully added to a vigorously stirred mixture of saturated aqueous NaHCO₃ (220 mL) and EtOAc (110 mL) until two clear phases had formed (about 15-20 min). The phases were separated, the aqueous phase was extracted with EtOAc (3 x 110 mL), the combined organic extracts were washed with saturated aqueous NaHCO₃ (110 mL) followed by drying over MgSO₄. Concentration *in vacuo* and purification using FC

(EtOAc→EtOAc/acetone 1:1) afforded **65a** (170 mg, 0.26 mmol, 90%) as a pale yellow, viscous oil.

TLC: $R_f = 0.51$ (EtOAc, UV, CPS). **¹H-NMR** (400 MHz, CDCl₃): $\delta = 7.53$ (ddd, $J = 15.0, 11.6, 6.1, 1$ H), 7.23 - 7.20 (m, 2 H), 6.86 - 6.83 (m, 2 H), 6.12 (d, $J = 11.6, 1$ H), 5.81 (d, $J = 15.1, 1$ H), 5.23 - 5.16 (m, 2 H), 4.71 - 4.69 (m, 2 H), 4.48 (dd, $J = 11.8, 1.5, 1$ H), 4.41 (dd, $J = 11.8, 2.7, 1$ H), 4.42 - 4.11 (m, 1 H), 4.17 - 4.05 (m, 4 H), 3.98 - 3.91 (m, 1 H), 3.77 (s, 3 H), 3.74 - 3.69 (m, 2 H), 3.60 - 3.56 (m, 1 H), 3.54 - 3.46 (m, 3 H), 2.89 - 2.76 (br s, 1 H), 2.60 (ddd, $J = 15.2, 14.5, 8.1, 1$ H), 2.47 - 2.40 (m, 1 H), 2.37 - 2.24 (m, 2 H), 2.17 - $.12$ (m 1 H), 2.09 - 2.04 (m, 1 H), 2.03 - 1.98 (m, 1 H), 1.98 - 1.95 (m, 1 H), 1.95 - 1.93 (m, 1 H), 1.92 (s, 3 H), 1.91 - 1.88 (m, 1 H), 1.81 - 1.70 (m, 2 H), $1.69, 1.68$ (d, $J = 1.1, 3$ H), 1.31 (t, $J = 7.1, 6$ H). **¹³C-NMR** (100 MHz, CDCl₃; due to the diastereomeric nature of the product, the number of signals in the ¹³C-spectrum exceeds the number of carbon atoms): $\delta = 167.0, 159.3, 145.7, 145.6, 144.0$ (2C), $140.6, 140.5, 134.9, 134.8, 130.2, 129.4, 129.0, 126.8$ (2C), $120.1, 120.0, 113.9, 109.0$ (2C), 78.3 (2C), $75.7, 72.9$ (2C), $71.0, 70.8, 70.5, 70.4, 65.4$ (d, $J = 5.1$), 65.3 (d, $J = 5.1$), 62.1 (d, $J = 6.5$), 62.0 (d, $J = 6.5$), $61.1, 55.3, 41.3$ (d, $J = 6.2$), 41.2 (d, $J = 6.2$), $41.2, 41.0, 40.6, 40.6, 38.3, 38.2, 33.6$ (d, $J = 138$), 33.5 (d, $J = 138$), $25.1, 24.8, 17.2, 17.1, 16.5$ (d, $J = 6.0$) (2C). **IR** (thin film): $\tilde{\nu} = 3388, 2935, 2909, 2864, 1707, 1633, 1612, 1513, 1442, 1367, 1247, 1222, 1148, 1023, 975, 890, 802$ cm⁻¹. **HRMS** (ESI): calcd for C₃₅H₅₄O₁₀P [(M+H)⁺]: 665.3449; found: 665.3438. **[α]_D²⁴**: $+6.06^\circ$ (c = 0.99, CHCl₃).



(1R,2E,5R,8E,10Z,14E,17R)-5-(((4-methoxybenzyl)oxy)methyl)-3,11-dimethyl-19-methylene-6,21-dioxabicyclo[15.3.1]henicosa-2,8,10,14-tetraene-7,13-dione (**91**)

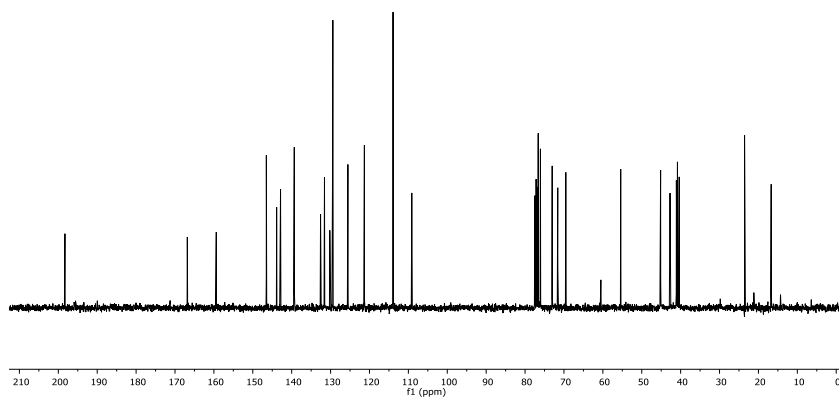
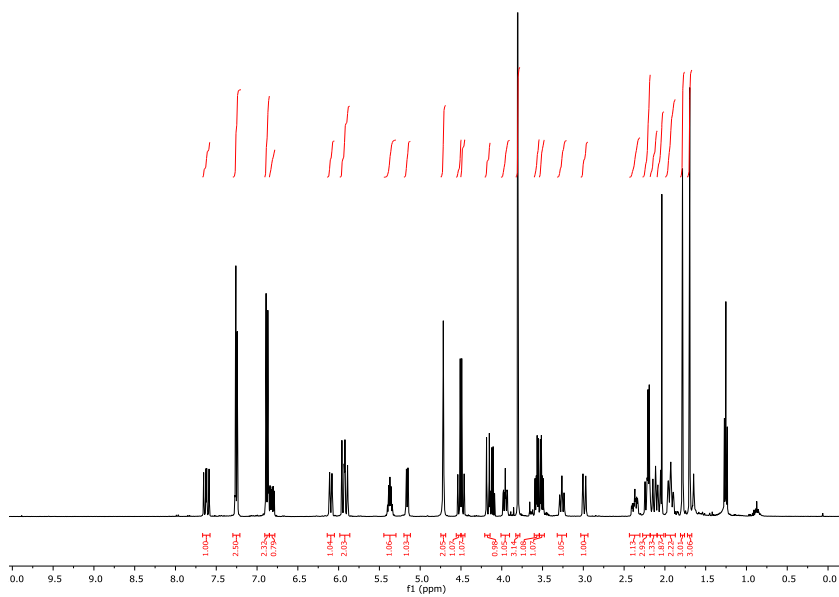
**91**

To a solution of **65a** (275 mg, 0.42 mmol, 1.00 equiv.) in DCM (18 mL) was added DMP (1.24 g, 2.91 mmol, 7.00 equiv.) at room temperature. After 2 h stirring at room temperature, a mixture of DCM (90 mL), saturated aqueous NaHCO₃ (90 mL), and saturated aqueous Na₂S₂O₃ (90 mL) and stirring was continued for 10 min, when two almost clear phases had formed. The phases were separated, the aqueous phase was extracted with DCM (3 x 150 mL), and the combined organic extracts were dried over MgSO₄ and concentrated *in vacuo*.

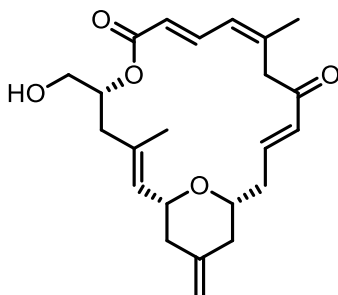
The crude product was dissolved in THF (127 mL) and H₂O (3.2 mL) was added, followed by freshly activated Ba(OH)₂•0.8H₂O (51 mg, 0.30 mmol, 0.8 equiv.) at 0 °C. The cooling bath was removed after 30 min and stirring was continued at room temperature for additional 15 min more; Et₂O (60 mL) and NaHCO₃ (30 mL) were then added and the solution was washed once with saturated aqueous NaHCO₃ (30 mL) and then with brine (1 x 30 mL). The combined aqueous phases were washed once with Et₂O (20 ml) then the combined organic phases were dried over MgSO₄ and concentrated *in vacuo*. The resulting yellow oil was purified using FC (EtOAc/Hex 1:3) to afford **91** (121 mg, 0.24 mmol, 63% over two steps) as a colorless oil.

TLC: R_f = 0.40 (EtOAc/Hex 1:3, UV, KMnO₄, CPS). **¹H-NMR** (400 MHz, CDCl₃): δ = 7.62 (dd, *J* = 15.1, 11.6, 1 H), 7.27-7.24 (m, 2 H), 6.90-6.86 (m, 2 H), 6.83 (ddd, *J* = 16.2, 9.8, 4.4, 1 H), 6.10 (d, *J* = 11.6, 1 H), 5.94 (d, *J* = 15.1, 1 H), 5.92 (d, *J* = 16.4, 1 H), 5.40-5.34 (m, 1 H), 5.17 (dd, *J* = 8.1, 0.9, 1 H), 4.74-4.70 (m, 2 H), 4.52 (d, *J* = 11.8, 1 H), 4.48 (d, *J* = 11.8, 1 H), 4.17 (d, *J* = 13.6, 1 H), 3.96 (ddd, *J* = 11.3, 8.1, 2.5, 1 H), 3.81 (s, 3 H), 3.58 (dd, *J* = 10.4, 6.0, 1 H), 3.51 (dd, *J* = 10.4, 4.9, 1 H), 3.30-3.24 (m, 1 H), 3.00 (d, *J* = 13.5, 1 H), 2.37 (dddd, *J* = 15.0, 10.1, 4.4, 2.0, 1 H), 2.26-2.20 (m, 1 H), 2.20 (d, *J* = 6.7, 2 H), 2.16-2.11 (m, 1 H), 2.11-2.05 (m, 1 H), 1.97-1.89 (m, 2 H), 1.79 (s, 3 H), 1.70 (d, *J* = 1.1, 3 H). **¹³C-NMR** (100 MHz, CDCl₃): δ = 198.3, 166.9, 159.4, 146.5, 143.9, 142.9, 139.4, 132.6, 131.6, 130.2, 129.5, 129.5, 125.6, 121.3, 114.0, 109.1, 76.7, 76.1, 73.1, 71.6, 69.6, 55.4, 45.2, 42.8, 41.1, 40.9, 40.4, 23.6, 16.8. **IR** (thin film): $\tilde{\nu}$ = 3016, 2923, 2852, 1713, 1668, 1635, 1614, 1513, 1463, 1360, 1281, 1249, 1215, 1176,

1152, 1086, 1035, 978 cm⁻¹. **HRMS** (ESI): calcd for C₃₁H₃₈NaO₆ [(M+Na)⁺]: 529.2561; found: 529.2549. **[α]_D²⁴**: +185.60° (c = 1.05, CHCl₃).



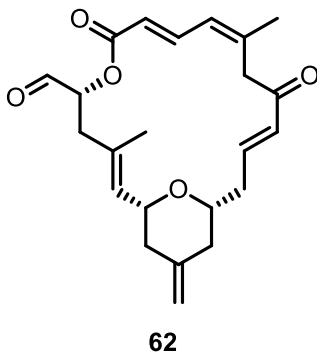
(1R,2E,5R,8E,10Z,14E,17R)-5-(hydroxymethyl)-3,11-dimethyl-19-methylene-6,21-dioxabicyclo[15.3.1]henicosa-2,8,10,14-tetraene-7,13-dione (62a)



62a

To a solution of **91** (21 mg, 0.054 mmol, 1.00 equiv.) in DCM (2.5 mL) was added H₂O (0.5 mL) followed by DDQ (43 mg, 0.190 mmol, 3.50 equiv.) at room temperature. The mixture was vigorously stirred for 3 h; then saturated aqueous NaHCO₃ (25 mL) and DCM (25 mL) were added and the phases were separated. The aqueous phase was extracted with DCM (3 x 25 mL) and the combined organic extracts were dried over MgSO₄ and concentrated *in vacuo*. Purification of the residue using FC (EtOAc/Hex 1:1) delivered **62a** (13.8 mg, 0.036 mmol, 86%) as a brown-yellow viscous liquid.

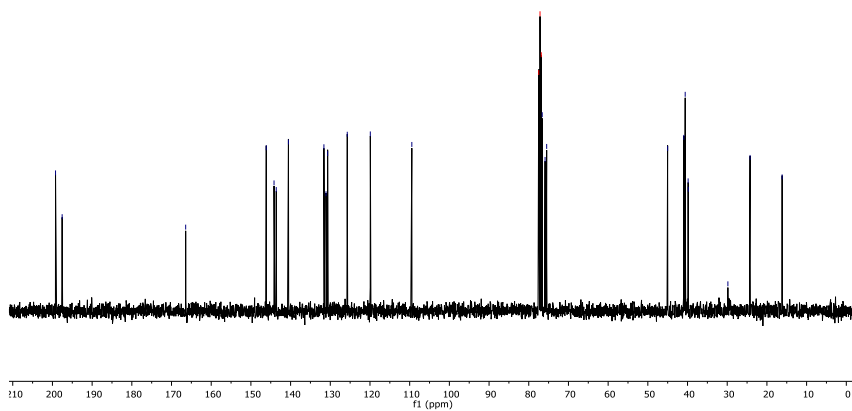
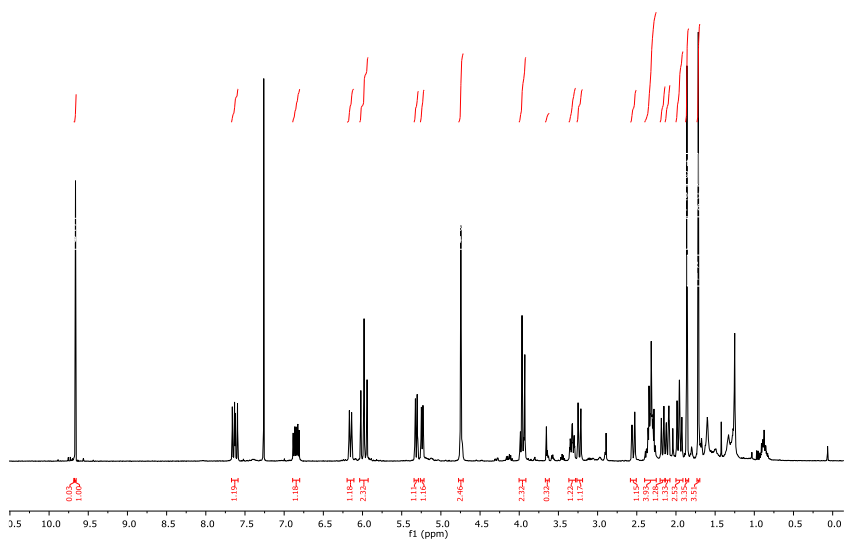
TLC: $R_f = 0.30$ (EtOAc/Hex 1:1, UV, CPS). **$^1\text{H-NMR}$** (400 MHz, CDCl_3): $\delta = 7.64$ (dd, $J = 15.1, 11.6, 1\text{ H}$), 6.84 (ddd, $J = 16.2, 9.6, 4.6, 1\text{ H}$), 6.11 (d, $J = 11.7, 1\text{ H}$), 5.94 (d, $J = 15.1, 1\text{ H}$), 5.93 (d, $J = 16.5, 1\text{ H}$), 5.28 (dddd, $J = 10.8, 5.9, 4.1, 2.1, 1\text{ H}$), 5.19 (d, $J = 8.0, 1\text{ H}$), 4.73 (d, $J = 1.6, 1\text{ H}$), 4.73 (d, $J = 1.6, 1\text{ H}$), 4.14 (d, $J = 13.7, 1\text{ H}$), 3.97 (ddd, $J = 11.2, 8.2, 2.7, 1\text{ H}$), $3.77\text{--}3.70$ (m, 2 H), 3.29 (ddt, $J = 11.8, 9.5, 2.1, 1\text{ H}$), 3.04 (d, $J = 13.7, 1\text{ H}$), 2.38 (dddd, $J = 15.1, 10.1, 4.6, 2.0, 1\text{ H}$), $2.30\text{--}2.08$ (m, 5 H), $1.98\text{--}1.91$ (m, 2 H), 1.81 (s, 3 H), 1.73 (d, $J = 1.2, 3\text{ H}$). **$^{13}\text{C-NMR}$** (100 MHz, CDCl_3): $\delta = 198.1, 167.1, 146.5, 143.9, 143.3, 139.8, 132.6, 131.6, 129.6, 125.6, 121.0, 109.2, 76.7, 76.1, 71.9, 65.4, 45.2, 42.1, 41.1, 40.8, 40.3, 23.7, 16.8$. **IR** (thin film): $\tilde{\nu} = 3389, 2925, 2853, 1715, 1669, 1634, 1553, 1449, 1436, 1357, 1280, 1259, 1148, 1086, 1049, 1019, 976, 799\text{ cm}^{-1}$. **HRMS** (ESI): calcd for $\text{C}_{23}\text{H}_{30}\text{NaO}_5$ [(M+Na) $^+$]: 409.1985; found: 409.1985. **$[\alpha]_D^{24}$** : $+203.31^\circ$ (c = 0.69, CHCl_3).

(+)-Dactylolide (**62**)

To a stirred solution of **62a** (13.8 mg, 0.036 mmol, 1.00 equiv.) in DCM (3 mL) was added DMP (91 mg, 0.21 mmol, 6.00 equiv.) at room temperature and stirring was continued for 1 h then a mixture of saturated aqueous NaHCO₃ (30 mL) and saturated aqueous Na₂S₂O₃ (30 mL) was added and stirring was continued for 10 min until two clear phases were formed. The phases were separated then the aqueous phase was extracted with DCM (3 x 50 mL), the combined organic phases were dried over MgSO₄, concentrated *in vacuo* then purified using FC (EtOAc/Hex 1:3→1:2→1:1) affording **62** (10.6 mg, 0.028 mmol, 77%) of a colourless solid.

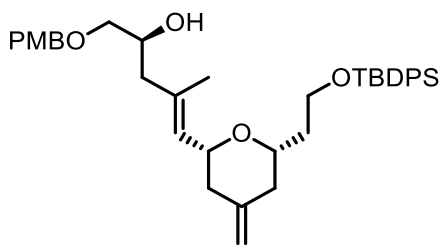
TLC: R_f = 0.57 (EtOAc/Hex 1:1, UV, CPS or KMnO₄). **¹H-NMR** (400 MHz, CDCl₃): δ = 9.67 (s, 1 H), 7.63 (dd, *J* = 15.1, 11.6, 1 H), 6.85 (ddd, *J*

= 16.2, 8.6, 6.0, 1 H), 6.16 (d, $J = 11.7$, 1 H), 6.03-5.94 (m, 2 H), 5.32 (dd, $J = 11.3$, 2.5, 1 H), 5.24 (d, $J = 8.0$, 1 H), 4.75 (d, $J = 1.6$, 1 H), 4.75 (d, $J = 1.6$, 1 H), 3.97 (ddd, $J = 11.5$, 8.1, 2.7, 1 H), 3.94 (d, $J = 14.3$, 1 H), 3.33 (ddt, $J = 11.1$, 8.7, 2.7, 1 H), 3.24 (d, $J = 14.5$, 1 H), 2.55 (d, $J = 14.3$, 1 H), 2.36-2.28 (m, 3 H), 2.19-2.15 (m, 1 H), 2.14-2.09 (m, 1 H), 1.99-1.93 (m, 2 H), 1.87 (s, 3 H), 1.72 (d, $J = 0.9$, 3 H). $^{13}\text{C-NMR}$ (100 MHz, CDCl_3): $\delta = 199.2$, 197.6, 166.4, 146.1, 144.2, 143.6, 140.6, 131.6, 131.1, 130.7, 125.7, 119.9, 109.5, 76.6, 75.9, 75.5, 45.0, 40.9, 40.6, 39.9, 39.8, 24.3, 16.2. **IR** (thin film): $\tilde{\nu} = 2936$, 2858, 1733, 1716, 1706, 1670, 1635, 1438, 1355, 1278, 1256, 1144, 1086, 1050, 978, 890 cm^{-1} . **HRMS** (ESI): calcd for $\text{C}_{23}\text{H}_{29}\text{O}_5$ [(M+H) $^+$], 385.2010, found: 385.2012. $[\alpha]_D^{25}$: +162.44 $^\circ$ (c = 0.18, MeOH).



5.6. Synthesis of 19-*epi*-(+)-dactylolide (**64**)

(*S,E*)-5-((2*R*,6*S*)-6-(2-((*tert*-butyldiphenylsilyl)oxy)ethyl)-4-methylenetetrahydro-2*H*-pyran-2-yl)-1-((4-methoxybenzyl)oxy)-4-methylpent-4-en-2-ol (**69**)

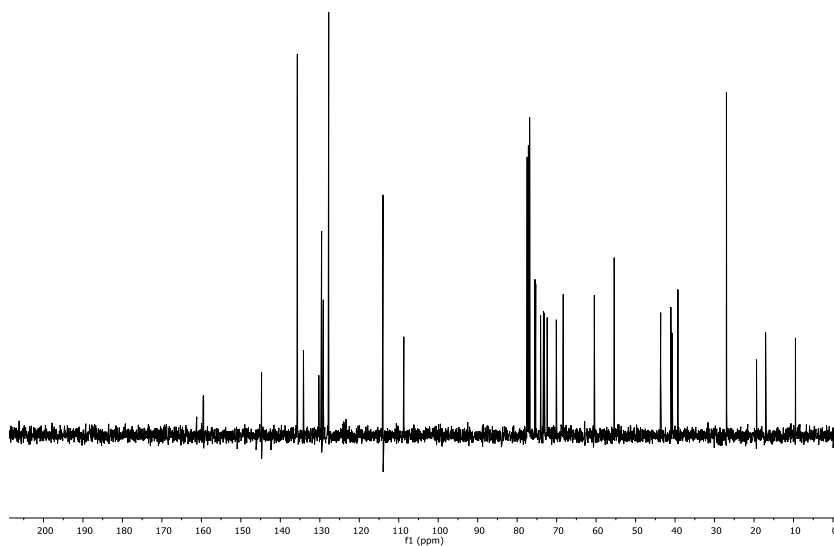
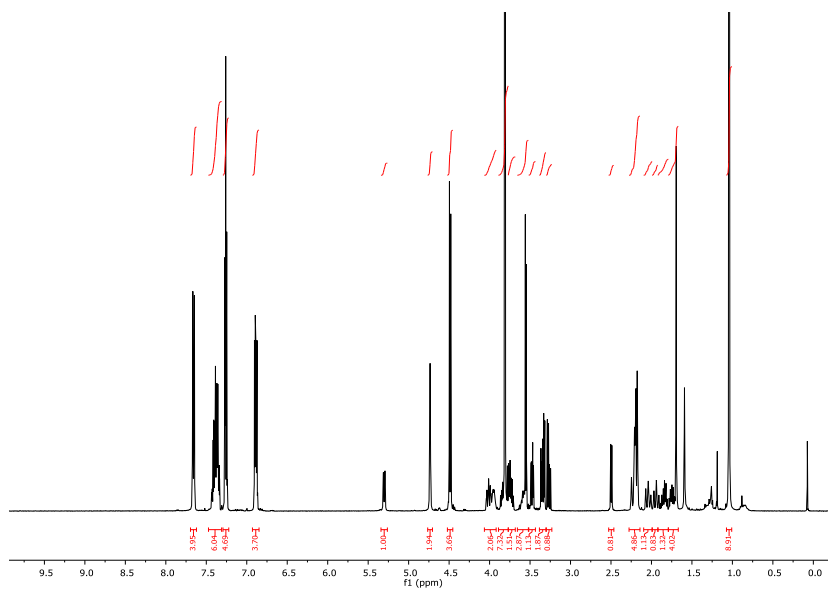


69

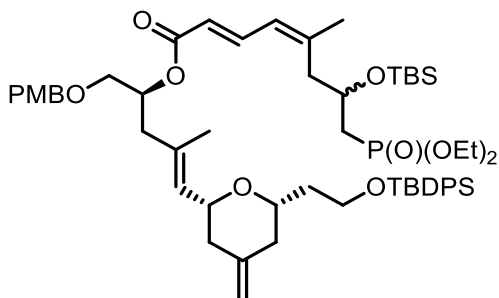
Vinyl iodide **72** (700 mg, 1.28 mmol, 1.00 equiv., azeotropically dried once with 2 mL of acetonitrile or toluene right before use) was dissolved in dry toluene (13 mL) and the solution was cooled to $-78\text{ }^{\circ}\text{C}$. *t*-BuLi (1.6M in pentane, 1.6 mL, 2.56 mmol, 2.00 equiv.) was then added and the near colorless solution was stirred for 30 min; it was then cooled to around -85 to $-90\text{ }^{\circ}\text{C}$ with liquid nitrogen and a solution of **71** (623 mg, 3.20 mmol, 2.50 equiv., azeotropically dried once with 2 mL of acetonitrile or toluene right before use) in dry toluene (4 mL) was added followed by $\text{BF}_3\cdot\text{OEt}_2$ (0.40 mL, 3.20 mmol, 2.50 equiv.; addition ca. 1 min after the addition of **71**) giving a pale yellow solution. Stirring was continued at $-78\text{ }^{\circ}\text{C}$ for 1 h; then the cooling bath was removed and

saturated aqueous NaHCO₃ (18 mL) and EtOAc (18 mL) were added. After the mixture had reached room temperature, the phases were separated and the aqueous phase was extracted with EtOAc (3 x 10 mL). The combined organic extracts were dried over MgSO₄, concentrated *in vacuo*, and the residue purified using FC (EtOAc/Hex 1:5) to give **69** (414 mg, 0.67 mmol, 52%) as a colorless oil.

TLC: R_f = 0.17 (EtOAc/Hex 1:5, UV, CPS). **¹H-NMR** (400 MHz, CDCl₃): δ = 7.68-7.65 (m, 4 H), 7.44-7.34 (m, 6 H), 7.28-7.24 (m, 2 H), 6.90-6.87 (m, 2 H), 5.29 (dq, *J* = 7.7, 1.2, 1 H), 4.75-4.73 (m, 2 H), 4.49 (s, 2 H), 3.99 (ddd, *J* = 10.9, 7.7, 2.7, 1 H), 3.98-3.91 (m, 1 H), 3.84 (ddd, *J* = 10.1, 8.0, 5.5, 1 H), 3.80 (s, 3 H), 3.74 (dt, *J* = 10.1, 5.7, 1 H), 3.60-3.54 (m, 1 H), 3.46 (dd, *J* = 9.5, 3.5, 1 H), 3.33 (dd, *J* = 9.5, 7.1, 1 H), 2.31 (d, *J* = 3.5, 1 H), 2.25-2.22 (m, 1 H), 2.20 (d, *J* = 6.8, 2 H), 2.16-2.12 (m, 1 H), 2.04-2.00 (m, 1 H), 1.97-1.90 (m, 1 H), 1.89-1.80 (m, 1 H), 1.77-1.71 (m, 1 H), 1.69 (d, *J* = 1.2, 3 H), 1.05 (s, 9 H). **¹³C-NMR** (100 MHz, CDCl₃): δ = 159.4, 144.7, 135.7, 135.7, 135.4, 134.1, 134.0, 130.2, 129.7, 129.5, 129.0, 127.7, 127.7, 114.0, 108.7, 75.5, 75.3, 73.7, 73.2, 68.6, 60.4, 55.4, 43.7, 41.0, 40.7, 39.2, 27.0, 19.4, 17.3. **IR** (thin film): $\tilde{\nu}$ = 3070, 2932, 2857, 1612, 1513, 1471, 1427, 1247, 1106, 1087, 1058, 1036, 998, 821, 702 cm⁻¹. **HRMS** (ESI): calcd for C₃₈H₅₀NaO₅Si [(M+Na)⁺]: 637.3320; found: 637.3313. **[α]_D²⁴**: -1.15° (c = 0.78, CHCl₃).



(2*E*,4*Z*)-(S,*E*)-5-((2*R*,6*S*)-6-(2-((*tert*-butyldiphenylsilyl)oxy)ethyl)-4-methylenetetrahydro-2*H*-pyran-2-yl)-1-((4-methoxybenzyl)oxy)-4-methylpent-4-en-2-yl 7-((*tert*-butyldimethylsilyl)oxy)-8-(diethoxyphosphoryl)-5-methylocta-2,4-dienoate (**90b**)

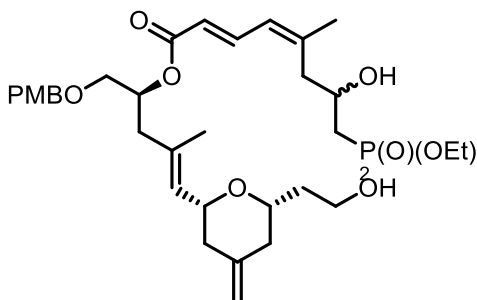
**90b**

To a solution of **67** (308 mg, 0.78 mmol, 1.20 equiv., co-evaporated once with 2 mL of toluene immediately before use) in toluene (6 mL) was added NEt_3 (0.24 mL, 1.69 mmol, 2.60 equiv.) followed by 2,4,6-trichlorobenzoyl chloride (0.15 mL, 0.98 mmol, 1.5 equiv.) giving a pale yellow mixture. After 1.5 h at room temperature, a solution of **69** (400 mg, 0.65 mmol, 1.00 equiv.) and DMAP (80 mg, 0.65 mmol, 1.00 equiv. co-evaporated together once with 2 mL of toluene immediately before use) in toluene (2 mL, plus additional 2 mL for rinsing) was added, immediately leading to a yellow suspension. After stirring at room temperature for 18 h saturated aqueous NaHCO_3 (10 mL), H_2O (10 mL), and EtOAc (10 mL) were added, the phases were

separated and the aqueous phase was extracted with EtOAc (3 x 10 mL). The combined organic extracts were dried over MgSO₄, concentrated *in vacuo*, and the residue was purified using FC (EtOAc/Hex 1:3→1:2→1:1) to give **90b** (289 mg, 0.28 mmol, 43%) as a pale yellow, viscous oil.

TLC: R_f = 0.54 (EtOAc/Hex 1:1, UV, CPS). **¹H-NMR** (400 MHz, CDCl₃): δ = 7.67-7.64 (m, 4 H), 7.59 (dd, J = 15.3, 11.9, 1 H), 7.43-7.32 (m, 6 H), 7.25-7.22 (m, 2 H), 6.87- 6.84 (m, 2 H), 6.07 (d, J = 11.8, 1 H), 5.80 (d, J = 15.2, 1 H), 5.26 (d, J = 7.8, 1 H), 5.21- 5.14 (m, 1 H), 4.73-4.71 (m, 2 H), 4.50 (d, J = 11.8, 1 H), 4.42 (dd, J = 11.8, 2.6, 1 H), 4.19-4.07 (m, 5 H), 3.96 (ddd, J = 10.9, 7.8, 2.6, 1 H), 3.85-3.80 (m, 1 H), 3.78 (s, br, 3 H), 3.72 (dt, 10.2, 5.5, 1 H), 3.60-3.51 (m, 1 H), 3.51-3.46 (m, 2 H), 2.64-2.54 (m, 2 H), 2.42 (dd, J = 13.7, 7.8, 1 H), 2.31 (ddd, J = 13.7, 5.7, 2.2, 1 H), 2.22 (d, J = 13.1, 1 H), 2.05 (d, J = 13.1, 1 H), 2.03-2.02 (m, 1 H), 1.99-1.97 (m, 1 H), 1.97-1.91 (m, 2 H), 1.89 (s, 3 H), 1.87-1.79 (m, 1 H), 1.76-1.71 (m, 1 H), 1.70 (s, 3 H), 1.32 (dt, J = 7.1, 3.0, 6 H), 1.03 (s, 9 H), 0.83 (s, 9 H), 0.06 (s, 3 H), -0.02 (s, 3 H). **¹³C-NMR** (100 MHz, CDCl₃): δ = 166.99, 159.34, 146.32, 144.81, 141.55, 141.40, 135.69, 134.50, 134.39, 134.15, 134.01, 130.34, 129.67, 129.57, 129.45, 127.74, 126.84, 126.77, 119.63, 118.77, 113.99, 113.91, 108.62, 75.59, 75.25, 73.28, 72.98, 70.96, 70.34, 69.98, 66.91, 66.79, 61.68, 60.44, 55.39, 41.72, 40.78, 39.28, 35.84, 34.58, 29.84, 26.97, 25.92, 25.18, 25.11, 19.36, 17.96, 16.98, 16.63, 16.56, 4.74, -4.56, -4.64. **IR** (thin film): $\tilde{\nu}$ = 2952, 2930, 2893, 2857, 1710, 1636, 1612, 1514, 1248, 1146, 1111, 1089, 1049, 1024, 823, 703 cm⁻¹. **HRMS** (ESI): calcd for C₅₇H₈₆O₁₀PSi₂ [(M+H)⁺]: 1017.5492; found: 1017.5490. **[α]_D²⁴**: -9.01° (c = 0.81, CHCl₃).

(2E,4Z)-(S,E)-5-((2R,6S)-6-(2-hydroxyethyl)-4-methylenetetrahydro-2H-pyran-2-yl)-1-((4-methoxybenzyl)oxy)-4-methylpent-4-en-2-yl 8-(diethoxyphosphoryl)-7-hydroxy-5-methylocta-2,4-dienoate (**65ab**)

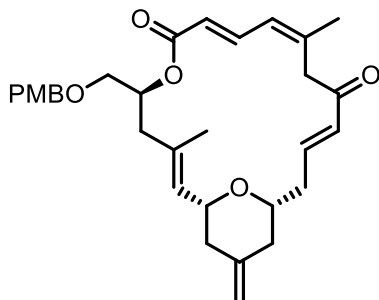
**65ab**

To a stirred solution of **90b** (280 mg, 0.28 mmol, 1.00 equiv.) in THF (11 mL) in a plastic tube was added 70% HF•py (2.8 mL) at 0 °C. The cooling bath was removed after 5 min and stirring was continued at room temperature for 14 h. The solution was then carefully added to a vigorously stirred mixture of saturated aqueous NaHCO₃ (220 mL) and EtOAc (110 mL) until two clear phases had formed (ca. 15 min). The phases were separated, the aqueous phase was extracted with EtOAc (3 x 110 mL), the combined organic extracts were washed with saturated aqueous NaHCO₃ (110 mL) followed by drying over MgSO₄. Concentration *in vacuo* and purification using FC

(EtOAc→EtOAc/acetone 1:1) afforded **65ab** (143 mg, 0.22mmol, 79%) as a pale yellow, viscous oil.

TLC: R_f = 0.51 (EtOAc, UV, CPS). **¹H-NMR** (400 MHz, CDCl₃): δ = 7.53 (ddd, J = 15.0, 11.6, 6.1, 1 H), 7.23-7.20 (m, 2 H), 6.86-6.83 (m, 2 H), 6.12 (d, J = 11.6, 1 H), 5.81 (d, J = 15.1, 1 H), 5.23-5.16 (m, 2 H), 4.71-4.69 (m, 2 H), 4.48 (dd, J = 11.8, 1.5, 1 H), 4.41 (dd, J = 11.8, 2.7, 1 H), 4.42-4.11 (m, 1 H), 4.17-4.05 (m, 4 H), 3.98-3.91 (m, 1 H), 3.77 (s, 3 H), 3.74-3.69 (m, 2 H), 3.60-3.56 (m, 1 H), 3.54-3.46 (m, 3 H), 2.89-2.76 (br s, 1 H), 2.60 (ddd, J = 15.2, 14.5, 8.1, 1 H), 2.47-2.40 (m, 1 H), 2.37-2.24 (m, 2 H), 2.17- .12 (m 1 H), 2.09-2.04 (m, 1 H), 2.03-1.98 (m, 1 H), 1.98-1.95 (m, 1 H), 1.95-1.93 (m, 1 H), 1.92 (s, 3 H), 1.91-1.88 (m, 1 H), 1.81-1.70 (m, 2 H), 1.69, 1.68 (d, J = 1.1, 3 H), 1.31 (t, J = 7.1, 6 H). **¹³C-NMR** (100 MHz, CDCl₃): δ = 166.97, 159.35, 145.65, 143.96, 140.50, 134.82, 130.27, 129.48, 129.07, 128.99, 126.82, 120.19, 113.93, 109.18, 78.77, 75.82, 73.00, 70.88, 70.45, 65.35, 62.25, 62.05, 61.50, 55.40, 41.50, 40.61, 40.47, 38.14, 34.17, 32.79, 25.02, 17.07, 16.54. **IR** (thin film): $\tilde{\nu}$ = 3388, 2935, 2909, 2864, 1707, 1633, 1612, 1513, 1442, 1367, 1247, 1222, 1148, 1023, 975, 890, 802 cm⁻¹. **HRMS** (ESI): calcd for C₃₅H₅₄O₁₀P [(M+H)⁺]: 665.3449; found: 665.3440. **$[\alpha]_D^{24}$** : -14.53° (c = 0.75, CHCl₃).

(1R,2E,5S,8E,10Z,14E,17R)-5-(((4-methoxybenzyl)oxy)methyl)-3,11-dimethyl-19-methylene-6,21-dioxabicyclo[15.3.1]henicosa-2,8,10,14-tetraene-7,13-dione (**91b**)



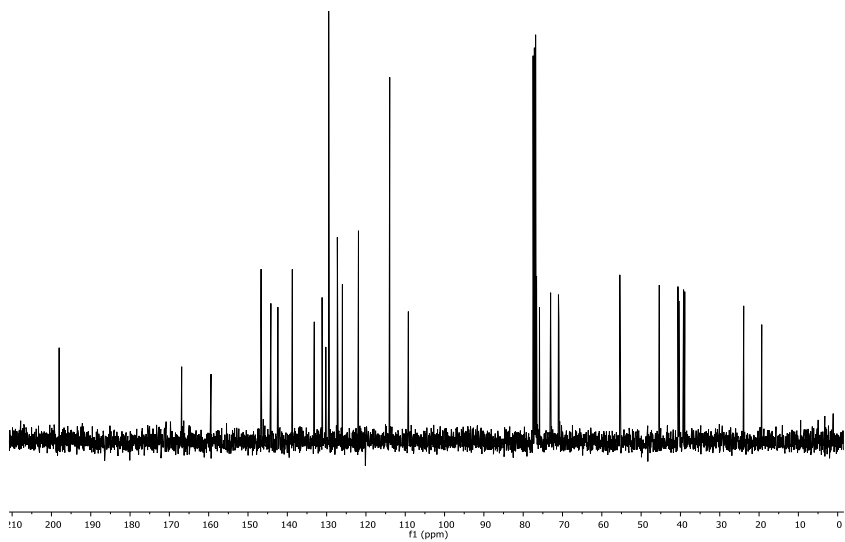
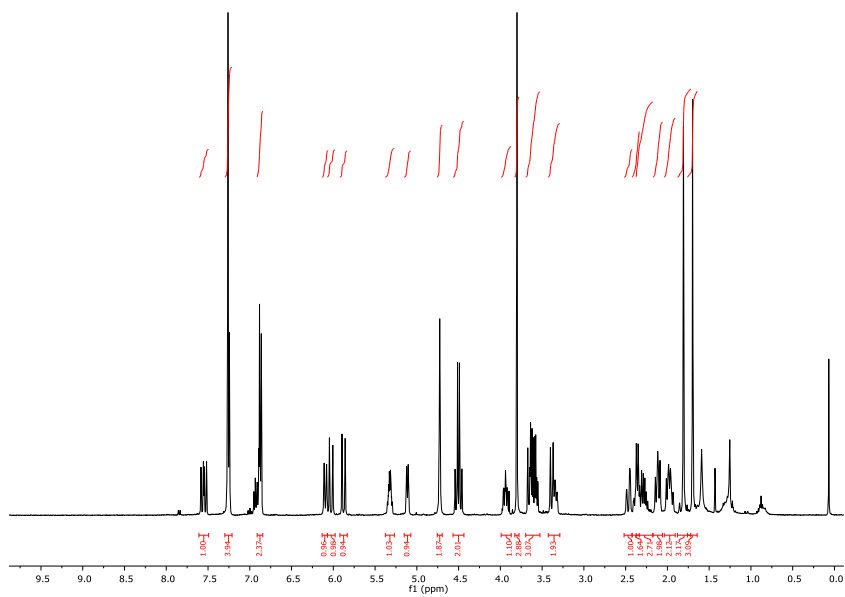
91b

To a solution of **65ab** (140 mg, 0.21 mmol, 1.00 equiv.) in DCM (5 mL) was added DMP (629 mg, 1.48 mmol, 7.00 equiv.) at room temperature. After 2 h stirring at room temperature, a mixture of DCM (45 mL), saturated aqueous NaHCO_3 (45 mL), and saturated aqueous $\text{Na}_2\text{S}_2\text{O}_3$ (45 mL) and stirring was continued for 10 min, when two almost clear phases had formed. The phases were separated, the aqueous phase was extracted with DCM (3 x 100 mL), and the combined organic extracts were dried over MgSO_4 and *in vacuo*.

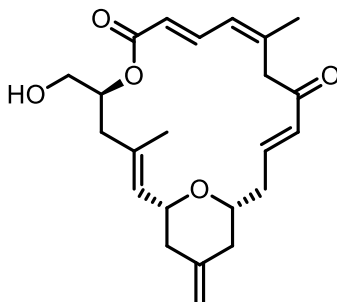
The crude product was dissolved in THF (60 mL) and H_2O (1.5 mL) was added, followed by freshly activated $\text{Ba}(\text{OH})_2 \cdot 0.8\text{H}_2\text{O}$ (25 mg, 0.14 mmol, 0.8 equiv.) at 0 °C. The cooling bath was removed after 30 min and stirring was continued at room temperature for additional 15 min more; Et_2O (30 mL) and NaHCO_3 (15 mL) were then added and the

solution was washed once with saturated aqueous NaHCO_3 (15 mL) and then with brine (1 x 15 mL). The combined aqueous phases were washed once with Et_2O (20 ml) then the combined organic phases were dried over MgSO_4 and concentrated *in vacuo*. The resulting yellow oil was purified using FC (EtOAc/Hex 1:3) to afford **91b** (37 mg, 0.073 mmol, 36% over two steps) as a colorless oil.

TLC: $R_f = 0.40$ (EtOAc/Hex 1:3, UV, KMnO_4 , CPS). **$^1\text{H-NMR}$** (400 MHz, CDCl_3): $\delta = 7.55$ (dd, $J = 15.1, 11.5$ Hz, 1H), 7.30 – 7.21 (m, 4H), 6.91 – 6.84 (m, 2H), 6.09 (d, $J = 11.5$ Hz, 1H), 6.03 (dt, $J = 16.1, 1.2$ Hz, 1H), 5.88 (d, $J = 15.1$ Hz, 1H), 5.32 (ddt, $J = 8.7, 5.4, 2.7$ Hz, 1H), 5.11 (dq, $J = 7.8, 1.4$ Hz, 1H), 4.73 (d, $J = 1.8$ Hz, 2H), 4.57 – 4.44 (m, 2H), 3.99 – 3.87 (m, 1H), 3.80 (s, 3H), 3.70 – 3.53 (m, 3H), 3.43 – 3.29 (m, 2H), 2.52 – 2.42 (m, 1H), 2.42 – 2.34 (m, 2H), 2.37 – 2.17 (m, 3H), 2.17 – 2.06 (m, 2H), 2.04 – 1.91 (m, 2H), 1.88 – 1.72 (m, 3H), 1.70 (d, $J = 1.3$ Hz, 3H). **$^{13}\text{C-NMR}$** (100 MHz, CDCl_3): $\delta = \delta$ 198.04, 166.87, 159.41, 146.67, 144.18, 142.40, 138.73, 133.14, 131.16, 130.21, 129.47, 127.27, 125.99, 121.90, 113.95, 109.21, 76.61, 75.86, 73.03, 71.03, 70.92, 55.42, 45.39, 40.63, 40.39, 39.20, 38.90, 23.91, 19.32. **IR** (thin film): $\tilde{\nu} = 3016, 2923, 2852, 1713, 1668, 1635, 1614, 1513, 1463, 1360, 1281, 1249, 1215, 1176, 1152, 1086, 1035, 978$ cm^{-1} . **HRMS** (ESI): calcd for $\text{C}_{31}\text{H}_{38}\text{NaO}_6$ [(M+Na) $^+$]: 529.2561; found: 529.2558. **$[\alpha]_D^{24}$** : +48.96° ($c = 0.98, \text{CHCl}_3$).



(1R,2E,5S,8E,10Z,14E,17R)-5-(hydroxymethyl)-3,11-dimethyl-19-methylene-6,21-dioxabicyclo[15.3.1]henicosa-2,8,10,14-tetraene-7,13-dione (62ab)

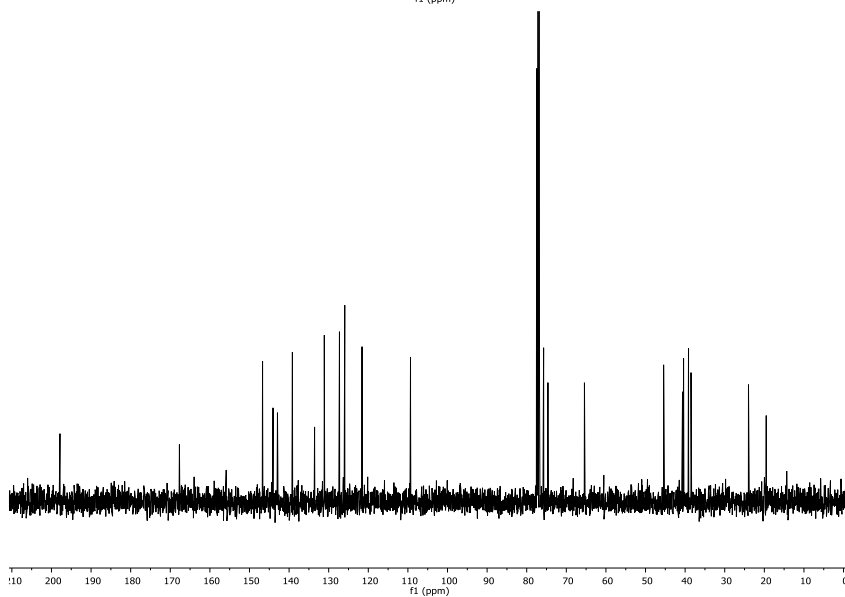
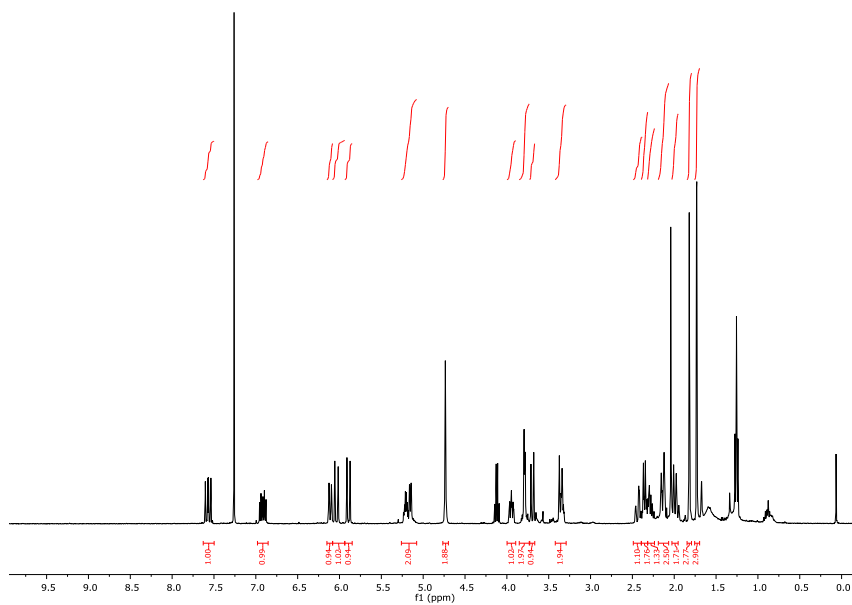


62ab

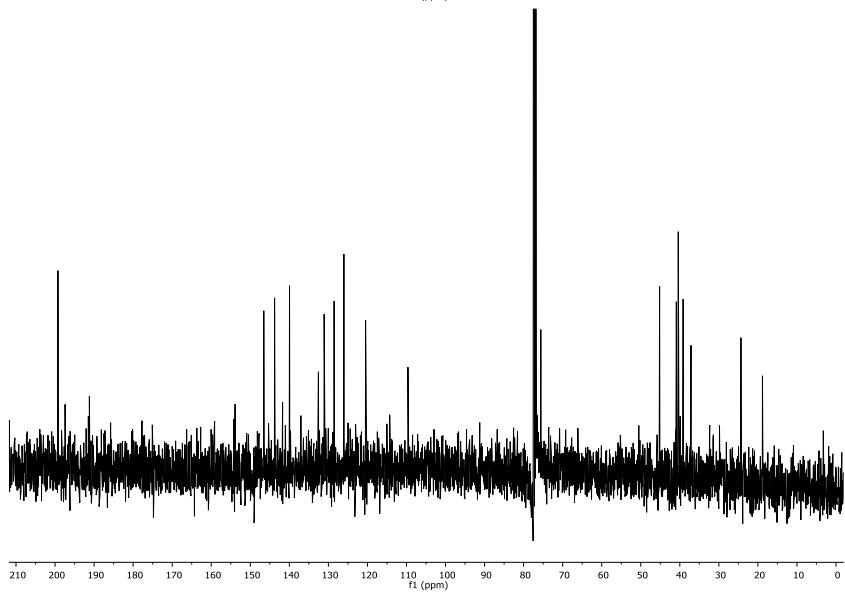
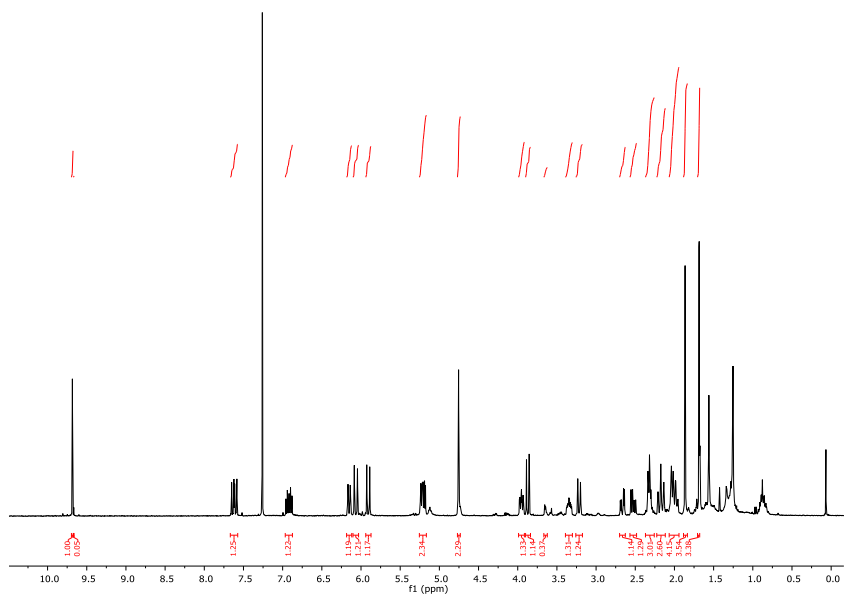
To a solution of **91b** (9 mg, 0.023 mmol, 1.00 equiv.) in DCM (1.5 mL) was added H₂O (0.29 mL) followed by DDQ (19 mg, 0.082 mmol, 3.50 equiv.) at room temperature. The mixture was vigorously stirred for 2 h; then saturated aqueous NaHCO₃ (15 mL) and DCM (15 mL) were added and the phases were separated. The aqueous phase was extracted with DCM (3 × 15 mL) and the combined organic extracts were dried over MgSO₄ and concentrated *in vacuo*. Purification of the residue using FC (EtOAc/Hex 1:3→1:2→1:1) delivered **62ab** (5.7 mg, 0.015 mmol, 65%) as a brown-yellow viscous liquid.

TLC: R_f = 0.30 (EtOAc/Hex 1:1, UV, CPS). **¹H-NMR** (400 MHz, CDCl₃): δ = 7.57 (dd, J = 15.1, 11.5 Hz, 1H), 6.92 (ddd, J = 16.2, 8.1, 6.7

Hz, 1H), 6.11 (d, $J = 11.6$ Hz, 1H), 6.08 – 5.94 (m, 1H), 5.89 (d, $J = 15.1$ Hz, 1H), 5.26 – 5.08 (m, 2H), 4.73 (d, $J = 1.9$ Hz, 2H), 3.95 (ddd, $J = 10.6, 7.6, 2.6$ Hz, 1H), 3.85 – 3.73 (m, 2H), 3.70 (dd, $J = 13.3, 0.8$ Hz, 1H), 3.42 – 3.29 (m, 2H), 2.49 – 2.39 (m, 1H), 2.39 – 2.32 (m, 2H), 2.28 (dddd, $J = 14.2, 8.2, 5.9, 2.2$ Hz, 1H), 2.19 – 2.07 (m, 3H), 1.99 (dq, $J = 11.0, 1.7$ Hz, 2H), 1.85 – 1.79 (m, 3H), 1.73 (d, $J = 1.3$ Hz, 3H). $^{13}\text{C-NMR}$ (100 MHz, CDCl_3): $\delta = 197.85, 167.69, 146.70, 144.06, 142.94, 139.17, 133.57, 131.11, 127.28, 125.94, 121.58, 109.34, 76.77, 75.73, 74.64, 65.42, 45.43, 40.65, 40.40, 39.14, 38.51, 24.00, 19.52$. **IR** (thin film): $\tilde{\nu} = 3389, 2925, 2853, 1715, 1669, 1634, 1553, 1449, 1436, 1357, 1280, 1259, 1148, 1086, 1049, 1019, 976, 799$ cm^{-1} . **HRMS** (ESI): calcd for $\text{C}_{23}\text{H}_{30}\text{NaO}_5$ $[(\text{M}+\text{Na})^+]$: 409.1985; found: 409.1978. $[\alpha]_D^{24}$: $+36.83^\circ$ ($c = 0.57, \text{CHCl}_3$).



1H), 6.92 (ddd, J = 16.2, 7.9, 7.0 Hz, 1H), 6.15 (d, J = 11.6 Hz, 1H), 6.07 (dt, J = 16.2, 1.3 Hz, 1H), 5.91 (d, J = 15.2 Hz, 1H), 5.26 – 5.17 (m, 2H), 4.75 (t, J = 1.8 Hz, 2H), 3.95 (ddd, J = 11.3, 7.6, 2.6 Hz, 1H), 3.87 (d, J = 13.8 Hz, 1H), 3.39 – 3.30 (m, 1H), 3.22 (d, J = 13.8 Hz, 1H), 2.66 (ddd, J = 15.7, 4.5, 1.3 Hz, 1H), 2.53 (dd, J = 15.8, 8.1 Hz, 1H), 2.37 – 2.26 (m, 3H), 2.23 – 2.12 (m, 3H), 2.07 – 1.94 (m, 4H), 1.86 (d, J = 1.2 Hz, 4H), 1.69 (d, J = 1.3 Hz, 3H). **¹³C-NMR** (100 MHz, CDCl₃): δ = 199.26, 197.44, 153.90, 146.55, 145.33, 143.78, 143.70, 141.73, 139.95, 137.04, 132.56, 131.09, 128.53, 126.03, 120.48, 109.63, 77.36, 76.79, 75.60, 45.18, 40.89, 40.40, 39.15, 37.14, 24.35, 18.84. **IR** (thin film): $\tilde{\nu}$ = 2936, 2858, 1733, 1716, 1706, 1670, 1635, 1438, 1355, 1278, 1256, 1144, 1086, 1050, 978, 890 cm⁻¹. **HRMS** (ESI): calcd for C₂₃H₂₉O₅ [(M+H)⁺], 385.2010, found: 385.2012. **[α]_D²⁵**: +28.7° (c = 0.20, MeOH).



THF (1 mL). The reaction mixture turned to orange over 15 minutes. The reaction was quenched adding NaHCO_3 (2.0 mL). The phases were separated then the aqueous phase was extracted with EtOAc (3 x 5 mL), the combined organic phases were dried over MgSO_4 , concentrated *in vacuo* then purified using FC (EtOAc/Hex 1:1, 2% Et_3N) as a mixture of both C20 epimers (93:7 *dr*) as a pale-yellow foam. Both epimers could be separated by HPLC on normal phase (compound is concentrated in EtOH. Column: Phenomenex Luna, $5\mu\text{ NH}_2$, 10x150 mm, *i*-PrOH/Hex (1:9), 5 mL/min, 25 °C, 266 nm, $R_t = 7.6$ min [(+)-zampanolide (**61**)], $R_t = 8.5$ min [C20-*epi*-(+)-**61**]) affording **61** (2.8 mg, 0.0058 mmol, 74%) of a colourless film.

TLC: $R_f = 0.40$ (EtOAc/Hex 1:1, UV, CPS). **$^1\text{H-NMR}$** (500 MHz, $\text{DMSO-}d_6$): $\delta = 8.35$ (d, $J = 8.9$, 1 H), 7.51 (dd, $J = 14.9$, 11.8, 1 H), 7.45 (dd, $J = 14.9$, 11.8, 1 H), 6.75 (ddd, $J = 16.3$, 8.6, 5.7, 1 H), 6.36 (t, $J = 11.3$, 1 H), 6.20 (d, $J = 11.9$, 1 H), 6.18 (br. s, 1 H), 6.00-5.94 (m, 1 H), 5.95 (d, $J = 15.9$, 1 H), 5.93 (d, $J = 15.1$, 1 H), 5.65 (d, $J = 11.4$, 1 H), 5.32 (dd, $J = 8.4$, 6.4, 1 H), 5.10 (d, $J = 7.7$, 1 H), 4.96 (dd, $J = 10.2$, 6.2, 1 H), 4.73 (br. s, 2 H), 4.13 (d, $J = 14.2$, 1 H), 3.86 (ddd, $J = 11.4$, 7.7, 1.8, 1 H), 3.26 (t, $J = 10.1$, 1 H), 3.00 (d, $J = 14.3$, 1 H), 2.35-2.26 (m, 3 H), 2.17 (d, $J = 12.7$, 1 H), 2.11-2.05 (m, 2 H), 1.89-1.86 (m, 1 H), 1.85-1.82 (m, 1 H), 1.79 (d, $J = 6.7$, 3 H), 1.74 (s, 3 H), 1.61 (s, 3 H). **$^{13}\text{C-NMR}$** (125 MHz, $\text{DMSO-}d_6$): $\delta = 197.3$, 165.6, 165.3, 145.9, 143.8, 143.0, 140.6, 139.5, 137.2, 132.5, 130.9, 129.0, 128.6, 125.1, 120.7, 119.2, 109.0, 76.0, 75.1, 72.9, 72.0, 44.9, 40.9, 40.3, 40.3, 39.3, 23.6, 18.3, 16.7. **IR** (thin film): $\tilde{\nu} = 3325$, 3015, 2960, 2924, 2853, 1708, 1664, 1634, 1604, 1520, 1431, 1355, 1281, 1259, 1213, 1147, 1085, 1050, 1034, 1025, 802 cm^{-1} . **HRMS** (ESI): m/z : calcd for $\text{C}_{29}\text{H}_{37}\text{NNaO}_6$ [(M+Na) $^+$]:

518.2513; found: 518.2509. $[\alpha]_D^{24}$: +226.12° (c = 0.084 in CHCl₃, deactivated before use over basic Alox).

6. Bibliography

- [1] J. Mann, *Nat. Rev. Cancer* **2002**, 2, 143.
- [2] G. Cragg, D. Kingston, D. Newman, in *Anticancer Agents from Nat. Prod. Second Ed.*, CRC Press, **2011**, pp. 1–4.
- [3] V. J. Paul, *Explor. Chem. Ecol.* **1992**.
- [4] D. G. I. Kingston, D. J. Newman, *Curr. Opin. Drug Discov. Devel.* **2002**, 5, 304–316.
- [5] Y.-Z. Shu, *J. Nat. Prod.* **1998**, 61, 1053–1071.
- [6] D. J. Newman, G. M. Cragg, *J. Nat. Prod.* **2007**, 70, 461–477.
- [7] M. S. Butler, *Nat. Prod. Rep.* **2008**, 25, 475–516.
- [8] G. M. Cragg, P. G. Grothaus, D. J. Newman, *Chem. Rev.* **2009**, 109, 3012–3043.
- [9] D. J. Newman, G. M. Cragg, K. M. Snader, *J. Nat. Prod.* **2003**, 66, 1022–1037.
- [10] D. G. I. Kingston, D. J. Newman, *Nat. Prod. Chem. Biol. First Ed. Ed. by Natanya Civjan* **2012**, 325–349.
- [11] R. Montaser, H. Luesch, *Future Med. Chem.* **2011**, 3, 1475–1489.
- [12] F. Flam, *Science* **1994**, 266, 1324–5.

- [13] M. E. Maier, *Nat. Prod. Rep.* **2009**, *26*, 1105–1124.
- [14] M. F. Clarke, J. E. Dick, P. B. Dirks, C. J. Eaves, C. H. M. Jamieson, D. L. Jones, J. Visvader, I. L. Weissman, G. M. Wahl, *Cancer Res.* **2006**, *66*, 9339–9344.
- [15] H. Clevers, *Nat. Med.* **2011**, *17*, 313–9.
- [16] T. Reya, S. J. Morrison, M. F. Clarke, I. L. Weissman, *Nature* **2001**, *414*, 105–111.
- [17] M. B. Insan, V. Jaitak, *Mini Rev. Med. Chem.* **2014**, *14*, 20–34.
- [18] R. Pardal, M. F. Clarke, S. J. Morrison, *Nat. Rev. Cancer* **2003**, *3*, 895–902.
- [19] L. Han, S. Shi, T. Gong, Z. Zhang, X. Sun, *Acta Pharm. Sin. B* **2013**, *3*, 65–75.
- [20] R. Tannishtha, S. J. Morrison, M. F. Clarke, I. L. Weissman, *Nature* **2001**, *414*, 105–111.
- [21] S. J. Scales, F. J. de Sauvage, *Trends Pharmacol. Sci.* **2009**, *30*, 303–312.
- [22] M. Varjosalo, J. Taipale, *Genes Dev.* **2008**, *22*, 2454–2472.
- [23] P. W. Ingham, A. P. McMahon, *Genes Dev.* **2001**, *15*, 3059–3087.
- [24] P. Kogerman, T. Grimm, L. Kogerman, D. Krause, A. B. Unden, B. Sandstedt, R. Toftgard, P. G. Zaphiropoulos, *Nat Cell Biol* **1999**, *1*, 312–319.
- [25] D. M. Stone, M. Murone, S. Luoh, W. Ye, M. P. Armanini, A. Gurney, H. Phillips, J. Brush, A. Goddard, F. J. de Sauvage, et al., *J. Cell Sci.* **1999**, *112* (Pt 2, 4437–48.

- [26] D. Amakye, Z. Jagani, M. Dorsch, *Nat. Med.* **2013**, *19*, 1410–1422.
- [27] L. L. Rubin, F. J. de Sauvage, L. L. Rubin, F. J. de Sauvage, F. J. de Sauvage, *Nat. Rev. Drug Discov.* **2006**, *5*, 1026–1033.
- [28] J. Xie, M. Murone, S. M. Luoh, a Ryan, Q. Gu, C. Zhang, J. M. Bonifas, C. W. Lam, M. Hynes, a Goddard, et al., *Nature* **1998**, *391*, 90–92.
- [29] U. Tostar, C. J. Malm, J. M. Meis-Kindblom, L. G. Kindblom, R. Toftgård, A. B. Undén, *J. Pathol.* **2006**, *208*, 17–25.
- [30] M. D. Taylor, L. Liu, C. Raffel, C. Hui, T. G. Mainprize, X. Zhang, R. Agatep, S. Chiappa, L. Gao, A. Lowrance, et al., *Nat. Genet.* **2002**, *31*, 306–310.
- [31] N. Takebe, P. J. Harris, R. Q. Warren, S. P. Ivy, *Nat Rev Clin Oncol* **2011**, *8*, 97–106.
- [32] L. Fan, C. V. Pepicelli, C. C. Dibble, W. Catbagan, J. L. Zarycki, R. Laciak, J. Gipp, A. Shaw, M. L. G. Lamm, A. Munoz, et al., *Endocrinology* **2004**, *145*, 3961–3970.
- [33] A. Ruiz i Altaba, P. Sánchez, N. Dahmane, A. i Altaba, P. Sánchez, N. Dahmane, *Nat. Rev. Cancer* **2002**, *2*, 361–372.
- [34] S. Coni, P. Infante, A. Gulino, *Biochem. Pharmacol.* **2013**, *85*, 623–628.
- [35] P. Infante, R. Alfonsi, B. Botta, M. Mori, L. Di Marcotullio, *Trends Pharmacol. Sci.* **2015**, *36*, 547–558.
- [36] R. L. Yauch, G. J. P. Dijkgraaf, B. Alicke, T. Januario, C. P. Ahn, T. Holcomb, K. Pujara, J. Stinson, C. A. Callahan, T. Tang, et al., *Science (80-)*. **2009**, *326*, 572 LP-574.

- [37] M. Lauth, Å. Bergström, *Proc. ...* **2007**, *104*, 8455–60.
- [38] J. M. Hyman, A. J. Firestone, V. M. Heine, Y. Zhao, C. a Ocasio, K. Han, M. Sun, P. G. Rack, S. Sinha, J. J. Wu, et al., *Proc. Natl. Acad. Sci.* **2009**, *106*, 14132–7.
- [39] J. Kim, J. J. Lee, J. Kim, D. Gardner, P. a Beachy, *Proc. Natl. Acad. Sci. U. S. A.* **2010**, *107*, 13432–13437.
- [40] P. Infante, M. Mori, R. Alfonsi, F. Ghirga, F. Aiello, S. Toscano, C. Ingallina, M. Siler, D. Cucchi, A. Po, et al., *EMBO J.* **2015**, *34*, 200–17.
- [41] N. P. Pavletich, C. O. Pabo, *Science* **1993**, *261*, 1701–7.
- [42] M. L. Verdonk, J. C. Cole, M. J. Hartshorn, C. W. Murray, R. D. Taylor, *Proteins Struct. Funct. Bioinforma.* **2003**, *623*, 609–623.
- [43] Y.-H. Bian, S.-H. Huang, L. Yang, X.-L. Ma, J.-W. Xie, H.-W. Zhang, *World J. Gastroenterol.* **2007**, *13*, 1659–1665.
- [44] A. N. Gerber, C. W. Wilson, Y.-J. Li, P.-T. Chuang, *Oncogene* **2006**, *26*, 1122–1136.
- [45] A. Ruiz i Altaba, P. Sanchez, N. Dahmane, *Nat Rev Cancer* **2002**, *2*, 361–372.
- [46] P. Sanchez, A. M. Hernández, B. Stecca, A. J. Kahler, A. M. DeGueme, A. Barrett, M. Beyna, M. W. Datta, S. Datta, A. Ruiz i Altaba, *Proc. Natl. Acad. Sci. United States Am.* **2004**, *101*, 12561–12566.
- [47] S. Coni, P. Infante, A. Gulino, *Biochem. Pharmacol.* **2013**, *85*, 623–628.
- [48] A. A. Abu-Hashem, M. M. Youssef, *Molecules* **2011**, *16*, 1956–

- 1972.
- [49] A. Gaspar, M. J. Matos, J. Garrido, E. Uriarte, F. Borges, *Chem. Rev.* **2014**, *114*, 4960–4992.
- [50] R. S. Keri, S. Budagumpi, R. K. Pai, R. G. Balakrishna, *Eur. J. Med. Chem.* **2014**, *78*, 340–374.
- [51] J. Reis, A. Gaspar, N. Milhazes, F. M. Borges, *J. Med. Chem.* **2017**, acs.jmedchem.6b01720.
- [52] J. Reis, A. Gaspar, N. Milhazes, F. Borges, *J. Med. Chem.* **2017**, DOI 10.1021/acs.jmedchem.6b01720.
- [53] K. P. Ko, *Asian Pacific J. Cancer Prev.* **2014**, *15*, 7001–7010.
- [54] H. Hussain, I. R. Green, *Expert Opin. Ther. Pat.* **2017**, 1–12.
- [55] A. Lévai, *J. Heterocycl. Chem.* **2004**, *41*, 449–460.
- [56] K. Wahala, T. A. Hase, *J. Chem. Soc. Perkin Trans. 1* **1991**, 3005–3008.
- [57] H. SEKIZAKI, R. YOKOSAWA, C. CHINEN, H. ADACHI, Y. YAMANE, *Biol. Pharm. Bull.* **1993**, *16*, 698–701.
- [58] J. D. S. Denis, J. S. Gordon Iv, V. M. Carroll, R. Priefer, *Synthesis (Stuttg.)* **2010**, 1590–1592.
- [59] K. F. Biegasiewicz, J. D. S. Denis, V. M. Carroll, R. Priefer, *Tetrahedron Lett.* **2010**, *51*, 4408–4410.
- [60] L. a. Paquette, H. Stucki, *J. Org. Chem.* **1966**, *31*, 1232–1235.
- [61] C. Ingallina, P. M. Costa, F. Ghirga, R. Klippstein, J. T. Wang, S. Berardozi, N. Hodgins, P. Infante, S. M. Pollard, B. Botta, et al.,

- Nanomedicine* **2017**, *12*, DOI 10.2217/nnm-2016-0388.
- [62] C. Ramarao, S. V Ley, S. C. Smith, I. M. Shirley, N. DeAlmeida, *Chem. Commun.* **2002**, 1132–1133.
- [63] N. Niccolai, 1947-, G. Valensin, 1946-, **1986**.
- [64] D. Neuhaus, M. P. Williamson, *J. Magn. Reson.* **1992**, *97*, 224.
- [65] L. V Goodrich, L. Milenković, K. M. Higgins, M. P. Scott, *Science* (80-.). **1997**, *277*, 1109 LP-1113.
- [66] J. Svård, K. H. Henricson, M. Persson-Lek, B. Rozell, M. Lauth, Å. Bergström, J. Ericson, R. Toftgård, S. Teglund, *Dev. Cell* **2006**, *10*, 187–197.
- [67] B. Manoranjan, C. Venugopal, N. McFarlane, B. W. Doble, S. E. Dunn, K. Scheinemann, S. K. Singh, *Cancer Lett.* **2013**, *338*, 23–31.
- [68] A. Po, E. Ferretti, E. Miele, E. De Smaele, A. Paganelli, G. Canettieri, S. Coni, L. Di Marcotullio, M. Biffoni, L. Massimi, et al., *EMBO J.* **2010**, *29*, 2646 LP-2658.
- [69] M. A. Jordan, K. Kamath, *Curr. Cancer Drug Targets* **2007**, *7*, 730–742.
- [70] M. A. Jordan, L. Wilson, *Nat. Rev. Cancer* **2004**, *4*, 253–265.
- [71] A. L. Risinger, F. J. Giles, S. L. Mooberry, *Cancer Treat. Rev.* **2009**, *35*, 255–261.
- [72] E. Mukhtar, V. M. Adhami, H. Mukhtar, *Mol. Cancer Ther.* **2014**, *13*, 275–284.
- [73] C. Dumontet, M. A. Jordan, *Nat. Rev. Drug Discov.* **2010**, *9*, 790–

- 803.
- [74] B. Gigant, C. Wang, R. B. G. Ravelli, F. Roussi, M. O. Steinmetz, P. A. Curmi, A. Sobel, M. Knossow, *Nature* **2005**, 435, 519–522.
- [75] R. J. Toso, M. A. Jordan, K. W. Farrell, B. Matsumoto, L. Wilson, *Biochemistry* **1993**, 32, 1285–1293.
- [76] M. A. Jordan, L. Wilson, *Biochemistry* **1990**, 29, 2730–2739.
- [77] B. T. Emmerson, *N. Engl. J. Med.* **1996**, 334, 445–451.
- [78] M. M. Cooney, W. van Heeckeren, S. Bhakta, J. Ortiz, S. C. Remick, *Nat Clin Pr. Oncol* **2006**, 3, 682–692.
- [79] E. Nogales, S. Grayer Wolf, I. A. Khan, R. F. Luduena, K. H. Downing, *Nature* **1995**, 375, 424–427.
- [80] K. Gerth, N. Bedorf, G. Höfle, H. Irschik, H. Reichenbach, *J. Antibiot. (Tokyo)*. **1996**, 49, 560–563.
- [81] D. M. Bollag, P. A. Mcquaney, J. Zhu, D. M. Bollag, P. A. Mcquaney, J. Zhu, O. Hensens, L. Koupal, J. Liesch, M. Goetz, et al., **1995**, 2325–2333.
- [82] Y. Zhao, X. Mu, G. Du, *Pharmacol. Ther.* **2016**, 162, 134–143.
- [83] E. Quiñoá, Y. Kakou, C. Phillip, *J. Org. Chem.* **1988**, 53, 3642–3644.
- [84] D. G. Corley, R. Herb, R. E. Moore, P. J. Scheuer, V. J. Paul, *J. Org. Chem.* **1988**, 53, 3644–3646.
- [85] L. M. West, P. T. Northcote, C. N. Battershill, *J. Org. Chem.* **2000**, 65, 445–449.

- [86] A. E. Prota, K. Bargsten, P. T. Northcote, M. Marsh, K. H. Altmann, J. H. Miller, J. F. D??az, M. O. Steinmetz, *Angew. Chemie - Int. Ed.* **2014**, *53*, 1621–1625.
- [87] J. LIU, M. J. TOWLE, H. CHENG, P. SAXTON, C. REARDON, J. WU, E. A. MURPHY, G. KUZNETSOV, C. W. JOHANNES, M. R. TREMBLAY, et al., *Anticancer Res.* **2007**, *27*, 1509–1518.
- [88] J. Tanaka, T. Higa, *Tetrahedron Lett.* **1996**, *37*, 5535–5538.
- [89] J. J. Field, A. J. Singh, A. Kanakkanthara, T. Halafihi, P. T. Northcote, J. H. Miller, *J. Med. Chem.* **2009**, *52*, 7328–7332.
- [90] A. B. Smith, I. G. Safonov, R. M. Corbett, *J. Am. Chem. Soc.* **2001**, *123*, 12426–12427.
- [91] A. B. Smith, I. G. Safonov, R. M. Corbett, *J. Am. Chem. Soc.* **2002**, *124*, 11102–11113.
- [92] A. Cutignano, I. Bruno, G. Bifulco, A. Casapullo, C. Debitus, L. Gomez-Paloma, R. Riccio, *Eur. J. Org. Chem.* **2001**, 775–778.
- [93] C. C. Sanchez, G. E. Keck, *Org. Lett.* **2005**, *7*, 3053–3056.
- [94] D. L. Aubele, S. Wan, P. E. Floreancig, *Angew. Chemie - Int. Ed.* **2005**, *44*, 3485–3488.
- [95] Q.-H. Chen, D. G. I. Kingston, *Nat. Prod. Rep.* **2014**, *31*, 1202–1226.
- [96] T. R. Hoye, M. Hu, *J. Am. Chem. Soc.* **2003**, *125*, 9576–7.
- [97] I. Louis, N. L. Hungerford, E. J. Humphries, M. D. McLeod, *Org. Lett.* **2006**, *8*, 1117–1120.
- [98] F. Ding, M. P. Jennings, *J. Org. Chem.* **2008**, *73*, 5965–5976.

- [99] J. Uenishi, T. Iwamoto, J. Tanaka, *Org. Lett.* **2009**, *11*, 3262–5.
- [100] S. Y. Yun, E. C. Hansen, I. Volchkov, E. J. Cho, W. Y. Lo, D. Lee, *Angew. Chemie Int. Ed.* **2010**, *49*, 4261–4263.
- [101] D. Zurwerra, J. Gertsch, K.-H. Altmann, *Org. Lett.* **2010**, *12*, 2302–2305.
- [102] B. Pera, M. N. Calvo-Vidal, S. Ambati, M. Jordi, A. Kahn, J. F. Díaz, W. Fang, K.-H. Altmann, L. Cerchietti, M. A. S. Moore, *Cancer Lett.* **2015**, *368*, 97–104.
- [103] J. J. Field, B. Pera, E. Calvo, A. Canales, D. Zurwerra, C. Trigili, J. Rodríguez-Salarichs, R. Matesanz, A. Kanakkanthara, S. J. Wakefield, et al., *Chem. Biol.* **2012**, *19*, 686–698.
- [104] A. E. Prota, K. Bargsten, D. Zurwerra, J. J. Field, J. F. F. Diaz, K.-H. Altmann, M. O. Steinmetz, *Science* (80-.). **2013**, DOI 10.1126/science.1230582.
- [105] C. Holohan, S. Van Schaeybroeck, D. B. Longley, P. G. Johnston, *Nat. Rev. Cancer* **2013**, *13*, 714–726.
- [106] D. Zurwerra, F. Glaus, L. Betschart, J. Schuster, J. Gertsch, W. Ganci, K. H. Altmann, *Chem. - A Eur. J.* **2012**, *18*, 16868–16883.
- [107] E. J. Corey, J. A. Katzenellenbogen, G. H. Posner, *J. Am. Chem. Soc.* **1967**, *89*, 4245–4247.
- [108] S. J. Mickel, G. H. Sedelmeier, D. Niederer, R. Daeffler, A. Osmani, K. Schreiner, M. Seeger-Weibel, B. Béro, K. Schaer, R. Gamboni, et al., *Org. Process Res. Dev.* **2004**, *8*, 92–100.
- [109] A. Chau, J.-F. Paquin, M. Lautens, *J. Org. Chem.* **2006**, *71*, 1924–1933.

- [110] Y. Oikawa, T. Yoshioka, O. Yonemitsu, *Tetrahedron Lett.* **1982**, *23*, 885–888.
- [111] K. Omura, D. Swern, *Tetrahedron* **1978**, *34*, 1651–1660.
- [112] D. L. J. Clive, K. S. K. Murthy, A. G. H. Wee, J. S. Prasad, G. V. J. Da Silva, M. Majewski, P. C. Anderson, C. F. Evans, R. D. Haugen, *J. Am. Chem. Soc.* **1990**, *112*, 3018–3028.
- [113] B. M. Trost, M. T. Rudd, *J. Am. Chem. Soc.* **2005**, *127*, 4763–4776.
- [114] R. Jasti, J. Vitale, S. D. Rychnovsky, *J. Am. Chem. Soc.* **2004**, *126*, 9904–9905.
- [115] J. P. Vitale, S. A. Wolckenhauer, N. M. Do, S. D. Rychnovsky, *Org. Lett.* **2005**, *7*, 3255–3258.
- [116] J.-F. Betzer, J. Ardisson, J.-Y. Lallemand, A. Pancrazi, *Tetrahedron Lett.* **1997**, *38*, 2279–2282.
- [117] J.-F. Betzer, F. Delalogue, B. Muller, A. Pancrazi, J. Prunet, *J. Org. Chem.* **1997**, *62*, 7768–7780.
- [118] J. Inanaga, K. Hirata, H. Saeki, T. Katsuki, M. Yamaguchi, *Bull. Chem. Soc. Jpn.* **1979**, *52*, 1989–1993.
- [119] I. Paterson, Y. Kap-Sun, *Tetrahedron Lett.* **1993**, *34*, 5347–5350.
- [120] I. Paterson, K.-S. Yeung, C. Watson, R. A. Ward, P. A. Wallace, *Tetrahedron* **1998**, *54*, 11935–11954.
- [121] D. B. Dess, J. C. Martin, *J. Org. Chem.* **1983**, *48*, 4155–4156.
- [122] A. K. Ghosh, X. Cheng, R. Bai, E. Hamel, *European J. Org. Chem.* **2012**, *2012*, 4130–4139.

- [123] R. Noyori, I. Tomino, Y. Tanimoto, M. Nishizawa, *J. Am. Chem. Soc.* **1984**, *106*, 6709–6716.
- [124] B. Botta, A. Gulino, M. Botta, M. Mattia, L. Di Marcotullio, P. Infante, F. Ghirga, S. Toscano, C. Ingallina, R. Alfonsi, *Multitarget Hedgehog Pathway Inhibitors and Uses Thereof*, **2014**.
- [125] C. W. Wullschleger, J. Gertsch, K.-H. Altmann, *Org. Lett.* **2010**, *12*, 1120–1123.

